# Further Exploration of EIT in Cancer Detection

**Martin Robert Brien BSc**

Thesis submitted for the degree of

Doctor of Philosophy

at the University of Leicester

Department of Engineering

University of Leicester

November 2011

# Abstract

Electrical Impedance Tomography (EIT) is a non-invasive detection technique which is able to distinguish between cancerous and non-cancerous cells.

This thesis addresses some of the issues associated with EIT system design. Initially a study was completed to source an improved voltage-to-current convertor for the current Leicester system. Two circuits were designed and simulated using PSpice software and compared for their responses and to ascertain the capacity for improvement through component advancement. Simulated results indicated that the Improved Howland circuit was superior for the specific needs of the Leicester group. Secondly, following a review of current techniques for improving the high frequency response of EIT systems, a theory for using a time response method as a solution was developed. The new method was directly compared to the existing frequency technique by analysing electronic phantom and organic samples with both systems. Finally an investigation was completed in the area of micro EIT which aimed to detect cancerous islets within mouse pancreata with aims to distinguish normal and cancerous cells, and, ultimately, to detect cancerous single cell “escapers”. Three methods were described. The initial technique tested in-vitro pancreata and results from this suggested that the approach was a viable method for indentifying the affected tissue; therefore additional methods were designed to test individual extracted islets.

In summary, the thesis provides an improved alternative V-to-I convertor for the Leicester group’s system, which has been adopted in experiments. The time response method investigation showed that it may provide a viable method that could, with further development and analytical refinement, improve the effectiveness of cell modelling in several interesting ways. Further investigation is suggested. The positive results provided by the whole pancreas testing are a convincing reason for further work to be conducted in this area, in particular work to enhance the diagnostic analysis of pancreata.

# Acknowledgements

I would like to thank my supervisor Prof. Da-Wei Gu for his guidance and calm nature which has been a great help at various points throughout my study.

I also thank Dr Wei Wang who provided me with the opportunity to complete this piece of work and provided much support along with various members of the De Montfort University Biomedical Research Group.

Special mention however must go to my colleagues from the group: Dr Ben Tunstall, Dr James Wheeler and Guofeng Qiao, who provided me with invaluable advice throughout my study.

I also acknowledge the financial support of the University of Leicester's Engineering Department.

I would like to extend my gratitude to Dr Richard Hopper and David Hirst who have been very kind on a number of occasions, and in doing so, have allowed my thesis to become a piece of work I can be proud of.

Finally, I would have not completed this work without my family and friends, in particular Eleanor and 'I am in love' who have provided both support and distraction.

# Declaration

The work presented within this thesis is the exclusive work of the author, Martin Brien, except where otherwise acknowledged. Furthermore the work presented has not been published or otherwise distributed by any person other than the author.

Martin Brien

November 2011

# Publication List by the Author

Wang W, Wang L, Brien M and Al-akaidi M. (2006) Study and comparison of the repeatability errors from different bio-electrodes under various conditions for *EIT Proceedings of VII EIT*, Seoul, Korea

Wang L, Wang W, Qiao G F, Brien M and Al-Akaidi M. (2006). Preliminary report of optimisation of in-vitro studies with an in-vitro specimen measuring system *Proceedings of VII EIT*, Seoul, Korea

Wang W, Wang L, Tunstall B, Brien M, and Gu D-W. (2006). Investigation on biomedical measurement accuracy in electrode-skin tests *Proceedings of XI IFAC MCBMS* **6** (1): 147-150

Wang W, Brien M, Gu D-W and Yang J (2007) A Comprehensive Study on Current Source Circuits In: *Proceedings of XIII ICEBI &VIII EIT*, Graz

Wang W, Gu D-W, Pelengaris S, Qiao G, Cheung L, Sze G, Tunstall B, Brien M and Epstein D (2008). Preliminary results from a study of pancreatic tissue for cancer identification using electrical impedance measurement *9th Electrical Impedance Tomography Conference,* Hanover, USA pg 130-133

# Table of Contents

# Table of Figures

## Chapter 1



## Chapter 2

## Chapter 3

## Chapter 4

## Chapter 5

# Table of Tables

# Glossary

**Agilent Vee** A visual programming environment used primarily for data acquisition, produced by Agilent

**Beta Cells** Cells within the Islets of Langerhans (see below) which produce insulin and amylin. Beta cells are the cells affected by the cancer researched in Chapter 5.

**C** The capacitance of a cell as represented within the 3-element Cole-Cole model

**Cole-Cole model** An electronic circuit which uses 3 elements to represent a biological cell

**Dispersion Frequency or Relaxation Frequency or Fr** The frequency which provides the lowest point of the imaginary part of the complex output of an EIT impedance curve

**Equipotential** Points which are all at the same potential

**Electrical Impedance Tomography (EIT)** A non-invasive medical imaging technique which provides an image representing the permittivity (or conductivity) of a body

**Electrical Impedance Mammography (EIM)** An application of EIT for the detection of breast cancer

**Faraday Cage** An enclosure which prevents external interference from electromagnetic fields

**Gain Bandwidth Product (GBP)** A property of an op-amp which describes the maximum bandwidth possible when operating at a gain of one

**Gastrointestinal Tract** The path through which digestion occurs, including the throat, stomach, intestines and colon

**Generalised Impedance Convertor (GIC**) An electronic circuit which uses the negative feedback capability of operational amplifier (see below) to provide a capacitive or inductive load

**Howland Model** A popular circuit which uses an operational amplifier to provide a constant current output

**Impedance** The complex value combining resistance and reactance characteristics of a circuit

**In-vitro** Literally meaning “within the glass”. It refers to experiments performed in a controlled environment, for example; excised cells within a petri dish.

**In-vivo** Literally meaning “within the living”. It refers to experiments performed on living organisms

**Islets of Langerhans** Islets within the pancreas which contain hormone producing cells

**LabVIEW** A graphical programming environment produced by National Instruments (NI)

**Mammary glands** Milk producing organs found in mammals

**Mammography** A process to form images of human breasts.

**Matlab** A technical computing software package produced by Mathworks

**Micro Electrode Array (MEA)** A device which contains a fixed set of small conducting points through which signals can be passed

**Multiplexer** An electronic device which selects a specific input from an array and sends it to a specific output

**Operational amplifier (Op-amp)** A high-gain differential electronic amplifier

**PSpice** An analogue and digital circuit simulator produced by OrCAD

**$R_R$ or R** The internal resistance of a cell as represented within the 3-element Cole-Cole model

**$R_S$ or S** The external resistance of a cell as represented within the 3-element Cole-Cole model

**RSC** The 3 components within the Cole model of a cell: $R_R$, $R_S$ and C

**Sensitivity** in mammography terms: A measure of how well a system can find lesions within tissue

**Specificity** in mammography terms: A measure of how well a system can identify lesions as malignant or benign

**Thorax** Part of the body between the head and the abdomen, also known as the chest in humans

**Ultrasound** A method of producing images by reflection of high frequency signals (above the limits of human hearing) from objects being imaged. The high frequency allows penetration of some materials

**Voxel** A "virtual point" element of volume within an object that can be homogenously characterised

**X-Ray** A high frequency form of electromagnetic radiation which is used to provide images of objects within a larger object of heterogeneous density

# Chapter 1 Cancer Detection

The early and reliable detection of cancers, particularly breast cancers in women, delivers substantial health and wellbeing benefits to our society and has attracted major medical and research activity in recent years. This thesis reports research on promising advances in detection and diagnostic techniques.

## 1.1 Cancer

The majority of cells within a human body undergo a constant reproduction process known as mitosis, in which they split apart to form two identical cells; by this method the body can form tissue and organs. This cell division continues at a relatively rapid pace until adulthood, at which point the body does not need to grow as much and the process is mainly used to heal wounds and replace cells which have died. [WILEY 2006]

Mitosis is a complicated process and has several phases in which chromosomes are replicated before the cell divides. Occasionally some cells reproduce abnormally, due to one or more of the phases not being completed successfully. When this occurs, the cells created are not exact copies of the original cells. The genetically mutated cells are different from the tissue surrounding them, therefore they grow independently, forming clusters which divide and multiply. This process creates

masses of mutated cells (or mutated tissue) which are distinct from the main body and known as tumours. [OXFORD 1994]

Tumours that have limited growth and do not spread into surrounding tissues are referred to as benign. They are, for the most part, harmless; although these tumours can cause problems by applying pressure to surrounding healthy cells.

Cancer refers to malignant tumours, which are tumours whose growth is uncontrolled and therefore are able to spread. They can spread both locally (known as invasion) and to distant sites; travelling via the bloodstream or the lymphatics (known as metastasis).

Cancer growth and spread may reach a point where it can kill the host. There are many eventual resulting causes of death, from affecting breathing function to upsetting the body's chemical balance, all of which stem from the destruction of healthy cells. [BLACKS 2005, WILEY 2006, TABER 1997]

## 1.2 Breast Cancer

Over 40,000 cases of breast cancer are diagnosed every year in the UK; this makes it the most common type of cancer in this country. Recent statistics show that around 1 in 9 women will develop breast cancer in their lives; men can also develop the

disease, though these account for only 1% of all breast cancer cases. [Cancer Research UK 2008a, ONS 2007]

There are several different types of Breast Cancer, the majority of them grow from glandular tissue and are known as adenocarcinomas. Within the breast there are two types of glandular tissue which can develop these cancers; the milk ducts, which can form Ductal cancer (approximately 85% of cases), and the milk lobes, which can be affected by lobular cancer (approximately 15% of cases). The other forms of breast cancer account for less than 1% of cases. [Cancer Research UK 2008a]

Breast cancer is the most prominent cause of death in women aged 35-54 years, accounting for up to 17% of all deaths. The number of women dying from the various forms of the disease has been decreasing since around 1990 due to advances in techniques for detecting and treating cancer. [Cancer Research UK 2008a]

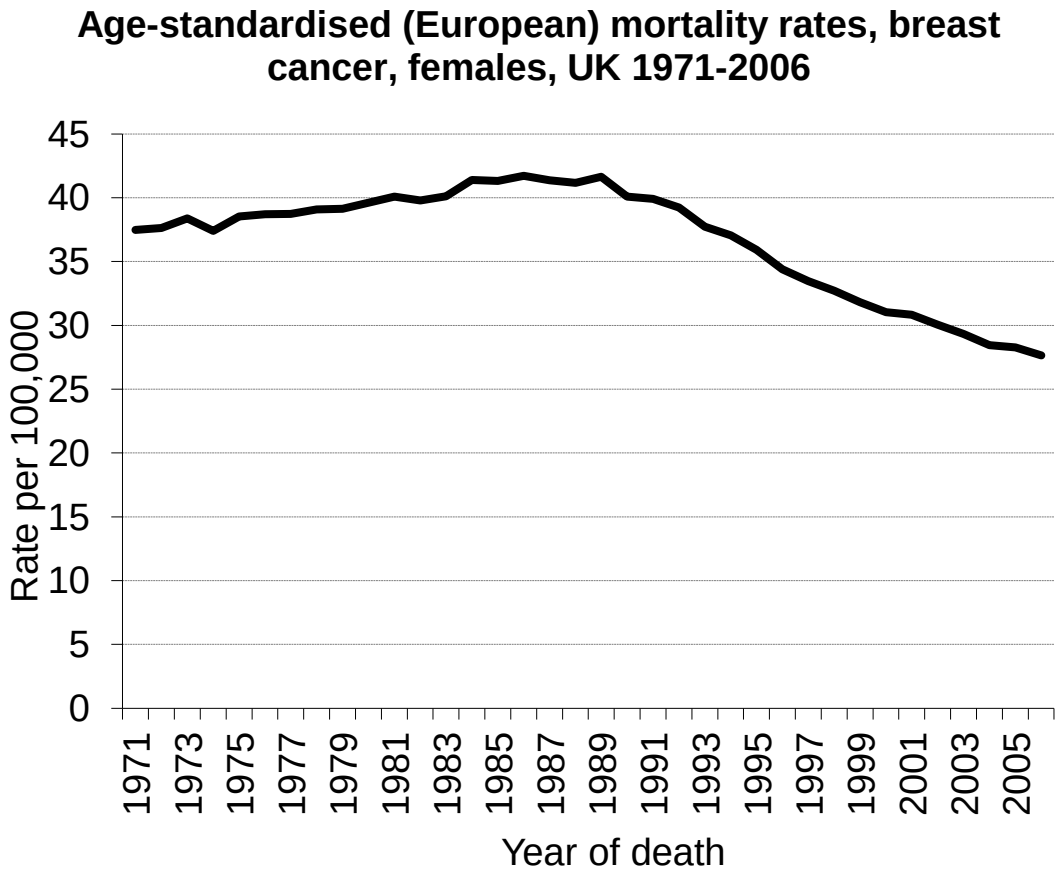


*Figure 1.1: Ages standardised (European) mortality rates, breast cancer, females, UK 1971-2005 [CANCER RESEARCH UK 2008b]*

## 1.3 Stages of Breast Cancer

Five different stages in the development of cancer have been outlined to ease the description of the disease within patients. They relate to how the disease has matured and, in some cases, spread around the body. Although the definition of each stage is clear, the disease is progressive, therefore late stage 1 cancer is little different from early stage 2. [Cancer Research UK 2008a]

### 1.3.1 Stage 0

Describes the earliest growth of a cancer, after the first cancer cells mutate during cell division. This level of disease is referred to as non-invasive as it is all in a concentrated area. Almost no cancers are discovered at stage 0.

### 1.3.2 Stage 1

Cancer which has grown, but has not yet surpassed 2cm in diameter. As in stage 0, this is also non-invasive as the cancer cells have not spread to any other parts of the body.

### 1.3.3 Stage 2

When the cancer has reached between 2 and 5 cm in size it becomes known as stage 2. It may also have spread to surrounding tissue, such as the lymph glands in the armpits.

### 1.3.4 Stage 3

This describes cancers that have grown beyond 5 cm and may have attached themselves to surrounding muscle or skin. At this stage the cancer still hasn't spread beyond the lymph glands.

Up to and including stage 3, tumours can often be removed completely through surgery with assisting radiotherapy for patients who are considered a high risk for reoccurrence. Also some younger patients may be treated with chemotherapy to shrink the tumour before surgery.

### 1.3.5 Stage 4

Stage 4 tumours can be of any size. It describes cancer that has spread to other parts of the body and is growing elsewhere. These are known as secondary cancers. [CANCER RESEARCH UK 2008a, KOPANS 1998]

## 1.4 Removal of Cancer

The earlier cancer is detected the easier it is to remove; if a tumour is small (stage 1) there is more chance of removing all the cancerous cells present, however once the tumour has grown and has begun spreading it will be more difficult to locate all of the mutated tissue, therefore the need for early detection is clear. If a benign lesion is discovered it can be removed fairly easily, however not all benign growths need to be removed and they can often be left alone if they are not uncomfortable for the patient. [BLACKS 2005]

Once cancer spreads it cannot usually be fully removed in surgery, instead the most suitable method, or combination of methods must be chosen to treat the cancer

most effectively. This also indicates that early detection is a very important factor in cancer diagnosis. [TABER 1997]

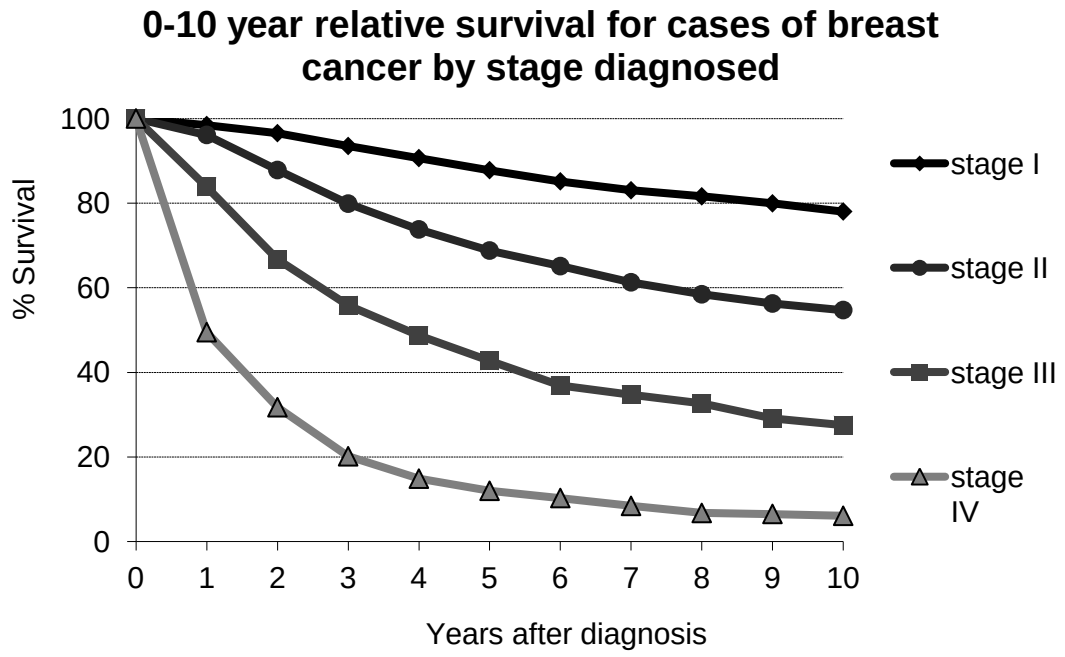


*Figure 1.2: 0-10 year relative survival for cases of breast cancer by stage diagnosed in the West Midlands 1985-1989 followed up to the end of 1999, as at January 2002 [Cancer Research UK 2008c]*

Figure 1.2 demonstrates how the chances of survival are much higher if the cancer is found at an earlier stage in its development. The graph does not show a curve for survival for stage zero, this is due to the low number of tumours detected at such an early stage. These statistics are now 9 years old, however this is latest study recognised by cancer research UK and they state that the outlook is better for

women diagnosed now due to improvements in screening and treatment. [Cancer Research UK 2008c]

## 1.5 Detection Techniques

There are many different techniques for detecting cancer, some of which are used within the medical industry already whilst others are still in the research and development stages. All the techniques have different advantages and disadvantages which can limit detection; a compromise is reached to provide the best detection available within each method.

All women are recommended to perform regular self examination to identify any changes or lumps, which can then be further investigated if necessary. In Britain there is a screening program in place for women aged 50 to 70 years in which they are regularly tested using an X-Ray mammogram.

### 1.5.1 X-Ray

X-Rays were first used to image breasts in 1930; tumours were identified. [Warren 1930]

X-Ray Mammography is currently the most common detection technique for breast cancer. An X-Ray image of the suspected tissue is taken and cancer cells can be seen as a change in the shade of the image produced. Cancerous cells occur as a dense

light section on an X-Ray image; this can however cause confusion between cancerous cells and dense, normal healthy tissue.

This test is considered to be invasive because ionising radiation enters the body. Exposure to X-Rays is often considered dangerous and may even be responsible for initiating cancer, particularly with multiple doses. Strict guidelines have been introduced in some countries regarding the radiation dose during these tests however, in order to improve the contrast of the image, increased radiation exposure is required. [TABER 1997, FENTIMAN 1998]

In order to acquire a successful image, the breast needs to be flattened; this compression improves the contrast on the image while reducing the dose of radiation that the breast is subjected to. It also restricts patient movement and allows the density of the image to be more uniform making it easier to identify tumours. However this compression can be very uncomfortable for many women. [IARC 2002]

Although the position of the lesion can be very clearly identified using X-Ray mammography unfortunately the technique cannot easily discern between benign and cancerous tumours. Therefore the test is often followed by further invasive surgery usually in the form of a needle biopsy in which cells are collected from the suspected area using a needle syringe and are tested *in vitro*. [TABER 1997]

Due to the higher density of tissue in younger breasts it is a lot harder to identify tumours and only 60% of cancer is detected in patients less than 50 years old. However for those over 50 years of age the detection rate rises to 90%. [FENTIMAN 1998]

This means X-Ray mammography is currently the most successful technique for discovering breast cancer and has become an integral part of a screening program throughout the UK which tests women aged 50-70 for breast cancer. There are many Mammography machines throughout the country which are available for anyone who may need the test.

The NHS budget for their breast screening programme was recently estimated to be around £75 million. On average, this amounts to around £45.50 for each patient. Clearly this figure is very high and anything which could help reduce this without compromising the results would be advantageous. [NHS 2007]

In America it is estimated that women in their 40s have a 30% chance of a false positive result in a mammography exam if they undertake yearly screening. These false positives can even lead to biopsy in some cases. It is also estimated that mammography screening has a 10% rate of false-negative results, that is where there is a cancer but it is not identified from the imaging test. [RADIOLOGYINFO 2008]

Although it is often preferable for false-positive patients to be recalled for further tests, as any new cancers may be identified, these further tests increase the cost of screening, it has also been shown to have a negative effect on the wellbeing of the patient, causing increased levels of anxiety in many cases. [BREWER 2007]

Currently X-Ray mammography is the best test available for screening for breast cancer. It is however not without its flaws and in view of this it is important for other avenues of cancer detection to be investigated. If a new technique can achieve a similar level of positive results without one of mammography's drawbacks (invasive X-Rays, uncomfortable for patients, etc), it may become the premier diagnostic instrument for cancer. However since X-Ray mammography is already well known and readily available for testing it will be some time until this is possible.

### 1.5.2 T-Scan

T-Scan is an early version of impedance imaging using electrodes, it furthered research towards Electrical Impedance Tomography (EIT) (discussed later), produced by Siemens Medical, which uses a hand held scanner similar to those used in ultrasound. The patient is earthed via an electrode held in the hand, the operator holds the scanner, which uses a square array of electrodes to apply an electric field to the breast and the impedance value indicates if the tissue is cancerous.

The unit was designed to work alongside X-Ray mammography and ultrasound as opposed to being a replacement. [ASSENHEIMER 2001]

T-Scan has been used clinically to identify a tumour which had already been discovered using X-Ray Mammography; unlike X-Ray, impedance imaging has the potential to distinguish between benign and cancerous growths. [FDA 1999b]

This impedance imaging cannot provide high resolution when compared to X-Ray mammography. The T-scan system produces 2D images which increase the difficulty in pin-pointing any cancers found for removal. Also since the breast is not held still and the patient generally lies on his or her back, or sits upright, the scanner can move the tissue around and therefore the position of the cancer is even harder to ascertain.

Although the FDA (Food and Drug Administration) approved the T-Scan for use throughout the US in 1999 it was never approved for clinical screening. [NCI 2008, FDA 1999a]

T-Scan was an important breakthrough for the impedance imaging community and made many people aware of the technique. Since it was designed following relatively early stages of research in the field the small number of electrodes employed and older computing software mean the system now looks primitive compared to modern EIT systems. Marketing T-Scan as a secondary diagnostic device meant that

the advantages of impedance imaging over X-Ray mammography were made clear, and this has encouraged further research into the field.

### 1.5.3 Magnetic Resonance Imaging

Magnetic resonance imaging works by sending an electro-magnetic pulse through the body, which excites protons within water molecules. An image can then be created based on the magnetic relaxation and phase changes within the cell; these changes are detected using antenna coils.

The test is very expensive to perform and can be lengthy to complete (sometimes up to an hour), during which the patient must stay completely still or the final image will become blurred. The MRI scanner itself is also a very expensive piece of equipment.

Also due to the large magnetic force involved, patients who may have metal in their body, for instance patients with a pacemaker or pins in bones, cannot undergo the test. MRI scanning for breast cancer is generally used as a second test after initial X-Ray mammography.

Since MRI has many applications within the medical industry, it is widely available for test purposes. It can be used to produce a highly detailed image, either 2D or 3D, but it cannot always tell the difference between cancerous and non-cancerous abnormalities though, with further research into the technique and the use of a

contrast agent to make the identification of tissue more clear it may yet be used more widely as a valid cancer detection technique.

In summary MRI is more sensitive than mammography and does not emit potentially dangerous X-Ray radiation, however it is less specific, very expensive and can be a difficult experience for patients. Currently the technique is more often used to understand issues brought about by breast implants. [KOPANS 1998, IARC 2002]

### 1.5.4 Ultrasound

Ultrasound breast scanning uses the same technique that is used when scanning for pregnancies. A scanner is used to transmit ultrasonic pulses into the body, and the scanner also acts as a receiver to detect the reflected pulses. It is a pain free method which involves no irritation to the patient. The images provided can be quite detailed and can often find lesions which are missed by X-Ray mammography as, with this technique, the images may provide the position of an unusual cell growth. However ultrasound provides a lower spatial resolution than mammography, therefore requires considerable operator skill in order to recognise small lesions and it is difficult to identify whether it is malignant or not without further investigation. [TSUI 2008, FENTIMAN 1998]

It is also worth noting that since many ultrasound scanners are hand held devices, this technique suffers from a similar problem of positioning as the T-Scan unit,

however ultrasound experimental units have been made which are not hand-held and they could provide a more accurate position of the growth.

Ultrasound is currently used as a tool in breast cancer detection alongside X-Ray mammography; it is used to distinguish certain types of lesions and also as a guide when completing a biopsy. [KOPANS 1998]

In summary Ultrasound has increased sensitivity, especially in denser breast tissue and there is no exposure to potentially dangerous X-Rays, however as with MRI it is both more expensive and less specific than X-Ray Mammography. [FENTIMAN 1998]

### 1.5.5 Electrical Impedance Tomography

Electrical Impedance Tomography (EIT), as briefly mentioned above, applies an electrical current to a body; an output is measured elsewhere and the impedance effects on the signal by the conductive tissue can be ascertained. This impedance can be plotted to show the values at different points within the body.

EIT was originally applied in layers, which could then be built up into 3D images; however, as more research has been completed, there are now many different approaches to measuring and plotting impedances, and 3D images can now be derived.

Although the T-scan system is not strictly EIT, as the image provided is a resistivity map rather than a topographic reconstruction, it is the most recognised impedance imaging-based application in the detection of breast cancer due to its approval for clinical use. Several EIT systems are approaching this level of maturity of investigation.

EIT can identify between benign and cancerous tumours; however the main drawback with the technique is the relatively low resolution available, due partly to the large impedances found at the electrode-skin interface, which can make accurate positioning of the lesion difficult. [HOLDER 2005, KAO 2008]

EIT is more specific than other detection techniques. It also has the potential to provide impressive sensitivity, though this relies heavily on the mesh model used. However due to the low spatial resolution the position of the tumour may not be correctly identified. The test is relatively comfortable for the patient and there is no exposure to X-Rays. [HOLDER 2005]

When referring to EIT used for breast cancer detection the term Electrical Impedance Mammography (EIM) is generally used.

EIT is discussed further in Chapter 2: EIT/EIM.

### 1.5.6 Other Techniques

There are several other techniques which are reported as having potential in this area of research. While none of the current techniques have a 100% detection rate there is room for investigation into new techniques which improve their performance.

Techniques such as Near-Infrared Imaging (NIR), Magnetic Induction Tomography (MIT) and Electromagnetic Probe (EM) are being investigated with the aim of use in detecting breast cancer. However they are at a relatively early stage in their research and it will be a long time before any of these can rival the current mammography techniques. [BOAS 2001, MIEOG 2011, SCHWEIGER 1999, SCHARFETTER 2007, SEQUIN 2009, ZHOU 2011]

### 1.5.7 Conclusion

The statistics described within this chapter show the dangers of cancer within today's society, the numbers of cancer victims have been increasing for some time and the need for improved medical facilities to cope with the disease are apparent. As discussed the early detection of cancer can result in much improved chances of survival.

It is clear that there is no single defining technique for detecting breast cancer, and most of the ones in use, mentioned above, are simply not accurate enough and

require further testing to confirm whether or not a tumour is present, or whether or not the tumour is malignant. The technique for finally answering these questions is generally biopsy which, as mentioned, involves taking a sample of the suspected tissue and testing it in a laboratory, obviously this is an invasive procedure, and could be unpleasant for the patient. If a test could be performed where the patient did not have to undergo this type of surgery to find out if cancer was present it would be preferable; this is what all breast cancer detection research is striving towards. [TABER 1997]

## 1.6 Thesis Outline

EIT has the potential to become a groundbreaking technique within cancer detection, however there are areas within it which need improving before this can be realised. This thesis looks at some of these areas and explores different avenues which may lead to improved detection and potentially save lives.

The potential of EIT is discussed in chapter 2, and includes a review of the Leicester group's contribution to the technique which provides a starting point for all the work described in the remaining chapters.

Chapter 3 discusses the issue of voltage to current converters which are required within all EIT systems and compares two known circuits with respect to bandwidth and output impedance. The investigation shows the benefits of both circuits and

discusses the needs within the Leicester group. The Improved Howland circuit is shown to provide a more suitable output and is recommended for future implementation.

The issue of restricted bandwidth is discussed further in Chapter 4 where two techniques presented by the Leicester group are investigated and an alternative approach is presented. Tests within the time domain are shown to be promising but the frequency approach currently provides more accurate results.

Finally an EIT system is described in Chapter 5 which can be adapted to allow measurements to be taken of mouse pancreata at different levels to compare cancerous and non-cancerous tissue. Tests completed on the whole pancreata suggest there are differences which could be used for identification however similar conclusions could not be drawn while testing individual islets. Improvements to the technique for future investigations are suggested which aim to improve the response at the islet level.

Each of these areas of EIT need to be improved if EIT is to compete with X-Ray Mammography and other better known cancer detection techniques and the novel contributions within these investigations are outlined in the thesis conclusions along with some further suggestions for work which was beyond the scope of this thesis.

# Chapter 2 EIT/EIM

Electrical Impedance Tomography (EIT) is a young detection technique with a huge amount of potential for medical diagnosis, not least for the diagnosis of cancer. Since it is such a relatively young technique it is still some way off being used in hospitals, especially since other techniques such as X-Ray already exist which can be used for similar purposes.

This chapter discusses how EIT has progressed since the first theory regarding a simplified electronic model was devised. The various systems built for EIM by the Leicester group are also described so that the progress made in this specific field can be observed.

Finally EIT is assessed in terms of its advantages and current shortcomings before discussing which parts of the technology need improving to help it reach its full potential.

## 2.1 Introduction to EIT

EIT, or EIT-style measurements, are used for many different applications throughout the world, from online monitoring and quality control of materials to the distribution of gas and liquids within pipelines. Much of this work is possible due to the non-

invasive nature of the technique; EIT can be used to describe the inside of an object without using intrusive radiation. EIT is used largely in diagnostic and analysis applications. This type of measurement is useful within the medical industry. In this field alone EIT methods have been used to image lung ventilation, gastric emptying, brain function and cancer growth, among other less publicised applications.

The applications described within this thesis are concerned with its use in the investigation of monitoring cancer growth.

The first known EIT experiments were completed under the term Applied Potential Tomography (APT). They are generally considered to be tests completed by D Barber and B Brown at Sheffield University who used a ring of electrodes to produce an image of a network of resistors. The first network was designed to be symmetrical for ease of measurements; however there was an unintentional wiring error which was identified from the results. This showed that it was possible to recognise a small change within a known array using this method. [BARBER 1984, BARBER 2005]

## 2.2 History

The roots of EIT were put down in 1940 when a paper released by Cole described an equation which allowed certain biological tissues to be characterised by a complex impedance curve across a frequency range; this equation is discussed further in chapter 4. The work presented was explored further by Cole & Cole in 1941 where

they described a plot of the real versus the imaginary parts of a complex permittivity across a frequency range. [COLE 1940, COLE & COLE 1941, MCADAMS 1995]

It took another 37 years before Henderson and Webster suggested the idea of impedance imaging in 1978, they designed a camera which could provide images of a thorax, however, by their own admission the images weren't good enough for any diagnostic purposes. [HENDERSON 1978]

Barber and Brown began their work in 1980; this initial work by the Sheffield group is considered the first real medical application of EIT, and was designed to provide images of the respiratory system, showing the inflation of the lungs (however their very first images were simply of a forearm to show the feasibility of the technique). The original system they produced became known as the Sheffield Mark 1 EIT system and was widely used in clinical studies; however it was never fully accepted as a clinical technique by medical staff, who already had access to CT and MRI equipment. [BARBER 1984, BARBER 2005]

Since this initial investigation several groups around the world have taken on the idea of using EIT for other medical imaging applications, with many different applications being considered including imaging of brain function, detection of cancer (in particular breast cancer), monitoring of the gastrointestinal tract among other less advanced areas of research such as monitoring temperature in hyperthermia patients (impedance and temperature have a linear relationship in

simple aqueous solutions). [POLLARD 2011, FORSYTHE 2011, SOULSBY 2006, HOLDER 2005]

EIT originally aimed to provide a visual output of various slices through an object (hence the term tomography[1]), allowing us to see any changes in electrical impedance at each level. More recently however EIT has taken on a 3D element; largely due to the advances in image reconstruction techniques using 3D meshes. The outputs from more advanced systems are generally viewed as a 3D model rather than in slices. This is an important step forward as the model created represents the tissue in a more realistic form, which can be used by doctors for easier diagnosis. [GRIEVE 2010, ADLER 2006]

This thesis is primarily concerned with the detection of cancer using EIT. Breast cancer imaging is the most popular application of this theory within the EIT community, largely because of the lack of bone and organs within the breasts; the images produced are therefore not distorted by the interference caused from large changes in density and impedance throughout the tissue. Also due to the protruding

[1] Tomography is a term derived from two Greek words; Tomo, meaning section or slice and Graph meaning to record or plot.

nature of breasts the application of electrodes around the tissue being investigated is decidedly easier than for other detection areas. [BARBER 2005, HARTOV 2005]

Early studies had measured the capacitance change in tumours compared to normal breast tissue which suggested that impedance measurements would be useful in the detection of breast cancer, however the first real EIT based study was conducted by Jossinet in 1985; this study again showed that a measurable difference was clearly apparent which led to further studies in the field by several groups. [JOSSINET 1985, MCADAMS 1995]

## 2.3 The Leicester Group

Dr Wei Wang worked at Sheffield University with Brian Brown and David Barber and produced several papers on EIT during his time there. He formed the Leicester group within De Montfort University's (DMU) engineering department in 1995. Dr Wang's idea was to use the EIT ideas he had worked on at Sheffield to build a detection technique for breast cancer, this theory was named EIM, as it was an EIT system for measuring the Mammary Glands. Working alongside Professor Malcolm McCormick the group made impressive early progress and was regarded as one of the most advanced groups in the world in this field. In 2005 the collaboration between members of the DMU EIM group and The University of Leicester's control systems group formed The Leicester EIM Group.

In October 2008 Dr Wang relocated to the University of Sussex, the majority of the research group moved with him, and there are no longer any members working in this field at De Montfort University. Since much of the work contained in this thesis was completed before this move the term 'The Leicester group' will be used to describe the research group.

Over the last 15 years the group worked on several different EIM systems which show the group's progress over the years and give an indication of the direction of the research generally. The different systems are detailed below giving a history of the work within the group.

### 2.3.1 Mk1

The original Leicester EIM system was only able to test in-vitro data in a specially designed in-vitro test chamber (ivTC).

In this system two pairs of differential electrodes were used in each test. The system used an RC oscillator (an oscillator which uses resistive and capacitive elements within its feedback loop to provide a phase shift of 0 degrees) to provide the input current signal while the software provided manual control of the frequencies used, with up to 31 different frequencies available.

Several tests were completed which provided promising results, and allowed the group to build a more ambitious, in-vivo based version of the system.

### 2.3.2 Mk2

The Mark 2 system was based on the idea of testing for breast lesions using electrodes built into a specially designed bra. The electrodes were positioned in rings within the bra and the electronics involved followed much of the same theory as the mark 1 model; however the hardware and software were updated to use a Direct Digital Synthesis (DDS) oscillator as the input (this provided the sinusoidal wave digitally, allowing more control when altering the input), which was controlled using digital signal processing, and programmed using the C programming language. All post test analysis was done within Matlab and the data was stored in a Microsoft Access database.

*Figure 2.1: DMU Mk 2 EIM System, used with permission [WANG 2007a]*

During the building of this system a new idea came about, which was to integrate the whole system into one software environment (rather than using 3 different programs). It also became apparent that due to the varying sizes of women to be

tested many different sized bras would need to be made in order to make this test useful on a wider scale and this would make the process a lot more difficult and expensive. [WANG 1998]

Unfortunately, therefore, no tests were completed using the Mark 2 system.

### 2.3.3 Mk3(a & b)

The Mark 3 system was the first system from the Leicester group to use a bed for test; this idea was already being used by other research groups as it allows all sizes of patient to be tested. A patient lies on the bed and the breast being imaged is placed into a depressed well which is lined with electrodes. [JOSSINET 1988]

Funding from Tianjin Virtual Bioengineering (TVB2001) paid for the redesign. The software system was mostly the same as in the Mk2 system involving several different programs and languages, however they were all integrated together using Matlab and Visual Basic so no further human interaction was needed to conduct a test.

A system was built for use in trials in China, which was known as the Mk3b system, however unfortunately ethical approval was never achieved due to the high standard of safety engineering required for medical instruments.

### 2.3.4 Mk4

The Mark 4 system was produced with funding from Lachesis and involved a new fully integrated all Matlab system, which controlled the input and output from the multiplexer (MUX) and Digital Signal Processor (DSP). The current signal, which is driven into the electrodes from a MUX, is created by sending the voltage output from the DSP through two converters, to create an analogue current source. The received voltage signal is collected at the multiplexer before being converted into digital format which is then sent to the DSP and computer system so that the impedance output can be calculated.

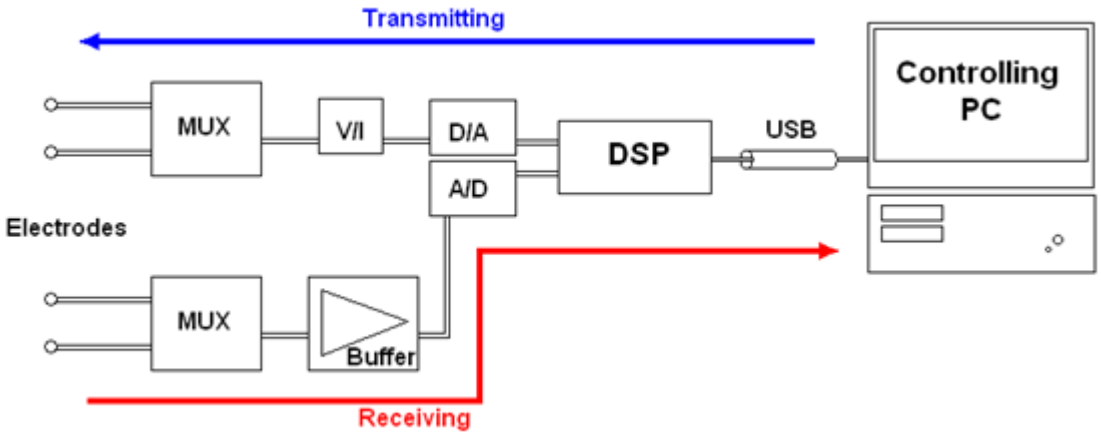


*Figure 2.2: Block diagram of hardware from the Mk4 Leicester EIM biomedical research system*

This system was also the first to use a saline bath, where the breast is immersed in a solution of known impedance to aid the conductivity between electrodes and tissue.

This theory was based on successful in-vitro tests which were conducted using a saline bath.

The working bed system was completed and a newly designed heating system was incorporated, heating the saline in the bath to make it more comfortable for the patient.

Although the system was completed in 2006 it did not receive ethical approval from the University due to issues with the safety of the saline bath being in such close proximity to the high mains voltages powering some of the electronics and therefore the project has not yet reached the second level of funding.

I worked extensively on this system and was the group leader for designing the front end user interface.

### 2.3.5 Mk4b

The Mark 4b system uses the same hardware as the Mark 4 system; however the software was changed completely. National Instrument's Labview was used throughout the whole system replacing Matlab, this was due to the group's close contact with NI and the potential of their interface for ease of programming. This decision was also made with the CEIMUS project in mind (see below), as it would mean both detection systems could use the same software and therefore be fully integrated.

This system was unfortunately abandoned when the majority of the group moved from De Montfort University in Leicester to the University of Sussex. The plan was to push this system for clinical trials using the 2nd instalment of the Lachesis funding; however with the move the funding was lost.

### 2.3.6 Ceimus Project (Current system)

The Leicester group are also involved in a project attempting to partner EIM with ultrasound, which has been name of the CEIMUS project (**C**ombined **EIM** and **U**ltra**S**ound).

The Ceimus project is the joint project between the Leicester group and the Diagnostic Sonar, who are experts at ultrasound imaging which combines the two techniques into one system for multi-modal imaging. The Mk4b software and hardware were used for the EIM part. The Ultrasound also uses an existing ultrasound system powered through LabVIEW. [DIAGNOSTICSONAR 2009]

This current system uses similar hardware for EIM as before. The ultrasound system in the Ceimus project was designed to be built around the existing Mk4b system.

### 2.3.7 2009 System Design

The most up to date system has several design features which are integral to the testing. These are discussed below.

The system is built into a portable hospital trolley, which allows height adjustment and has wheels allowing easy movement of the system. It has been fitted with specially designed cushioning for patient comfort.

The electrodes are positioned at the bottom of the saline well, this method (as previously mentioned) had been used for in-vitro tests and was considered successful enough to use within the main test unit. An earlier version used rings of electrodes up the sides of the well, enabling the imaging of slices of the breast.

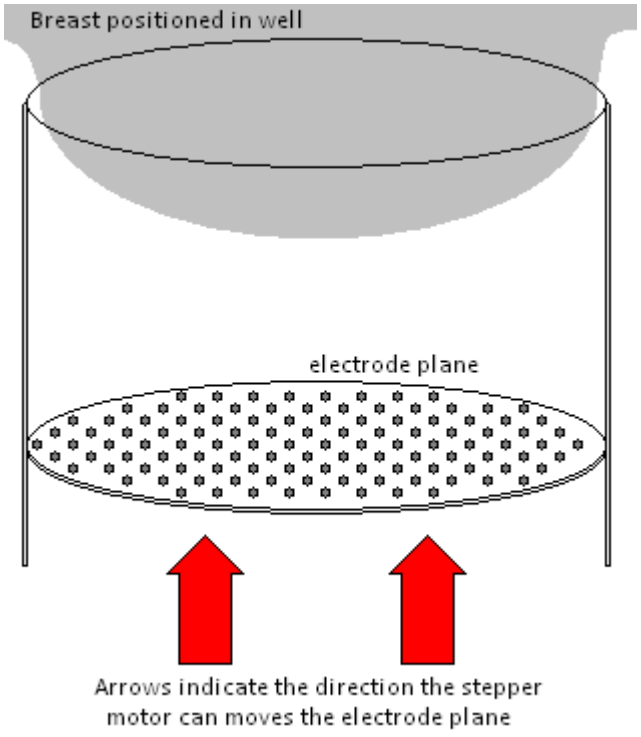


*Figure 2.3: Diagram showing the placement and movement of electrodes within the well.*

Due to the varying sizes of breasts the well was designed so that the bottom of it could be raised in order to move the electrodes closer to the tissue being imaged. This allows for better images, as the depth the current has to penetrate is less. This well is moved using a stepper motor, which allows steady movement and will be controlled by an operator to help reassure the patient. It is important to keep the well watertight, even when adjusting the stepper motor, as any leak may be dangerous for the patient.

The saline heating system was introduced to reduce patient discomfort. The saline solution is heated until close to body temperature before the patient is asked to lie on the trolley. A temperature-monitored tank of saline is heated under the trolley in a separate compartment from the drive and receive electronics. This saline is then pumped into the well surrounding the breast to be imaged and creating a conducting link between the electrodes and the tissue.

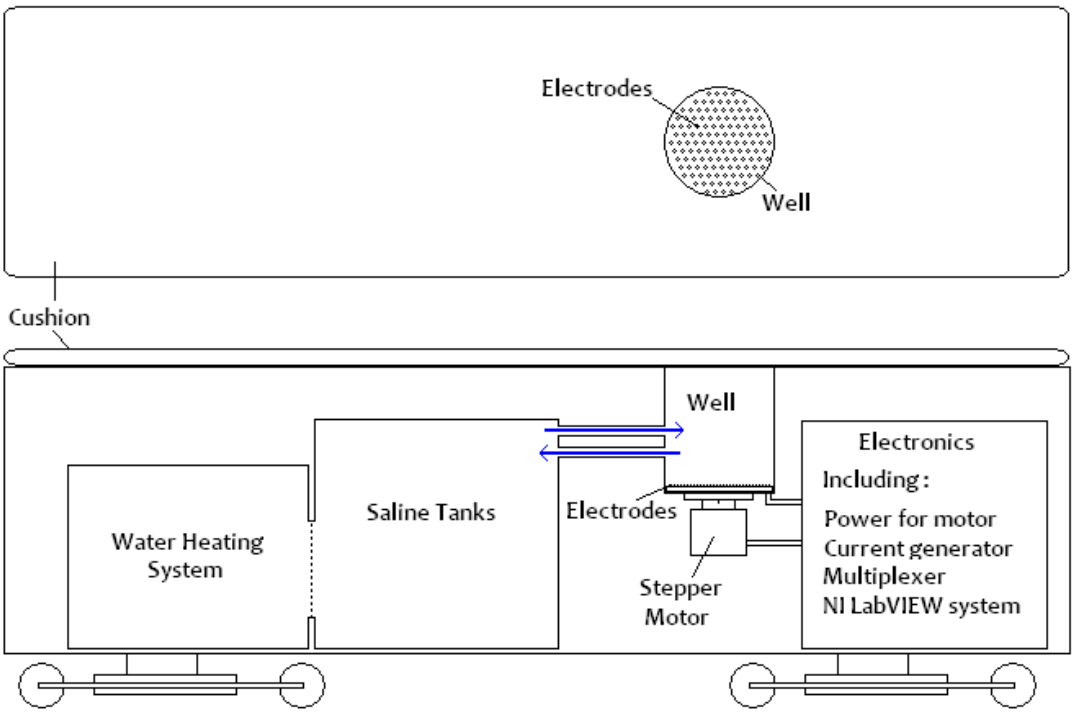


*Figure 2.4: Plan and side views of the trolley onto which the current EIM system is built*

The electrodes lining the bottom of the well are designed so that each of them can be programmed to either drive the current into the tissue, or be used to receive the output voltage (electrodes which can be switched between these two states are known as active electrodes). This allows more measurements to be taken by a lower number of electrodes, and therefore in a smaller area, which improves the resolution of the output images.

As can be seen in Figure 2.5 the electrodes at the bottom of the well are positioned in a repeated pattern, which can be split into many trapezoidal groups. These are the patterns which are used to make EIT measurements on the sample. The red

electrodes indicate the electrodes which inject the input current, while the blue electrodes show where the voltage measurements are recorded. Through the use of active electrodes this 4 electrode pattern can be repeated all over the grid providing a large amount of measurements.

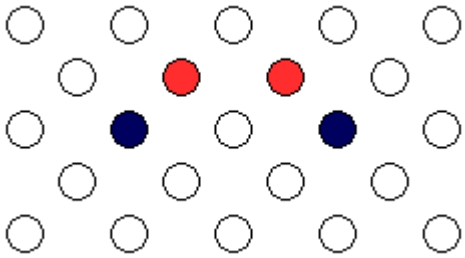

*Figure 2.5: Diagram showing the electrode grid, red electrodes are drive electrodes and blue are receive electrodes.*

## 2.4 Other Groups

There are several institutions around the world involved in advancing the field of EIT. Within this field breast imaging is being researched by a few different groups, some of the more recent results published by these groups are described in this chapter.

The Korean based Kyung Hee University group have recently presented their latest system known as KHU Mark2.5 EIT system [YOO 2011], it is the latest in a range of devices which began with the KHU Mark1 system which was used by several teams in the EIT field. The group provided a group from University College London with their Mark1 system who published some findings which compare the Korean system to

the UCH Mark2.5 EIT system. The London based system was designed specifically for EIT measurements of the head, initially to image severe acute stroke [MCEWAN 2006]. The outcome from the comparison showed that the UCH Mark2.5 system was superior for the tests which involved a saline tank phantom model to represent epileptical foci [FABRIZI 2009]. The Mark2 system was built following suggestions from groups who had used it as to how the system could be improved [OH 2011]. This system had a wider bandwidth (10 Hz to 1M Hz) and improved acquisition and signal processing components [WI 2009]. It has been used to investigate several EIT applications including breast cancer testing; their most recent publication presents a new image reconstruction method for breast EIT [LEE 2011]. The Mark 2.5 system incorporates a self-calibration element to the current source and voltmeters which maximise the performance of the overall system [YOO 2011].

The Dartmouth group have a patent application for a combined ultrasound and electrical impedance imaging system for detecting prostate cancer [HARTOV 2011]. This work has been completed while they also investigate breast cancer applications, their recent work has been complete in conjunction with the Middlesex university group, it describes an image reconstruction system which is designed specifically to work with an individual and relies on knowing the surface geometry of the patient [TIZZARD 2010], they have also recently provided the example of using an optical scanner to provide the breast geometry needed to complete their reconstruction images and show a successful example for a human volunteer [FORSYTH 2011].

A group from Yaroslavl State Medical academy in Russia have published a few papers. In 2008 they published findings of a clinical trial which showed EIT performed favourably when compared to other techniques [TROKHANOVA 2008]. Their most recent describes a theory for analysing the electrical conductivity of mammory glands in women who suffer with cancerous or precancerous growths and are taking oral hormonal contraceptives. The paper shows EIT being used alongside other techniques such as X-ray mammography and ultrasound on a selection of 355 women. The findings conclude that for this particular application EIT provides superior results to the other techniques as they do not show the affect of the hormone treatment as clearly [TROKHANOVA 2011].

A system known as MEM has been built by Impedance Medical Technologies in Russia. It is an update from their previous MEIK system which has been used in published trials such as those completed in Czech Republic in 2008 which compared the system to other techniques and concluded that EIT could be used as an adjunct to X-ray mammography or ultrasound, however acknowledged that improvements could be made to EIT with further research [PRASAD 2008]. The MEM device has been approved for medical trials however the system is based on a hand-held scanner, similar to the T-Scan, while most groups have moved onto to experimenting with bed-based systems which can improve repeatability of tests as discussed previously [IMT 2008].

There are other groups which use the systems described above, or have their own systems, some of these systems and relatively new and do not yet have any published results to compare to the older systems, for example this year a new system was presented by a German group at the EIT conference in Bath, UK [PIKKEMAAT 2011] and a Taiwanese group also published details of their new system at a conference in Singapore [HUANG 2011], the latter provided copper/Teflon based phantom results within the paper, the images could detect the phantom differences, however the system was limited to a frequency range of 100 Hz – 100K Hz, which is much smaller than some of the more popular EIT systems.

Unfortunately few of the publications regarding EIT, in particularly breast EIT, provide evidence of clinical trials. This is possibly due to the strict medical safety requirements which need to be met before trials are approved. Details of systems employed by some groups have been released, as mentioned above, and sometimes saline/agar phantom simulation results are provided. However much of the research within the EIT field is aimed at either suggesting further uses for EIT, for example Yamaguchi's recent paper which involves attempting to estimate visceral fat within a human abdomen [YAMAGUCHI 2011], or improving the reconstruction of images, shown by Attardo from the Dartmouth group who discusses the advancement of graphics processors in modern computers and how they affect the EIT image reconstruction process [ATTARDO 2011]. Image reconstruction is a vast subject on

which an entire thesis could easily be written; however it is not the main focus of this work.

## 2.5 EIT in Practice

### 2.5.1 Cell Impedance

A living cell is made up of a nucleus within intracellular fluid contained within a membrane, surrounding the cells within tissue is another fluid known as extracellular fluid. It was suggested by Fricke and Morse that the electrical impedance properties of different parts of the cell could be represented by resistors and capacitors in the formation shown below. Figure 2.6 shows how the various properties of the cell are represented and also shows how this circuit can be reduced to a simple 3 element model by considering series component values. [FRICKE 1925]

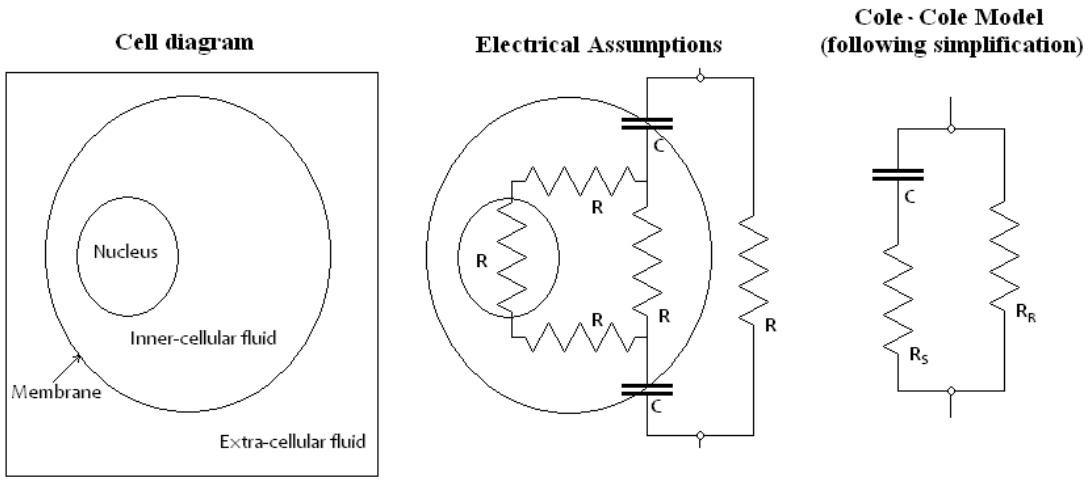


*Figure 2.6: How the 3-element Cole-Cole model can be achieved from assumptions based on the electrical properties of a cell*

The model derived in Figure 2.6 is a 3-element model of a living cell. Although the model was used initially in 1925, when Fricke and Morse used it to represent the electrical properties of cell suspension, this model has become known in EIT circles as the 'Cole-Cole' model, probably due to a misunderstanding of its origins and Cole's heavy use of it throughout his work, it is referred to in this thesis as such. [MCADAMS 1995, FRICKE 1925]

All tissues within a body are characterised with slightly different $R_R$, $R_S$ and C values in the model above. For example a nucleus of one type of cell may be denser, which will affect the impedance value, or the membrane may be weaker which could alter the capacitance across it. A change in impedance will affect the path of current through the tissue, if it is possible to detect and quantify this change the individuality of the impedance values will allow for the identification of cells. [COLE 1941, FOSTER 1989, HALTIWANGER 2003]

Various sources have reported substantial differences between normal and cancerous cells in terms of impedance measurements. Fricke provided the first set of results in 1926 which suggested the capacitance of the cell increased for cancerous tumours, when compared to benign tumours. Other studies since then have generally agreed with the idea that cancerous tissues have a lower impedance magnitude than normal tissues. Jossinet showed in 1998 that the various tissues

found within the breast can be identified using this technique. [FRICKE 1926, JOSSINET 1998]

### 2.5.2 EIT Realisation

EIT provides an image which represents the changes in the impedance of an object; this image is reconstructed from data collected following the application of a current via electrodes. Usually these electrodes are mounted directly onto the skin, however this approach can lead to errors due to large impedances found at the electrode-skin contact, which can cause lower resolution of the final image and a less accurate diagnosis. Several groups have begun investigating other methods of applying the current through non-contact electrodes to avoid this error.

The output is collected by two electrodes, the signal is then amplified and the voltage is recorded. In early systems the same electrodes were used for both drive and receive purposes, however it became apparent that impedances from these electrodes were included in the output results when this method was used. Instead a 4-electrode system is usually employed which allows the voltage readings to be taken directly from the sample, thus avoiding this extra impedance. An input current is applied through the drive electrodes $R_{Electrode1}$ and $R_{Electrode2}$. The known impedance from the receive electrodes, $R_{Electrode3}$ and $R_{Electrode4}$, is then compensated for within the amplifier used to record the voltage, due to the large input impedance of the voltage measuring device, the receive electrode impedances will be very low.

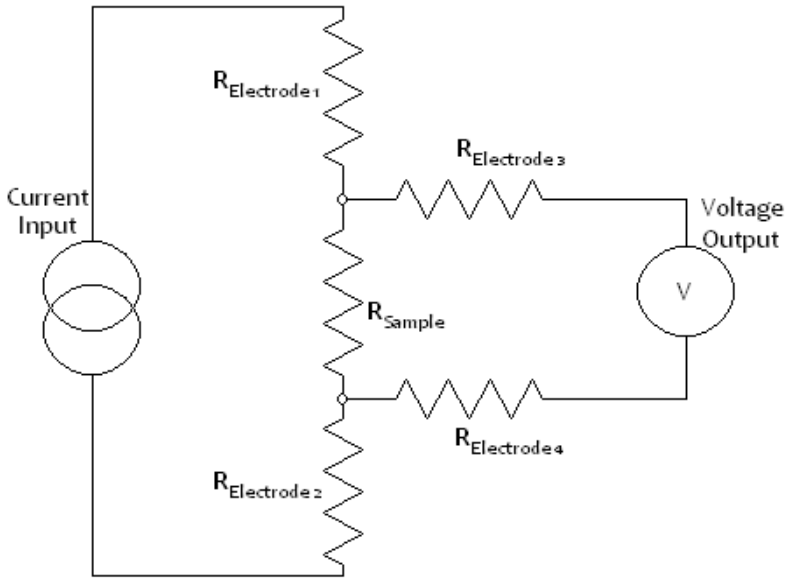


*Figure 2.7: A 4-electrode system showing how voltage is measured via a second pair of electrodes.*

Following the current input and the recorded voltage, output impedance measurements can be evaluated from the collected data by applying calculations based upon Ohm's law.

The input is in the form of a sinusoidal waveform, while the output is similar however it has different phase magnitude properties from the input. The data provided by a standard EIT system is a combination of in-phase and out-of-phase data; the in-phase data corresponds directly with the resistive elements within the sample, while the out-of-phase data has been affected by the reactive (in this case the capacitive) elements of the tissue.

The cables connecting the electrodes, although shielded, still produce stray capacitances and the effect of this can be significant. This alters the out-of-phase data considerably and therefore this data is often disregarded in favour of solely analysing the resistance based output. Some systems attempt to use this disregarded data by compensating for the stray capacitances, however this technique is not very widely employed due to the difficulties in reducing the errors.

There are many different frequency ranges employed within EIT, usually designed to suit the subject being tested. The Sheffield Mark 1 system employed only one frequency; all tests were recorded at 50 kHz. However most modern systems provide a bandwidth range and run tests which collect results at multiple frequencies. This type of data collection has become much more commonplace following the improvement in the speed of computers. [BARBER 2005]

### 2.5.3 Cole-Cole Model Response

EIT aims to provide component values for a cell model which can be used to identify the tissue within the sample tested. The cell model used depends on the opinion of the researchers; work presented here uses the Cole-Cole model as described earlier.

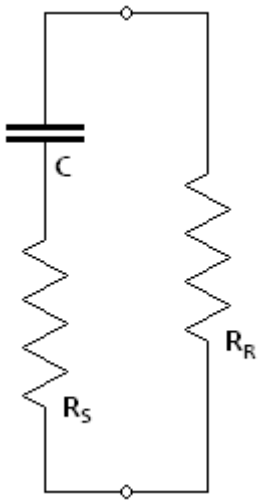


*Figure 2.8: The Cole-Cole cell Model*

A frequency response is provided by testing the sample over a frequency range. Some EIT tests require very high frequency measurements. The results from these tests are commonly shown in graphs separating the real and imaginary components of the complex domain. Convention states that the in-phase (resistive) data is considered as the real part, while the out-of-phase, capacitive response is described as imaginary.

At very low frequencies the capacitor acts as an open circuit so the initial value for the impedance relies on the value of $R_R$, at high frequencies the capacitor acts as a short circuit, therefore the final output value will be equal to $R_R$ in parallel with $R_S$.

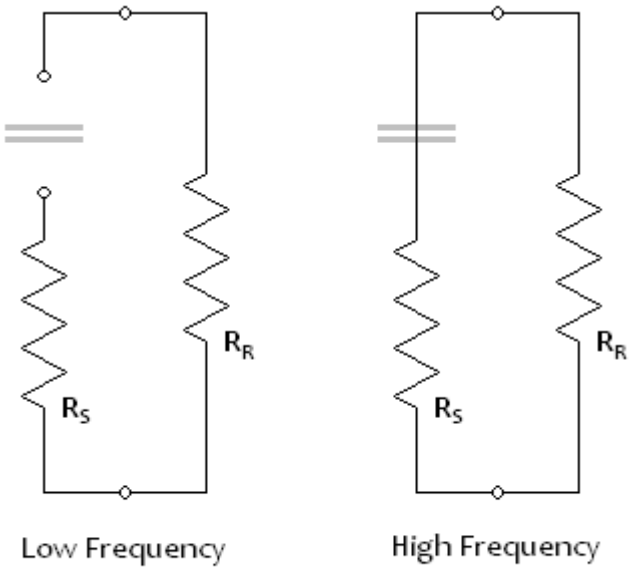


*Figure 2.9: How the Cole-Cole cell model responds to extreme frequency inputs*

The following values for $R_R$, $R_S$ and C were used to provide a frequency output curve.

*Table 2.1: Table showing example $R_R$, $R_S$ and C values*

| | Phantom 1 |
|---|---|
| $R_R$ | 50Ω |
| $R_S$ | 10Ω |
| C | 3.3nF |

The resulting curve of this model is shown below, it can be seen that the initial value is 50 Ohms, which is equal to $R_R$, where the capacitance acts as an open circuit. The final value is 8.33 Ohms which can be calculated from $R_R$ in parallel with $R_S$. The curve

describes the output of the circuit as the capacitor impedance changes as the frequencies increase.

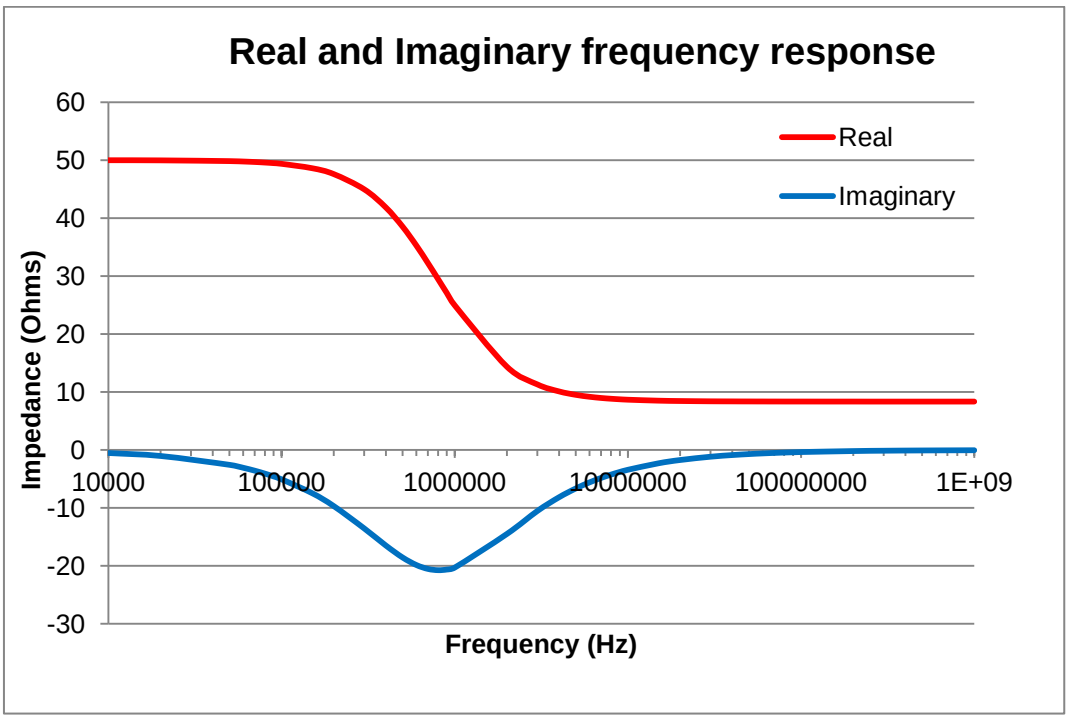


*Figure 2.10: Real and Imaginary frequency responses plotted against a logarithmic frequency scale*

The values shown in the graph above were calculated in Matlab using a program designed within the Leicester Research group from the $R_R$, $R_S$ and C values provided above. The imaginary curve provides the dispersion frequency at its lowest point, approximately 800 kHz in this example, which also indicates the point of steepest gradient on the real data curve.

### 2.5.4 Reconstruction of Images

This thesis is primarily concerned with enhancements to the measurement technology, but it is helpful to understand the available visualisation techniques generally used. Broadly there are two:

- **Back projection**, which offers a simple and intuitive understanding, and is based on assumptions about potential (voltage) behaviour within largely homogeneous material, however it can only provide 2D images

- **Mathematical Mesh and Sensitivity matrixes**, which, although more complex, has scope for sophisticated computational analysis with more input data, and, with sufficient computing power, offers higher resolution 3D visualisation

#### *2.5.4.1 Back Projection*

Back projection is a technique for locating impedance disturbances within a sample, based on assumptions about voltage behaviour within a largely homogeneous material.

Figure 2.11 shows a 16-electrode ring which can be used to scan a circular object, in reality many EIT electrode rings are not exactly circular however early reconstruction algorithms presented all output images as a circular slice. Non-circular images can be

acquired using modern systems, however due to shape of the breast tissue circular rings and their respective outputs are still often used.

A differential current input is applied via two of the electrodes (in the case below electrodes 1 and 2 are used). A voltage output can be read at each of the other pairs of adjacent electrodes.

The current does not flow directly between the input and output electrodes, however a volume of maximum sensitivity can be assumed to lie between these points and an impedance measurement representing this area can be calculated.

The curved lines in the diagram describe approximate equipotential paths driven by the current; they are plotted at a 90 degree angle to the electric field emanating from the input within homogeneous material. These lines are used to identify the volume of maximum sensitivity; the shaded area is this volume in respect to pairs (1, 2) and (7, 8).

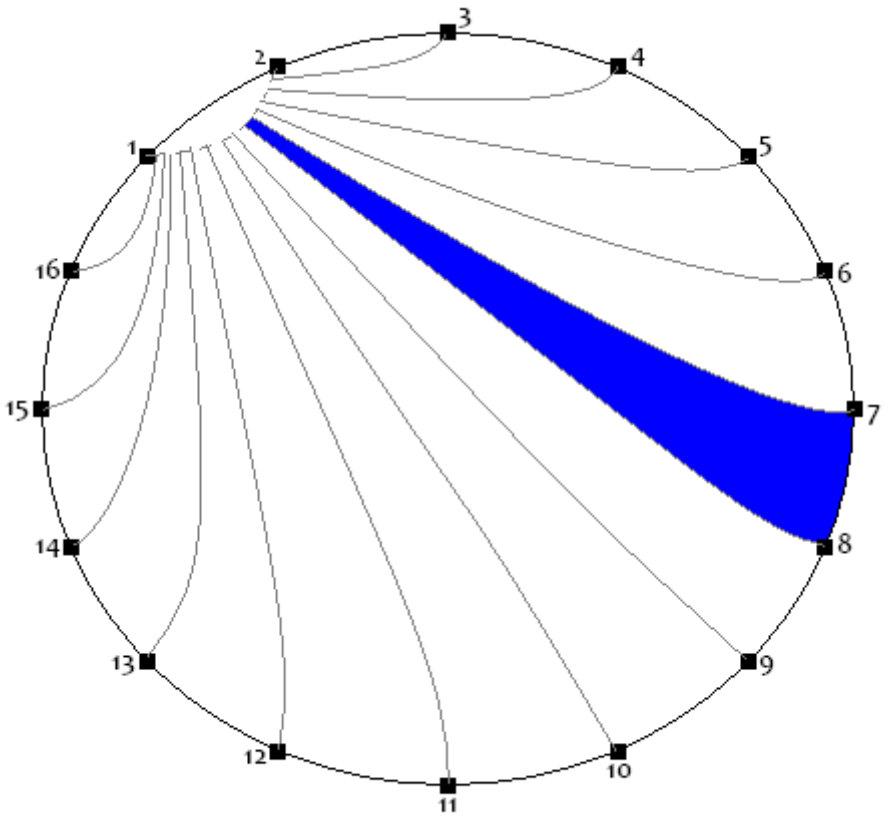


*Figure 2.11: A 16 electrode ring showing calculated equipotential lines when current is injected into homogeneous material via electrodes 1 and 2. This image was redrawn with reference to an image in [HOLDER 2005].*

The voltage is measured at each pair of electrodes around the ring, 2 and 3; 3 and 4; 4 and 5 etc. Impedance differences between tissues can be identified as a change from the measurement expected from an undistorted equipotential path.

Medically, any impedance change can be identified as cancerous or benign tissue.

Most modern EIT systems use electrode switching, so that any one electrode can be set to either drive the current into the sample, or receive the voltage measurement output; these are known as active electrodes. Active electrodes allow the drive electrode positions to be changed by high speed electronics and measurements taken with respect to multiple inputs. This sequence can be repeated around the whole ring until all pairs have provided the input. Following computer analysis the various impedance disturbances can then be mapped out within this cross section.

Figure 2.12 shows an example of how this method can be used to determine the position of a detected impedance change. Distortions of equipotential paths are detected at pairs of receive electrodes, for three different pairs of drive and receive electrodes. When paths are deflected by cancerous tissue, projecting the 3 images on top of each other will provide a location. The more electrodes included in the process, the more accurate the position that can be calculated. [HOLDER 2005]

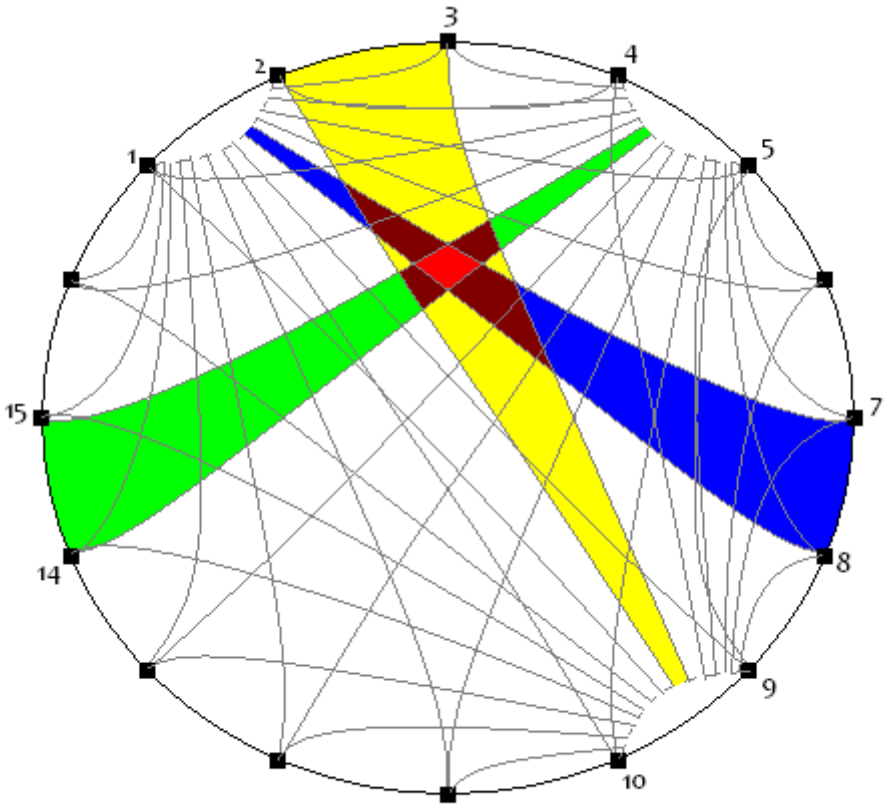


*Figure 2.12: Back projection method - how three impedance paths can be used provide the position of a tumour. This image was redrawn with reference to an image in [HOLDER 2005].*

### *2.5.4.2 Mathematical Mesh and Sensitivity Matrices*

The method of back projection assumes that the current flows directly between the drive electrodes and, at any one time the receive electrodes are the only place the voltage is measured. It does not fully consider the behaviour of potential through all parts of the sample and is therefore influenced by all of the variable impedances

within the object (although some more than others), not just those on the direct path.

In order to address this shortcoming a different technique has become widely used in the EIT communities known as a sensitivity matrix.

In this technique the sample being imaged is split into a mesh of small areas, called voxels as shown in Figure 2.13. Voxels can be any shape, in this example triangles are used to describe a similar circular area to that shown in the back-projection method.

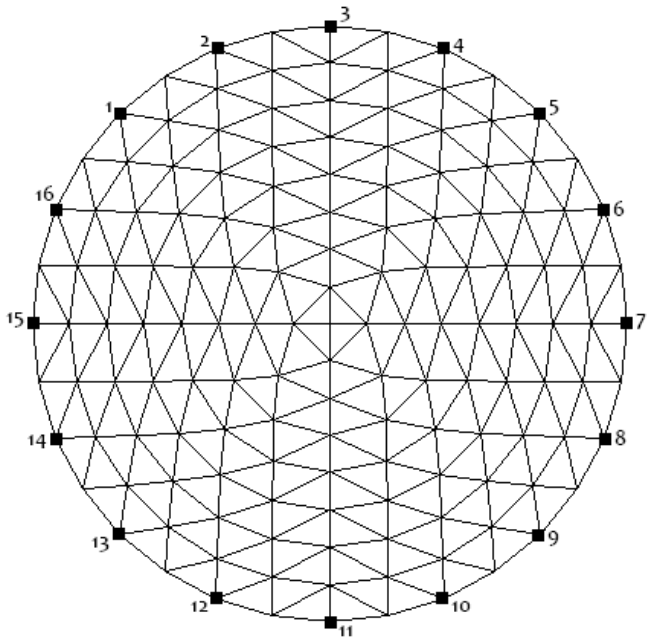


*Figure 2.13: Mesh example showing circular area split into 256 triangular voxels, electrodes are shown surrounding the sample and are numbered. This image was altered from a mesh built within EIDORS open source software [ADLER 2006]*

When current is applied via the electrodes it will flow throughout the sample, the voltages realised at each sample contribute to the output at the point of recording.

This output voltage is a combination of the voltages from each voxel, some contribute a larger ratio than others depending on 3 parameters attributed to the individual voxel, these parameters are: the resistivity of the voxel itself; the amount of current flowing through the voxel; and the distance the voxel is from the receive electrode.

Some of the contributions will be negligible; however calculations should include all data in order to produce an accurate output.

The factor of contribution for each voxel is called a Sensitivity Factor (S) and a mathematical matrix known as a Sensitivity Matrix can be compiled by collecting a factor for each voxel every time an output measurement is taken into a grid.

Table 2.2: Example of a Sensitivity Matrix

| ρ(a) | ρ(b) | ρ(c) | ρ(d) | | …ρ(#) | |
|---|---|---|---|---|---|---|
| $S_{a1}$ | $S_{b1}$ | $S_{c1}$ | $S_{d1}$ | | $S_{\#1}$ | Voltage output 1 |
| $S_{a2}$ | $S_{b2}$ | $S_{c2}$ | $S_{d2}$ | | $S_{\#2}$ | Voltage output 2 |
| $S_{a3}$ | $S_{b3}$ | $S_{c3}$ | $S_{d3}$ | | $S_{\#3}$ | Voltage output 3 |
| $S_{a4}$ | $S_{b4}$ | $S_{c4}$ | $S_{d4}$ | | $S_{\#4}$ | Voltage output 4 |
| | | | | | | |
| $S_{an}$ | $S_{bn}$ | $S_{cn}$ | $S_{dn}$ | | $S_{\#n}$ | Voltage output n |

Table 2.2 shows how using the sensitivity matrix the resistivity (ρ) of each voxel (a - #) can be related to the output voltages. The sensitivity matrix can be extended to include larger numbers of voltage measurements (it is not uncommon for several hundred measurements to be taken) or more voxels (which can number tens of thousands) which is often necessary.

Resistivity values for each voxel are estimated and varied individually within a computer simulation, the resulting changes of every voltage output is recorded which allows the calculation of the sensitivity factors within the matrix.

Once a sensitivity matrix has been compiled the recorded output voltages can be combined with it to provide actual values for the resistivity of each voxel within the

mesh. These resistivity values can be converted into an image to show an output in a more visual fashion, this allows faster recognition of a variation in resistivity.

*Figure 2.14: An example of an output from a mesh based EIT system. The colours represent differing impedances; the white voxels represent an alien object within a uniform sample. This image was altered from an image created within the EIDORS software [ADLER 2006]*

In Figure 2.14 the overall shade of the sample is similar, which represents normal tissue, however the lighter part suggests a different resistivity value can be found there, suggesting a tumour. The actual values calculated for these voxels can be investigated further in order to identify the anomaly.

As computer speeds continue to increase, the number of voxels within a mesh has increased. Furthermore 3D meshes have been built using a similar method, incorporating 3D voxel shapes such as tetrahedron, which allows the output image to be viewed as a 3D model, rather than a collection of slices. [HOLDER 2005]

## 2.6 Comparing the Techniques

In Chapter 1 a list of techniques used to detect breast cancer were discussed, most of these techniques are in a much more advanced stage of research than EIT, and several are currently used within hospitals and trusted by medical staff to provide results on real patients. Here, the various advantages and disadvantages of EIT are discussed and that provide arguments that show that research in this area is worth pursuing.

Following these discussions a list of advances which are required in order to allow EIT to achieve a status which could lead to regular use in hospitals is given.

### 2.6.1 Advantages

EIT has many advantages over rival techniques; some of these are inherent within any system, some others are based on theory and yet to be fully realised.

**Inexpensive,** EIT is a very cheap solution as all the software can be installed onto a standard PC while the hardware is generally built into already existing equipment – for example a hospital bed trolley. The electrodes are cheap to manufacture and the only seemingly expensive piece of equipment is the specially designed motorised and water-tight saline bath which holds the electrodes in place, however in comparison to an MRI scanner, or an x-ray machine the costs are minimal.

**Portability,** since the system can be built onto a trolley it can be taken almost anywhere, patients can be tested within a hospital, and no specific EIT room would be necessary. It may play a role in portable screening where the system is taken into a community to make access to a test easier for the patients.

**Speed,** scanning using EIT is a relatively fast process, each electrode configuration takes less than a millisecond to run, although in more complicated systems the amount of tests to be run may exceed several hundred configurations, this many tests are needed to provide enough data to identify resistivity values for each voxel, of which there may be well over a thousand. Image reconstruction for EIT has improved over recent years. 2D images have been reconstructed at a rate of 4 per second and have even been reconstructed on a mobile phone handset within 25 seconds. However the speed of reconstruction depends greatly on the complexity of the image required. 3D image reconstruction is also being improved with some studies showing images reconstructed within 10 minutes. [HOLDER 2010, EIDORS 2011, BORSIC 2010]

As the software designed for reconstruction improves the figures shown above will be reduced further. In comparison X-Ray mammography usually takes between 15 and 30 minutes. [IMAGINIS 2006]

**Easy to operate,** as mentioned previously, the main programs from which EIT systems are controlled are generally run from standard PCs, this means the

interfaces are usually built and controlled in a fashion most people are familiar with. In fact most of the operation involved in an EIT test would be saving the patient details onto a secure database, the test itself is able to run almost entirely automatically without much human involvement.

**Differences are obvious,** EIT is designed to recognise change at a cellular level and therefore the differences brought about by a tumour being present are, in theory, easily identifiable. If EIT does reach this potential no further testing would be necessary as any tumour found could be identified as cancerous or benign from the same scan, this would save the patient the needing to undergo the discomfort of biopsy.

**Non-invasive (incl. x-rays),** unlike many of the other techniques for cancer detection EIT is non-invasive, no elements of the test unit penetrate the test subject; no electrodes break the skin and the patient is not subjected to any ionising radiation. Also it has the further advantage that no heavy breast compression is necessary. Following the test the patient will be able to leave the hospital with no side-effects.

**Early detection possible,** as mentioned above, any change in the tissue should be enough to alter the results at the output, however clearly the smaller the change the harder it would be to detect. As EIT technology improves, in particular the reconstruction and analysis systems, it will be possible to detect cancer at earlier

stages. Other techniques require a certain level of growth before any tumours can be identified.

**Young people can be tested,** due to this cellular identification the density of the cells within the tested tissue will not affect the results, therefore younger people who have denser tissue (particularly in their breasts) can be tested using EIT and the results would be as reliable as that in mature adults. In other techniques the denser tissue can make it harder to identify tumours, while they show up more clearly in less dense tissue. Due to the nature of X-Ray Mammography extensive testing on young people has not been encouraged as the exposure to X-Rays at a young age are considered a health risk, EIT could provide this opportunity without endangering the patient.

**Digital storage,** since the whole process is computerised all the data involved in the test can be stored digitally and can be called upon for comparison if the patient re-visits the hospital for further tests. Since all the images are reconstructed from the raw data the data itself can be stored and as improvements are made on imaging algorithms new images can be provided from the older data for better diagnosis and comparison.

**Further application,** there are further advantages to be gained from EIT, as more testing is done other types of tissue will become recognisable and EIT may find further uses within medical diagnosis. [HOLDER 2005]

### 2.6.2 Shortcomings

EIT has several shortcomings that will need to be overcome before it can realise its potential of being installed in hospitals for completing diagnostic tests. In this section issues are identified which need further research so that they can be addressed and solutions found. This progress may allow EIT to realise its potential as a diagnostic tool.

**Resolution,** the main issue with EIT is the spatial resolution of the output which makes it very difficult to pinpoint any abnormal growths, in addition the resolution is not uniform and therefore it can be worse at certain points within the image. Major contributors to this resolution issue are the limited number of voltage measurements, noise interference and high impedance found at the electrode-skin interface.

**Skin impedance,** since the technique is non-invasive the current is applied via an electrode-skin contact, this contact has variable impedance which can grossly affect the test results. The impedance can decrease the output resolution as the final impedance measured at the output will include this contact impedance. Also, some of the contacts may have lower impedance than others, which could bias the measurements towards certain electrodes. Skin abrasion before applying the electrodes is required by some EIT systems as it makes for more uniform impedance over the various contact points, however this can be uncomfortable for the patient.

**Electrical noise interference and safety,** there is a trade-off between safety and the strength of the signal that can be applied. For safety EIT uses very small signals (See Chapter 3 for more details). These small signals mean that any inherent or external noise can have a large effect. Some systems need to be placed in a suitably shielded room to avoid any interference from electrical fields provided by other equipment which may be in close proximity.

Since EIT is a relatively new technique it is overshadowed by older, more familiar techniques, as a consequence, it has the handicap of being compared to these throughout its development and therefore its shortcomings have been highlighted further.

These other techniques are trusted within the medical industry and medical staff are already trained to use them. This means that any EIT system hoping to be used regularly needs to prove that it is better than the current techniques, as anything less than that would involve a lot of change for little gain, and may be difficult to engineer throughout the health services which may prove to be an expensive process.

This has made it difficult for EIT prototypes to be accepted onto medical trials. Although many groups around the world are working on EIT there are currently no fully functioning up-to-date prototypes being widely tested. Two previous systems have been accepted and used for large scale clinical trials; the Sheffield Mark 1

system; and a hand held system called T-Scan which was produced by Siemens Medical. Clinical trials in various medical facilities did not prove popular and currently it is very rare to find a system available for testing. [BARBER 2005, HARTOV 2005]

### 2.6.3 Improvement Opportunities

EIT is still a young detection technique and in that respect there are several parts of modern EIT systems which still need improving before the system can be fully considered a rival to any of the current techniques for breast cancer detection. Some of these areas a discussed below.

Electrode-skin contact, the electrode-skin contact can cause problems within an EIT system, as described above. This impedance issue can be improved by treating the skin directly before applying the electrodes, but this is only a partial (and uncomfortable) solution.

There are several attempts being made which may improve this issue within the EIT community, the majority of groups are now altering their approach to try and apply the current through another method than contact electrodes. The Saline bath is the technique being investigated by the Leicester Group, while other researchers are investigating different non-contact electrodes, including magnetic induction of current.

**Current input,** the current driven into the tissue via the electrodes needs to be a steady current with a large bandwidth and high output impedance. The bandwidth needs to be large in order to provide outputs up to the high frequencies needed to acquire good EIT measurements (the DMU group specification stated up to 10 MHz). The output impedance needs to be high to ensure that the output current value isn't affected by the impedance of the tissue being measured.

Several different approaches have been attempted to reach a good current output, most systems use a form of voltage to current converter in order to achieve this output, there are many different circuits which can achieve this and each group has a slightly different requirement for their own system. Chapter 3 offers a design and approach suited to the needs of the Leicester group.

**Control system,** An EIT system needs to process a large amount of information, from raw measured data to compiling sensitivity matrices. All this data needs to be stored in a secure database and the various functions need to be controlled from a program which has user-friendly interface as the majority of operators are likely to be hospital staff who are not necessarily trained in computing techniques.

**High frequency measurements,** Modern EIT systems collect measurements over a very large bandwidth, as mentioned earlier. This allows the values of R,

S and C from the Cole-Cole model to be calculated accurately. Unfortunately the high frequency measurements are difficult to achieve as most input sources and measurement devices begin to lose their accuracy when frequencies increase to 1MHz and above. Also, the input sources may be unintentionally loaded with capacitances, even a small 20pF capacitor load can have a large detrimental effect on the drive current bandwidth.

Improved systems with larger bandwidths need to be designed, which can cope with the high standards needed within EIT.

**Reconstruction of images,** Reconstruction algorithms are being regularly improved and updated, as can be seen by the speed of improvements for 3D EIT. These need to keep updating as the raw data can only be refined to a certain level, the analysis of this data and reconstruction of images convert these measurements into a diagnostic tool. [HOLDER 2005]

One reason this part of EIT has improved quickly is the release of EIDORS software which is open source software compiled by leading experts in the field of reconstruction and is regularly updated with the most modern techniques from various groups all round the world. This allows everyone the chance to see how the techniques are improved and add their own ideas into the software for others to use and improve further. [ALDER 2006]

## 2.7 Standardisation

Another major issue within the EIT research community is the level and extent of research group inter-communication.

At the ICEBI 2007 conference in Graz, Dr P De Vries was asked to talk about the advances needed for EIT to be considered for use at medical facilities; he offered an outside view of the leading EIT research groups and gave a lecture describing the flaws in the research approach of the various EIT groups in regards to communication. He summarised by describing this apparent lack of communication as the major factor in why EIT is not already more widely used for clinical trials [DEVRIES 2007].

Clearly it is healthy to have competition within research as this will encourage continued progress and improvements within the field, however there are many arguments which suggest an open approach to research would benefit the progress made across the field. If all researchers were aware of the current research being undertaken by each group it would be easier for the research to advance. This approach could also encourage new researchers to become involved in the community.

It is important for inventors to protect their work by filing patents as too often the people responsible for a piece of work do not receive the credit they deserve.

Nevertheless, at a research level these legal issues can create barriers which may discourage other scientists from becoming involved in a worthwhile research area.

Although Dr De Vries' lecture concentrated on the negative aspects of EIT research some areas of EIT were described as commendable, such as the EIDORS software project for reconstruction. This software development encourages various experts in the field to add their expertise into an open source application which can be used to reconstruct images from the raw data. Some groups still prefer to design their own reconstruction algorithms, however most have committed to the project [ADLER 2006, DEVRIES 2007].

Since 2007 EIDORS has continued it's work and has released updated versions of it's image reconstruction software [EIDORS 2011]. Furthermore as a direct result of the Graz conference a project was begun which became known as Graz consensus Reconstruction algorithm for EIT (GREIT), this involved many of the leading researchers within the EIT field and aims to provide improved EIT image reconstruction [ADLER 2009]. Following this initial paper several others have been published which further the joint research project [GRYCHTOL 2011, YANG 2010]. If other research within the EIT field could take a similar approach to sharing their progress EIT would stand a much better chance of becoming a popular technique in hospital environments.

## 2.8 Combining Multiple Diagnostic Techniques

A novel idea being tested by the Leicester group (as documented earlier), among others, is the idea of combining EIT with another detection technique. In theory the results from both techniques can be used to achieve the advantages of both techniques. This has been used within the industry by complementing the X-ray mammography technique by using ultrasound to provide further information regarding lesions found during a screening.

The Leicester group is attempting to put both EIT and ultrasound into the same diagnostic setup so one test will actually provide the results from both techniques, it is hoped that these techniques together may provide an output which is more useful than either technique used individually. Using the improved resolution of ultrasound alongside the identification abilities of EIT could produce a new impressive imaging technique.

## 2.9 Conclusion

EIT has the potential to be a very useful diagnostic technique over a wide range of medical fields. The research into cancer detection using EIT has provided very promising results with several groups investigating the use of the technique for different cancers.

For breast cancer detection there are already several techniques, discussed in chapter 2, which are used as diagnostic tools, although these techniques have drawbacks they are currently more advanced than any EIT system available. Leicester has one of the leading research groups in breast cancer detection using EIT. Since 1995 they have designed and built several EIT systems which have introduced new ideas to the screening process. The group is currently building a new system which should be ready for clinical trials late in 2010, if this goes ahead the group will confirm their status as a forerunner in field.

The ultimate aim for EIT in this case would be to become the primary technique for breast cancer detection. This is a long term plan and although it cannot currently compete with X-Ray Mammography it is clear that EIT has some advantages which X-Ray Screening cannot provide, most notably identification of malignant tissue. EIT has several drawbacks, such as low spatial resolution, which are preventing it from being able to challenge the existing techniques. However as more research is completed further improvements are being made to the latest systems and the effects of these issues are being reduced. As research on EIT continues to improve, it will become able to provide a superior diagnosis to traditional screening systems.

There are still a lot of issues which need addressing before this can come to fruition, many of which are being researched by various groups throughout the world. Each problem needs to be assessed and a solution developed before EIT can be seriously

considered as a replacement to X-Ray Mammography. There may be some issues which simply cannot be solved due to the nature of the technique, already some research groups are trying to find other ways around these problems, such as employing a secondary technique within their system to compensate for these drawbacks.

Chapter 3 provides a solution to one of the major issues within EIT systems, two voltage to current convertors are compared and their benefits are tested and discussed, the chapter provides a preferred option which is specific to the needs of the Leicester group.

# Chapter 3 Circuit Design

An important element in any EIT system is the current source, this source needs to provide an accurate current to be sent to the drive electrodes.

The current needs to be stable over the selected frequency range while maintaining high output impedance. Following iterations of their system an empirical method provided the DMU group with a specification of 5 MHz at -3 dB bandwidth.

Due to the living tissue safety act there is a limit on the current allowed to be passed through the human body, to reduce the risk of burning and causing necrosis. A.C. currents must stay below 5mA (d.c. must stay below 100uA); this must be considered a priority when designing the output circuitry. [BSI 1989]

This chapter compares two circuits considered for use as a current source within the Leicester group's system. One is an optimised version of the common 'Improved Howland' model while the 2$^{nd}$ incorporates a Generalised Impedance Convertor (GIC) in an attempt to improve the output signal. The circuit designs are explained and a comparison of the outputs is made with respect to bandwidth limitations and output impedance values through PSpice computer simulation using the Orcad software package.

Further testing describes the effect of changing the op-amps within the circuitry and finally the outputs are documented with varied capacitance loads to simulate the effect of impedances within the body.

The author was responsible for all the work presented in this chapter, including all PSpice modelling and mathematical working. A paper was written by the Author which contained the majority of the findings reproduced here, it presented at the 13th International Conference on Electrical Bioimpedance combined with the 8th Conference on Electrical Impedance Tomography in Graz, Austria in 2007. [WANG W 2007b]

## 3.1 Howland Model Circuit

The majority of current sources used in EIT systems are actually voltage-to-current (V-to-I) converters.

The Leicester system was based on this approach; a V-to-I converter was needed in order to supply the electrodes with an input current. There were several important characteristics which needed to be considered while designing and comparing the various options.

The most important factor was that the current should be produced over a large bandwidth to allow the investigation to include high frequencies as well as the more

common lower values. The specification for this particular investigation, as mentioned above, was 5 MHz -3 dB bandwidth.

High output impedance was also required since this would provide better stability for the current source (an ideal current source has infinite output impedance as this ensures the load resistance has no effect on the output current).

Furthermore, the idea of using active electrodes had been discussed and it was decided that the most efficient way of producing electrodes which could act as either current drive or voltage receive points would be to build the current source directly onto the back of the electrode ring. This was done in order to reduce the length of cable in the system; the cable could have a capacitive effect. Therefore the components involved needed to be small.

Previously the group had used circuits based on the Howland Model, which uses an op-amp feedback loop to provide a consistent output current. This approach was well trusted by all involved and it was decided to provide a new circuit based on this theory.

An American group who were also studying current circuits within EIT had produced a paper suggesting a Modified Howland Circuit connected to a Generalised Impedance Converter, in an inductance providing configuration, could provide

extremely high output impedance. The performance of this circuit was also investigated in this work. [ROSS 2003]

### 3.1.1 Howland Circuit Theory

The simplest form of V-to-I is a voltage source driving a load resistance; unfortunately the current produced by this circuit is dependent on the value of the Load resistance

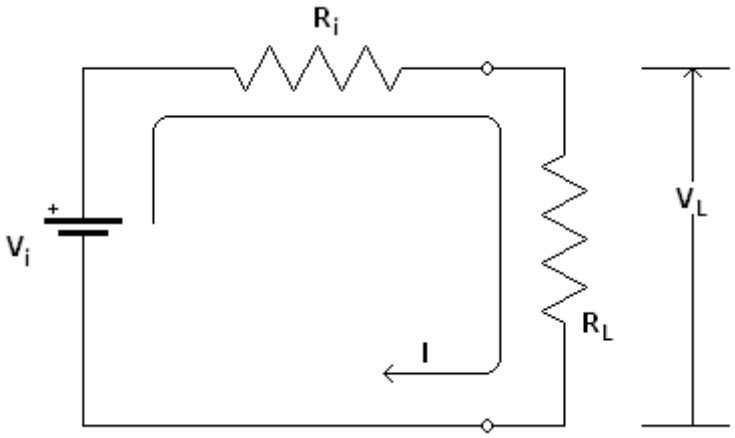


*Figure 3.1: Simple V-to-I current source*

The Output Current $\mathrm{I}$ through $\mathrm{R_L}$ can be calculated by:

$$I = \frac{V_i - V_L}{R_i} = \frac{V_i}{R_i + R_L} \qquad (3.1)$$

As can be seen $I$ is dependent on $R_L$, therefore this cannot be relied upon to provide the same current when the electrode is attached to a different material, or even a different part of the body.

The Howland model is a well known V-to-I converter which uses a non-inverting op-amp implementation to produce a helper voltage which mirrors the original Voltage input. The output can be controlled accurately provided the feedback resistors are balanced.

Figure 3.2 shows a variation on the Howland Model with a second current source ($V_{i2}$), with 2 voltage sources the circuit can be regarded as a differential V-to-I converter.

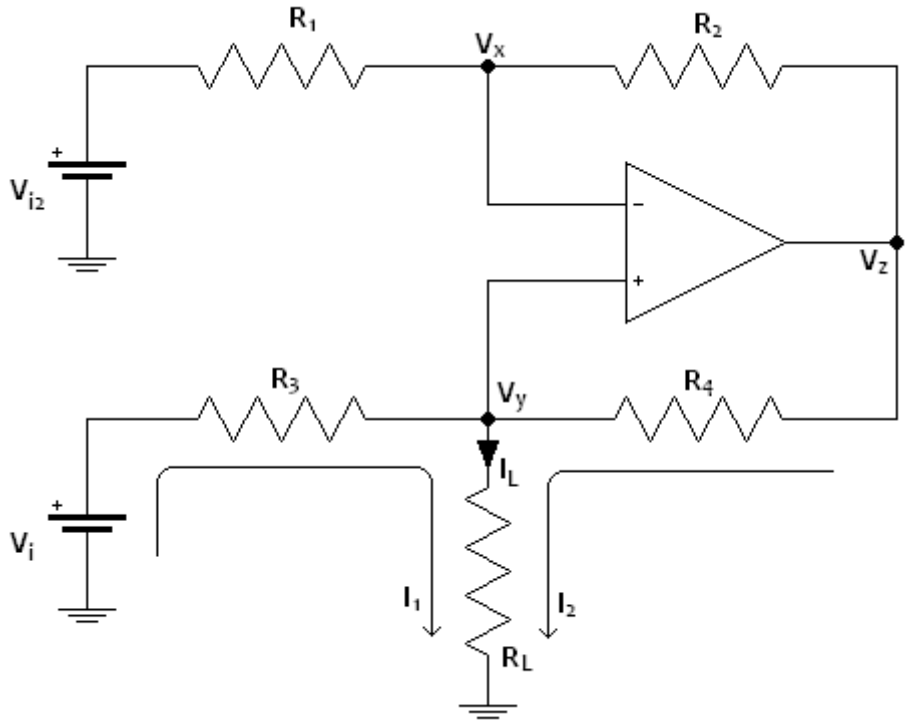


*Figure 3.2: Differential V-to-I converter based on the Howland Model*

Current $I_1$

$$I_1 = \frac{V_i - V_y}{R_3} \tag{3.2}$$

Current $I_2$

$$I_2 = \frac{V_z - V_y}{R_4} \tag{3.3}$$

The non-inverting op-amp configuration gives

$$V_z = V_x\left(\frac{R_2 + R_1}{R_1}\right) - V_{i2}\left(\frac{R_2}{R_1}\right) \quad (3.4)$$

Assuming the two inputs to the op-amp are equal: $V_x = V_y$ and that $R_2 = R_1$

$$V_z = 2V_y - V_{i2} \quad (3.5)$$

Also, assuming $R_3 = R_4$

$$I_2 = \frac{2V_y - V_{i2} - V_y}{R_3} \quad (3.6)$$

Since $I_L = I_1 + I_2$

$$I_L = \frac{V_i - V_y}{R_3} + \frac{2V_y - V_{i2} - V_y}{R_3} = \frac{V_i - V_{i2}}{R_3} \quad (3.7)$$

In order to eliminate the second current source so that the whole circuit can be run off one voltage input $V_i$ can be shorted to ground, $V_i=0$, the resulting output is:

$$I_L = -\frac{V_{i2}}{R_3} \quad (3.8)$$

Again it can be seen that the current output is not dependant on the load resistance, therefore the current source can be used to drive the EIT electrodes.

## 3.2 The Improved Howland Model

Due to the nature of the Howland model for current conversion the output current level is quite small. As the feedback resistance values decrease (reaching similar or lower values than the load resistance) the op-amp is forced to provide a higher voltage output to compensate for the effect of the load resistance, often this is impossible as op-amps can only source voltages up to the value of their power supply voltages.

The Improved Howland model attempts to provide a solution to this issue. The operation is similar to the standard Howland model however this modified version includes an extra resistor, shown below as $R_5$, which reduces the amount of voltage the op-amp needs to provide in order to give the correct output current. [PARKER 2005, PEASE 2008, HOROWITZ 1989]

The Leicester group proved empirically that the Improved Howland model also provided better Output Impedance values. It was shown through computer

simulation that slight adjustments of $R_3$ (as low as 0.001%) can allow for this improvement. This second attribute is the main reason the Improved Howland circuit chosen for this investigation.

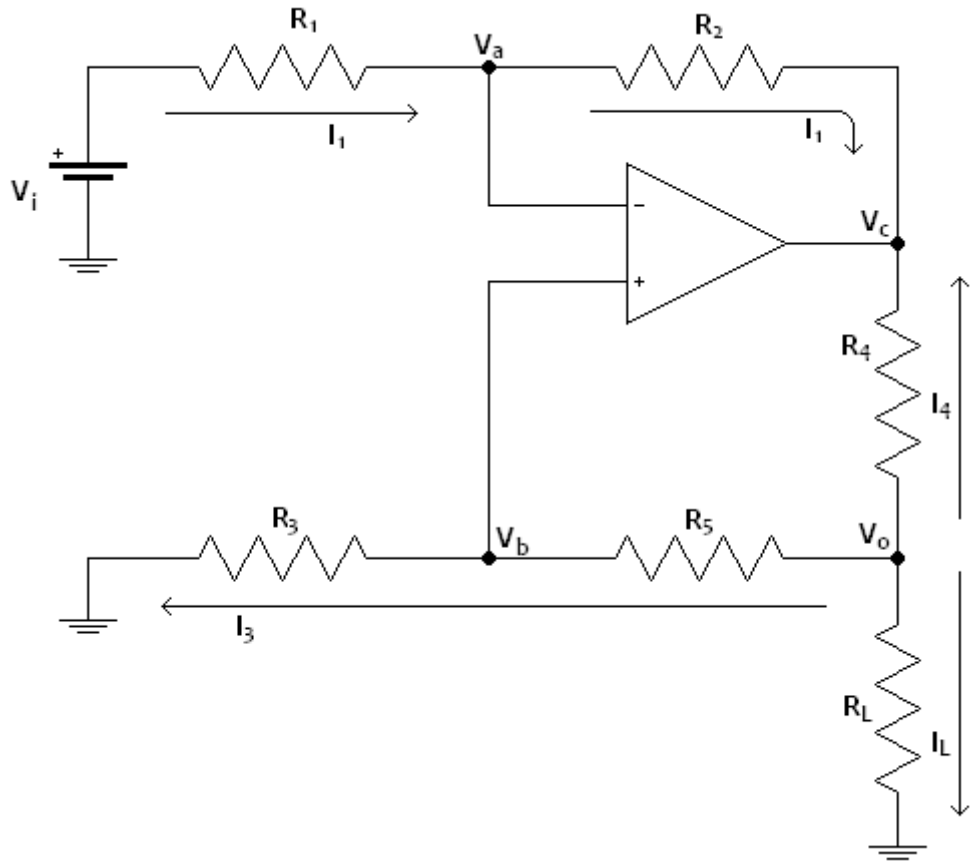


*Figure 3.3: The Improved Howland Model*

From Kirchoff's current law and Ohm's law

$$-I_L = I_4 + I_3 = \frac{V_o - V_c}{R_4} + I_3 \quad (3.9)$$

Since $V_a = V_b$

$$-I_L = \frac{(V_o - V_b) - (V_c - V_a)}{R_4} + I_3 \quad (3.10)$$

Therefore

$$-I_L = \frac{V_{R5} - (-V_{R2})}{R_4} + \frac{I_3.R_4}{R_4} = \frac{I_3.R_5 - (-I_1.R_2)}{R_4} + \frac{I_3.R_4}{R_4} \quad (3.11)$$

Rearranged to give

$$-I_L = I_3\frac{(R_5 + R_4)}{R_4} + I_1\frac{R_2}{R_4} \quad (3.12)$$

Further

$$-I_L = \frac{V_b}{R_3}\frac{(R_5 + R_4)}{R_4} + \frac{(V_i - V_a)}{R_1}\frac{R_2}{R_4} \quad (3.13)$$

And finally

$$-I_L = V_b \frac{(R_5 + R_4)}{R_3.R_4} - V_a \frac{R_2}{R_1.R_4} + V_i \frac{R_2}{R_1.R_4} \quad (3.14)$$

Due to the potential divider within the circuit

$$V_a = V_b = \frac{V_o.R_3}{R_3 + R_5} \quad (3.15)$$

Therefore

$$-I_L = \frac{V_o.R_3}{R_4(R_3 + R_5)} \left( \frac{(R_4 + R_5)}{R_3} - \frac{R_2}{R_1} \right) + V_i \frac{R_2}{R_1.R_4} \quad (3.16)$$

Or

$$I_L = \frac{V_o.R_3}{R_4(R_3 + R_5)} \left( \frac{R_2}{R_1} - \frac{(R_4 + R_5)}{R_3} \right) - V_i \frac{R_2}{R_1.R_4} \quad (3.17)$$

It can therefore be shown that if

$$\frac{R_2}{R_1} = \frac{(R_4 + R_5)}{R_3} \quad (3.18)$$

$$I_L = -\frac{V_i.R_2}{R_1.R_4} \tag{3.19}$$

This shows that the output current is not dependant on the value of $R_L$ and instead relies simply on the input voltage and 3 balanced resistors.

The output impedance of the Improved Howland circuit can be calculated as follows:

$$I_L = \frac{V_o.R_3}{R_4(R_3+R_5)}\left(\frac{R_2}{R_1}-\frac{(R_4+R_5)}{R_3}\right) - V_i\frac{R_2}{R_1.R_4} \tag{3.20}$$

First short the input voltage to ground:

$$I_L = \frac{V_o.R_3}{R_4(R_3+R_5)}\left(\frac{R_2}{R_1}-\frac{(R_4+R_5)}{R_3}\right) \tag{3.21}$$

The output impedance $Z_{out} = V_o/I_L$

$$Z_{out} = \frac{V_o}{I_L} = \frac{R_1.R_4(R_3+R_5)}{R_2.R_3-(R_4+R_5)R_1} \tag{3.22}$$

It can be seen here that the output impedance is dependent on $R_3$, however the Output current calculated earlier was only dependant on $R_1$, $R_2$, $R_4$ and the input

voltage. This allows the value of $R_3$ to be tweaked to improve output impedance performance.

Clearly if this is altered, the matched resistors assumed in equation (3.9) which create the output current will change, however if the value is only slightly altered (approx 1%) the output current will hardly be affected.

## 3.3 The Generalised Impedance Converter

All versions of the Howland Model can be described as being based on a negative Impedance Converter (NIC) which applies both positive and negative feedback. Basic amplifiers built using op-amps, inverting or non-inverting, use only negative feedback. The NIC uses both types of feedback simultaneously to create a scaled negative impedance value.

The Generalized Impedance Converter (GIC) is based on combining two NICs to create a circuit which can replicate the effect of a different form of impedance. In this example resistors and capacitors can be used to create an inductance. [HOROWITZ 1989]

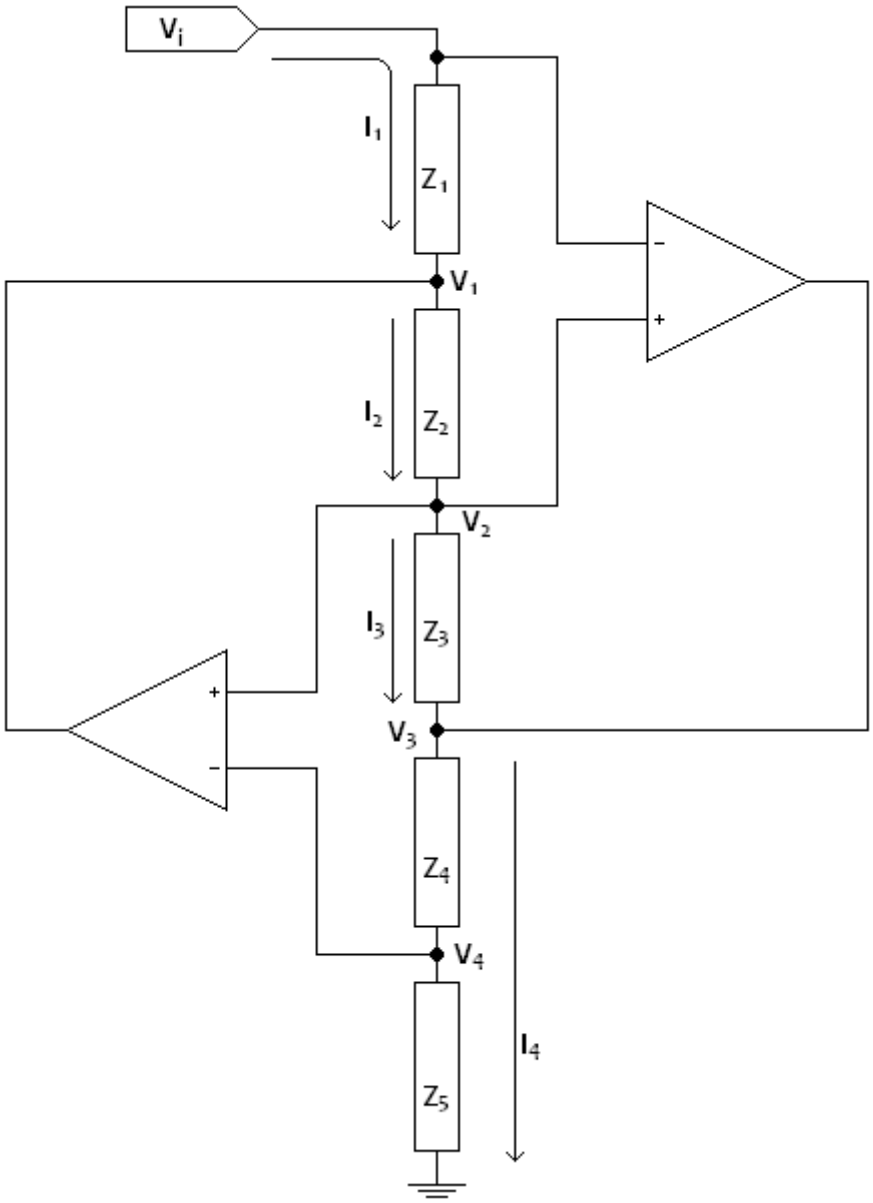


*Figure 3.4: Generalised Impedance Converter*

Given that the inputs for op-amps are equal to each other, it can be said that

$$V_i = V_2 = V_4 \tag{3.23}$$

Also, an op-amp draws no current

$$I_4 = \frac{V_4}{Z_5} = \frac{V_i}{Z_5} \tag{3.24}$$

From these initial assumptions you can work back up through the circuit as follows

$$V_3 = V_4 + I_4.Z_4 = V_i + \frac{V_i.Z_4}{Z_5} \tag{3.25}$$

$$I_3 = \frac{V_2 - V_3}{Z_3} = \frac{V_i}{Z_3} - \frac{\left(V_i + \frac{V_i.Z_4}{Z_5}\right)}{Z_3} = -\frac{V_i.Z_4}{Z_3.Z_5} \tag{3.26}$$

$$V_1 = V_2 + I_3.Z_2 = V_i + \left(-\frac{V_i.Z_4}{Z_3.Z_5}\right).Z_2 \tag{3.27}$$

$$I_1 = \frac{V_i - V_1}{Z_1} = \frac{V_i}{Z_1} - \frac{\left(V_i - \frac{V_i.Z_2.Z_4}{Z_3.Z_5}\right)}{Z_1} = \frac{V_i.Z_2.Z_4}{Z_1.Z_3.Z_5} \tag{3.28}$$

Therefore the input impedance $V_i/I_1$ can be described as

$$Z_i = \frac{Z_1.Z_3.Z_5}{Z_2.Z_4} \tag{3.29}$$

If either $Z_2$ or $Z_4$ are capacitances then the input impedance becomes inductive in nature

$$Z_i = \frac{Z_1.Z_3.Z_5}{Z_2.(\frac{1}{jwC_4})} = \frac{jwC_4.Z_1.Z_3.Z_5}{Z_2} \quad (3.30)$$

Assuming all the other impedances are resistances the inductance value can be calculated from

$$L = \frac{C_4.R_1.R_3.R_5}{R_2} \quad (3.31)$$

Inductance, in impedance terms, is the opposite of capacitance; reactance can be inductive or capacitive depending on its polarity, negative reactance is capacitive. It was suggested that an inductive element may reduce the effect of capacitance on the standard Howland model, and may improve the bandwidth of the output.

## 3.4 Comparison & Results

The outputs from two different circuits were compared to one another; the first was an 'Improved Howland' model in series with a GIC, the second was simply the 'Improved Howland' part of the circuit. Both circuits were optimised to achieve the best current stability.

The circuits were built in the electronics simulator PSpice. Graphs showing the current output across the Load resistor were produced and compared.

Initially the Howland circuits were built using an OPA 620 operational amplifier; the group have previously used these amplifiers in their systems due to their low noise, which is integral to EIT systems. However this op amp has been discontinued by the manufacturer and therefore it would be foolish to base the whole system on its output therefore outputs were taken using an ideal op-amp, modelled by PSpice, to show the potential output from the circuits.

The current design for the system has the current driven into the V-to-I circuit coming from a multiplexer, this multiplex has a built in capacitance, depending on the multiplexer the capacitance can be different, therefore the circuits were tested at 20pF and 100pF loading also (these tests were completed while still using the ideal op-amps).

For the graphs plotted in the next section values for Output Impedance were calculated at 1Kohm Loading.

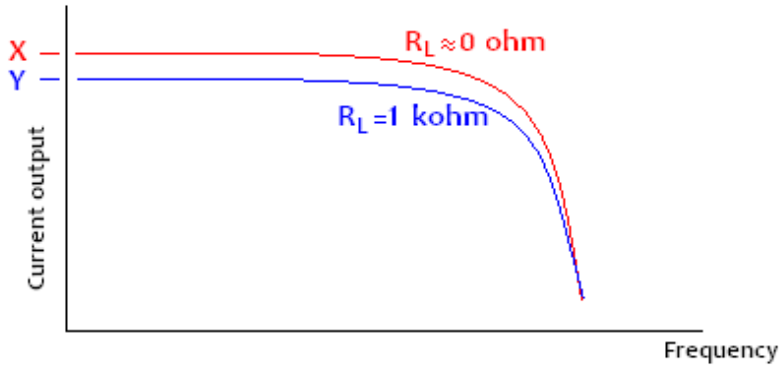


*Figure 3.5: Simplified output example from V-to-I showing outputs from two resistance loads*

X on the graph represents the initial output current under ideal conditions, when $R_L \approx 0\ \Omega$.

While Y represents initial output current when $R_L = 1\ k\Omega$.

Output impedance can be found using the equation:

$$Z_{out} = \frac{1000 \times Y}{X - Y} \tag{3.32}$$

This is because the equation can be reduced to show:

$$Z_{out} = \frac{V_{out}}{I_{out}} \tag{3.33}$$

It can be seen that since $R_L$ is 1kohm.

$$V_{out} = 1000 \times Y \tag{3.34}$$

X-Y represents the output change induced by the resistor, $R_L$.

So it can be said that X-Y is the current through $R_L$, or the output current.

$$I_{out} = X - Y \tag{3.35}$$

The -1dB and -3dB bandwidths of each output were also calculated and shown in the tables alongside output impedance.

### 3.4.1 Howland-GIC Circuit Performance

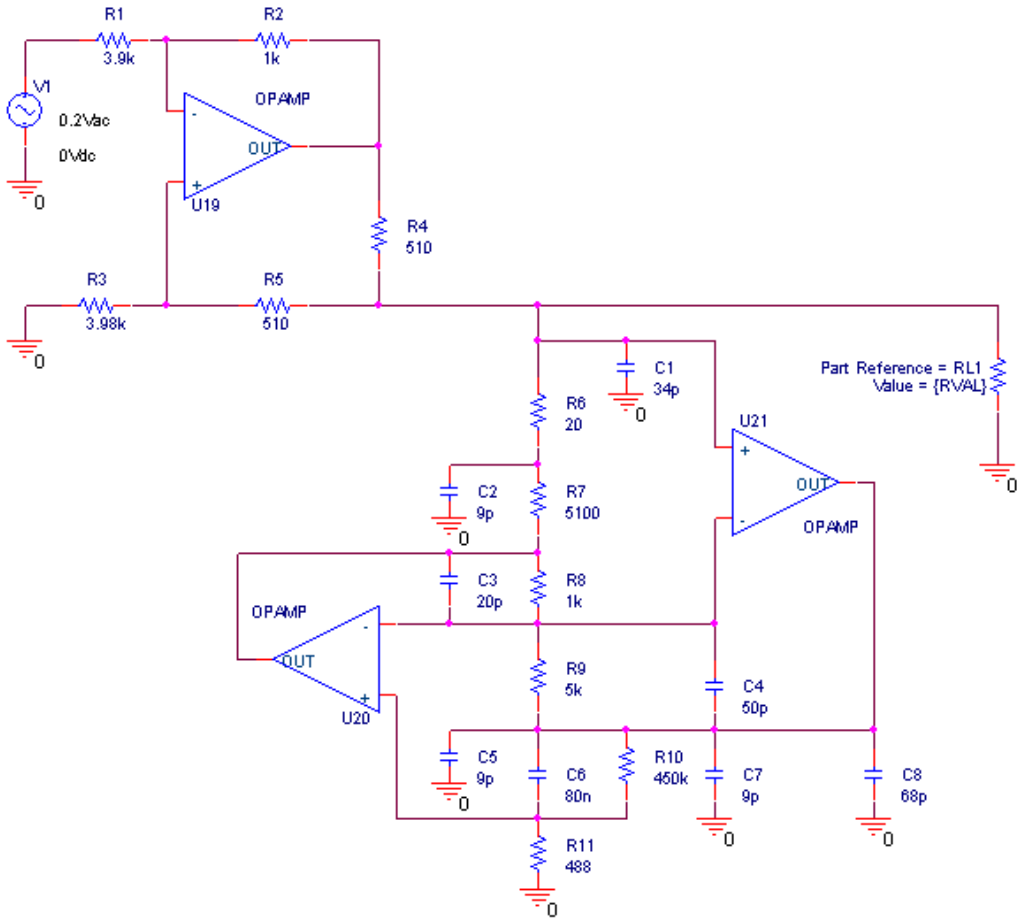


*Figure 3.6: PSpice computer simulation model of Improved Howland in series with GIC*

This circuit was designed by an American group whose intention was to create a current source with high output impedance, the paper described a circuit which was a very simple GIC circuit, however, following private discussions with the authors various extra components were included to model stray capacitances. [ROSS 2003]

The circuit was simulated in PSpice using the OPA620 chip for comparison. Although now discontinued the Leicester Group has experience of utilising this amplifier in previous hardware systems and had a large quantity in stock for use on the project.

The simulations were run over a wide frequency range. The –1dB and –3dB points were measured (the frequency at which the magnitude drops below 90uA and 70uA respectively) and the output impedance at 1 KΩ loading was calculated for varying $R_L$ values of 0.1Ω (to model the ideal response), 1kΩ, 2kΩ and 4KΩ.

#### *3.4.1.1 OPA 620 Performance*

The following graphs show the response of the circuit under the described conditions. Each graph contains 4 curves representing 0.1Ω, 1KΩ, 2KΩ and 4KΩ $R_{L1}$ loading.

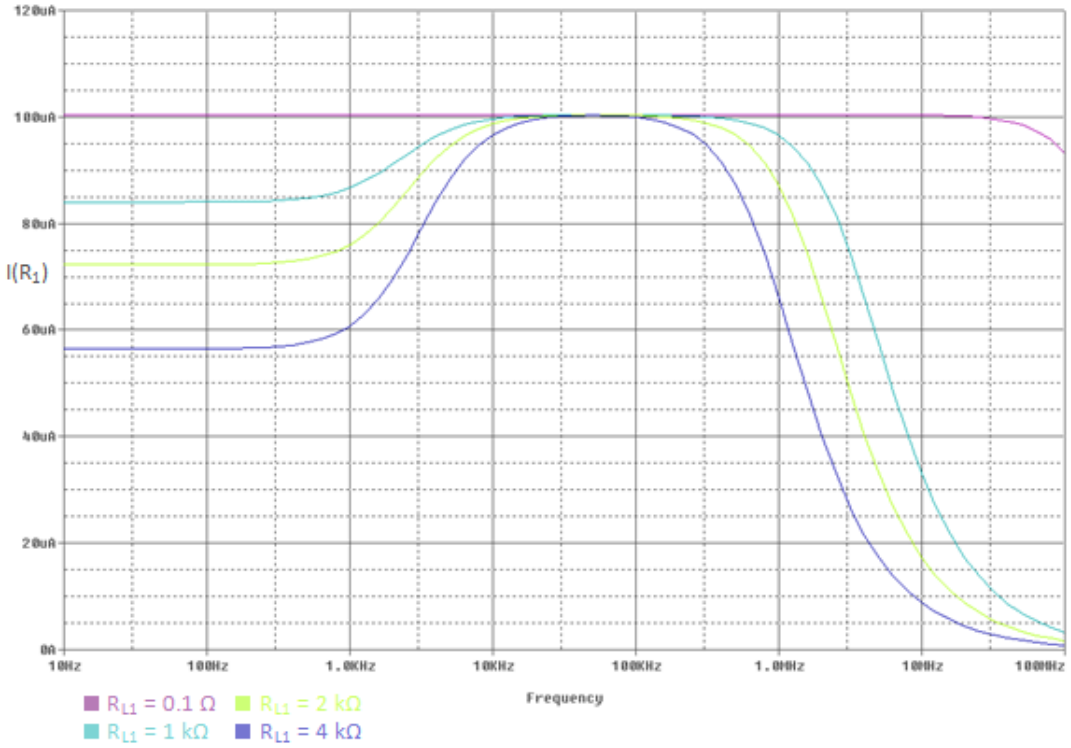


*Figure 3.7: Howland-GIC circuitry frequency response with OPA620*

Figure 3.7 shows the frequency response of the Howland/GIC circuit when using the OPA620 op-amp, it can clearly be seen how the outputs peak between 10 KHz and 100 KHz, and this means that any Output Impedance values attained would only be for one instance rather than constant. It can also be seen how the response is low at frequencies lower than 10 KHz, although EIT is normally concerned with high frequencies, some lower frequency data could prove to be of use and this type of output may not be able to provide it.

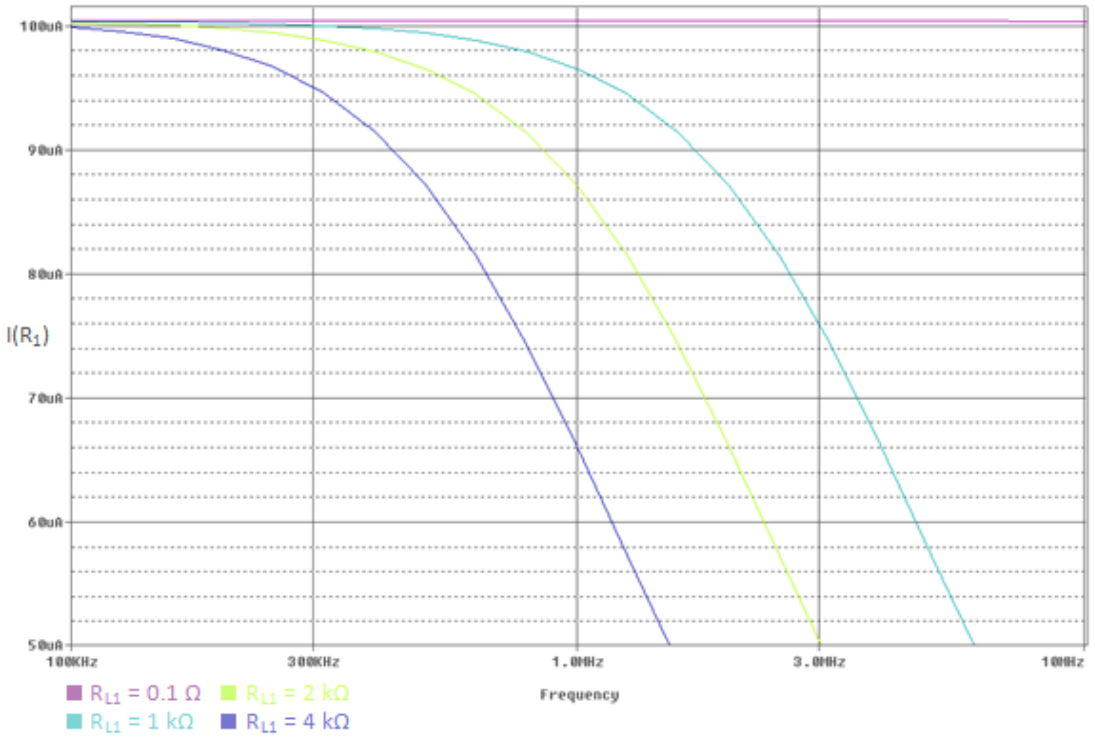


*Figure 3.8: Howland-GIC dB points with OPA620*

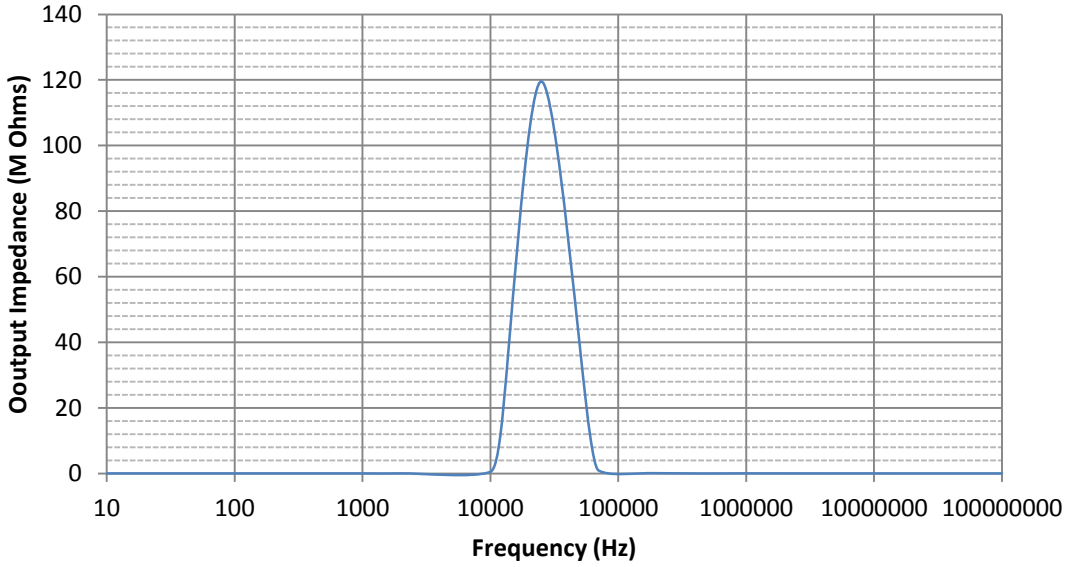


*Figure 3.9: Howland-GIC Output Impedance Curve with OPA620*

The drop off providing bandwidth data can be seen easier in Figure 3.8, while Figure 3.9 shows the Output Impedance curve which highlights how the nature of the circuitry provides a peak output impedance rather than a constant value, both the -1dB and -3dB bandwidths along with the Output Impedance ($Z_{out}$) values are provided in Table 3.1.

Table 3.1: Howland-GIC response with OPA620 $R_3$ = 4015.6 Ω

| $R_L$ | -1dB Bandwidth | -3dB Bandwidth | $Z_{out}$ at 1 KΩ loading |
|---|---|---|---|
| 0.1Ω | >100 MHz | >100 MHz | 120 MΩ (peak) |
| 1KΩ | 1.7 MHz | 3.6 MHz | |
| 2KΩ | 847.5 KHz | 1.8 MHz | |
| 4KΩ | 424.9 KHz | 894.1 KHz | |

The output impedance falls rapidly, only remaining at 120MΩ at 26.8 KHz, it was already as low as 2.7 MΩ by 100 KHz. This circuit also limits the bandwidth to below 5 KHz for the higher loading values.

#### *3.4.1.2 Ideal OP-AMP Performance*

It has been noted that the OPA620 is discontinued therefore the circuit was tested again using an ideal op-amp in the PSpice simulation so that any restrictions applied by the circuitry itself will become apparent. The circuit was optimised by altering the $R_3$ resistor, the optimised value for $R_3$ in this case was 3980Ω. Figure 3.10 shows the outputs gained from these simulations. A graph for Output Impedance is not provided as it is similar in form to Figure 3.9: Howland-GIC Output Impedance Curve with OPA620 with a lower peak value as described in Table 3.2: Howland-GIC response with ideal op-amps $R_3$ = 3980 Ω.

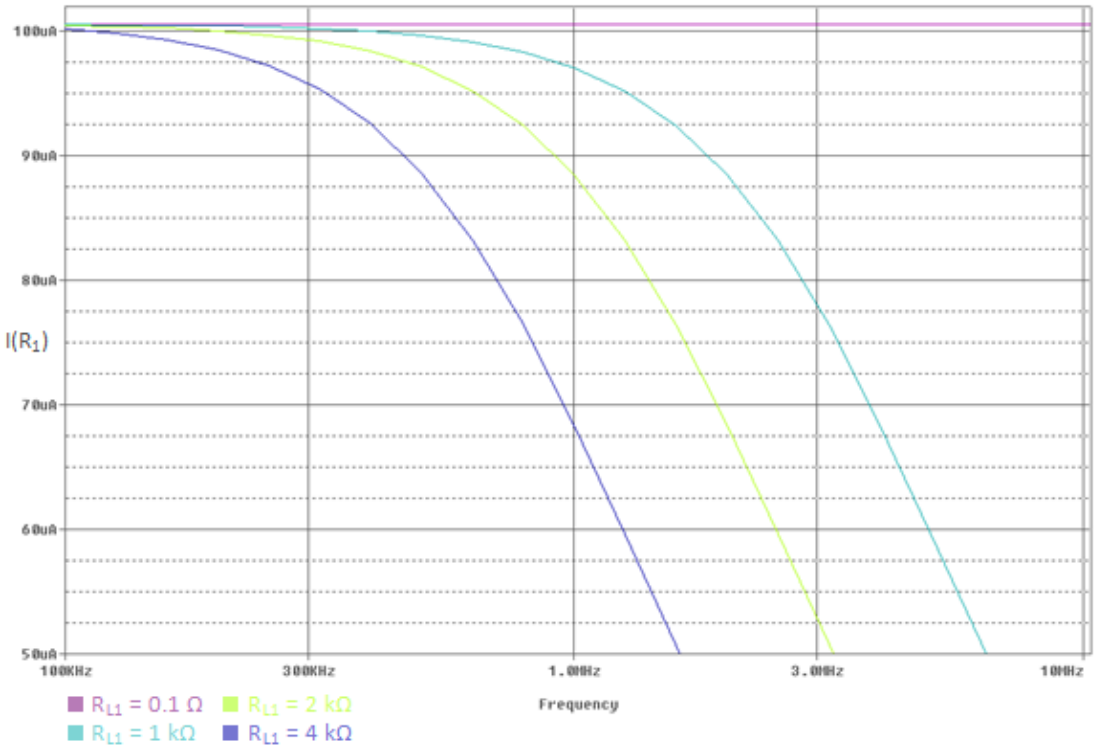


*Figure 3.10: Howland-GIC dB points with ideal op-amps*

Table 3.2 shows the values attained for bandwidth and Output Impedance ($Z_{out}$).

*Table 3.2: Howland-GIC response with ideal op-amps $R_3$ = 3980 Ω*

| $R_L$ | -1dB Bandwidth | -3dB Bandwidth | $Z_{out}$ at 1 KΩ loading |
|---|---|---|---|
| 0.1Ω | >100 MHz | >100 MHz | 91.8 MΩ (peak) |
| 1KΩ | 11.8 MHz | 3.8 MHz | |
| 2KΩ | 904.9 KHz | 1.9 MHz | |
| 4KΩ | 453.2 KHz | 949.6 KHz | |

The output impedance again falls rapidly, this response shows that the Howland-GIC circuitry is limiting the output; ideal op-amps will introduce no capacitance into the system. In this case the results are very similar to the previous OPA620 simulations and therefore we can conclude that the effect due to the circuit is greater than any resulting from the chosen op-amps.

#### *3.4.1.3 20 pF Loading*

The circuit was simulated with a parallel loading capacitance of 20pF, this is an approximation of the loading value gained with a 16 electrode system, even though it has been shown that the output from the GIC model is limited by its circuitry, it was hoped that the inductance would cancel some of the capacitance and thereby improve the overall bandwidth. Ideal op-amps were once again used to measure the output.

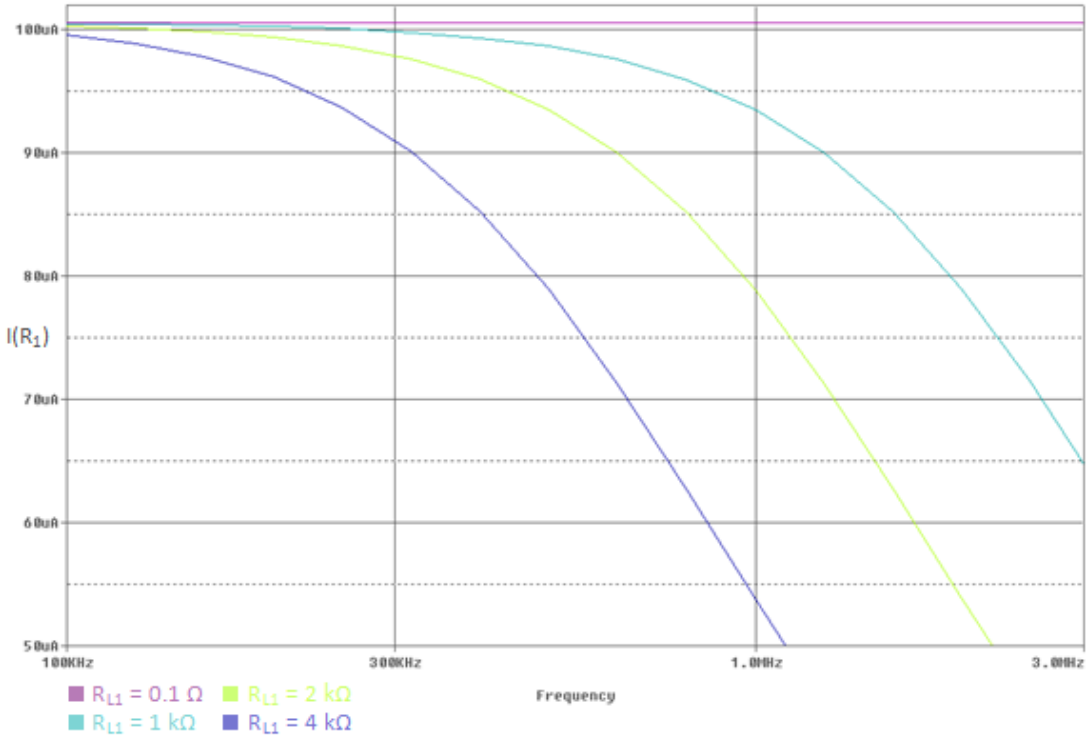


*Figure 3.11: Howland-GIC dB points with 20pF loading*

Figure 3.11 is condensed into Table 3.3 where the bandwidth can be seen along with the Output Impedance ($Z_{out}$) values.

*Table 3.3: Howland-GIC response with 20pF loading $R_3$ = 3980 Ω*

| $R_L$ | -1dB Bandwidth | -3dB Bandwidth | $Z_{out}$ at 1 KΩ loading |
|---|---|---|---|
| 0.1R | >100 MHz | >100 MHz | 92.1 MΩ (peak) |
| 1K | 1.3 MHz | 2.6 MHz | |
| 2K | 632.1 KHz | 1.3 MHz | |
| 4K | 318.3 KHz | 652.0 KHz | |

#### *3.4.1.4 100pF Loading*

The multiplexer used within the DMU Mk3a system loads the current source output with a capacitance of up to 100pF, therefore a simulation was used to see the effect of this on the model, as previously ideal op-amps were used.

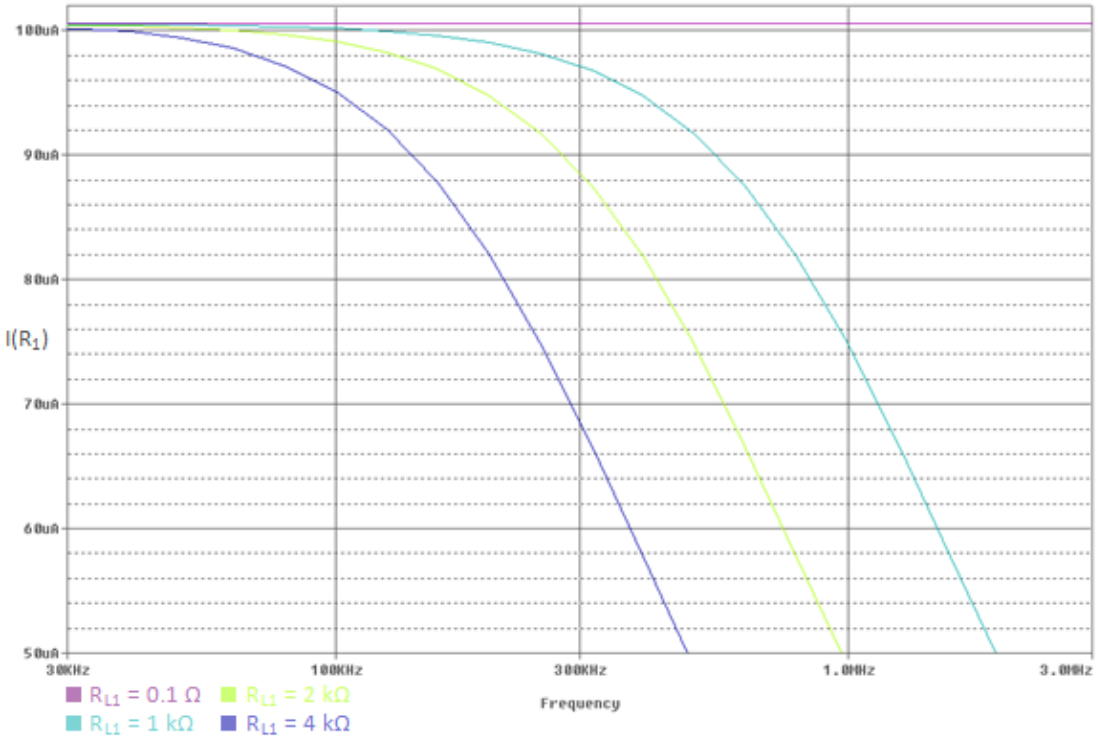


*Figure 3.12: Howland-GIC dB points with 100pF loading*

*Table 3.4: Howland-GIC response with 100pF loading $R_3$ = 3980 Ω*

| $R_L$ | -1dB Bandwidth | -3dB Bandwidth | $Z_{out}$ at 1 KΩ loading |
|---|---|---|---|
| 0.1R | >100 MHz | >100 MHz | 76 MΩ (peak) |
| 1K | 547.8 KHz | 1.1 MHz | |
| 2K | 275.0 KHz | 570.0 KHz | |
| 4K | 140.0 KHz | 300.0 KHz | |

In these two simulations (20pF and 100pF loading) the output can be seen to simply degrade depending on the capacitive loading applied.

### 3.4.2 Improved Howland Performance

The resistor values used in following simulations were, for $R_1$, $R_2$, $R_4$ and $R_5$ set to 1K, while $R_3$ was altered in order to optimise the circuit for the chosen op amp.

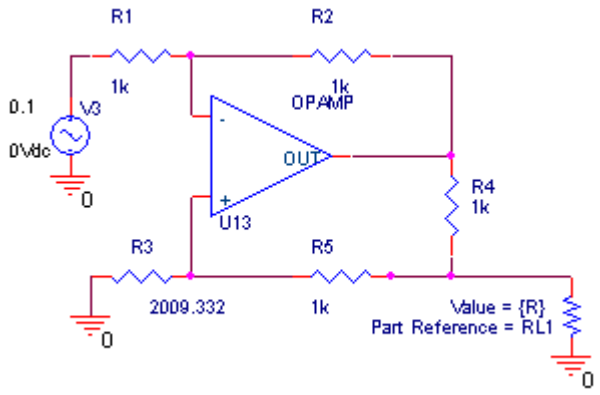


*Figure 3.13: PSpice computer simulation model of Improved Howland circuit*

The values shown are the optimised values for use with an OPA620 op-amp.

The improved Howland circuit gave the output shown in Figure 3.14, it is clear that this response appears much better than the improved Howland-GIC version initially due to the lack of low frequency drop off.

### 3.4.2.1 OPA 620 Performance

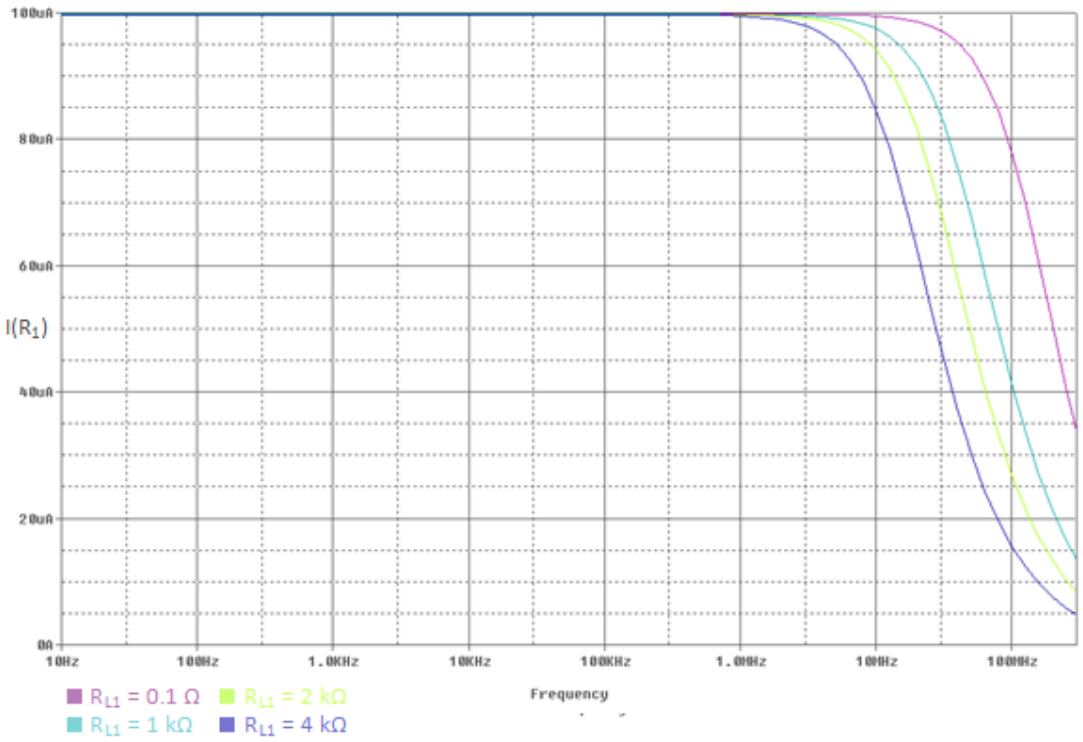


*Figure 3.14: Improved Howland frequency response with OPA620*

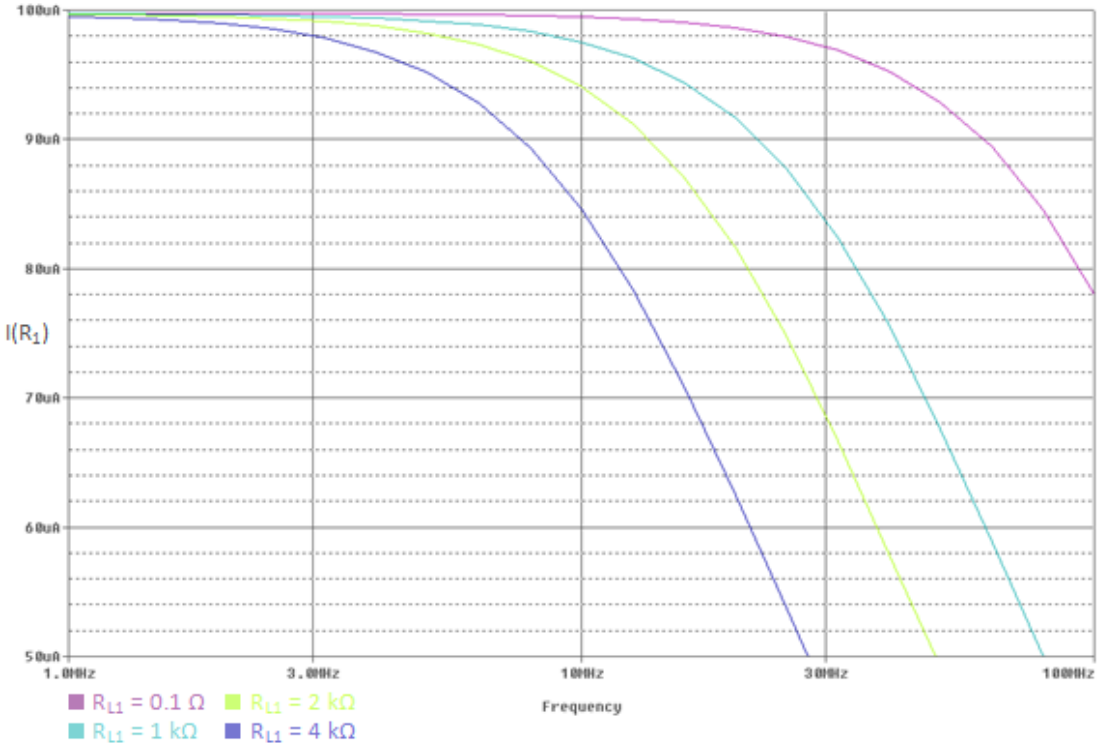


*Figure 3.15: Improved Howland dB points with OPA620*

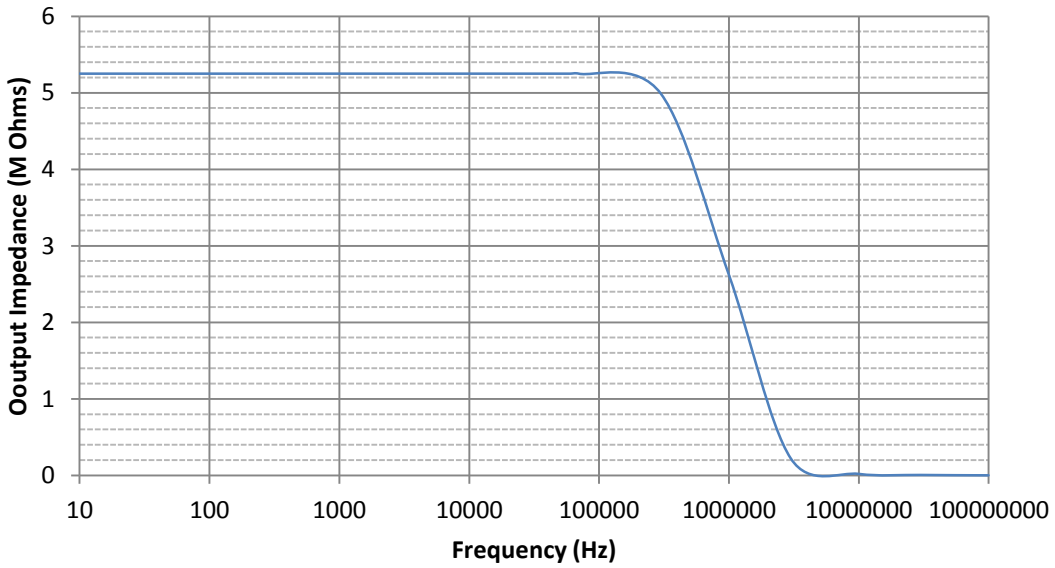


*Figure 3.16: Improved Howland Output Impedance difference with OPA620*

The curve shown in Figure 3.16 shows how the output impedance for the Improved Howland circuit has a more consistent Output Impedance level which drops off after 100K Hz. As before the results shown in Figure 3.15 and Figure 3.16 are reproduced in Table 3.5.

*Table 3.5: Improved Howland response with OPA620 $R_3$ = 2009.332 Ω*

| $R_L$ | -1dB Bandwidth | -3dB Bandwidth | $Z_{out}$ at 1 KΩ loading |
|---|---|---|---|
| 0.1Ω | 59.8 MHz | >100 MHz | 5.3 MΩ |
| 1KΩ | 21.8 MHz | 46.7 MHz | |
| 2KΩ | 13.5 MHz | 28.7 MHz | |
| 4KΩ | 7.6 MHz | 16.2 MHz | |

The output impedance was steady at 5.3MΩ up to around 200 KHz and is still as high as 4.9 MΩ by 300 KHz.

### *3.4.2.2 Ideal OP-AMP Performance*

For the tests involving the ideal op-amps the $R_3$ value was optimised to 2 KΩ as this gave the best response.

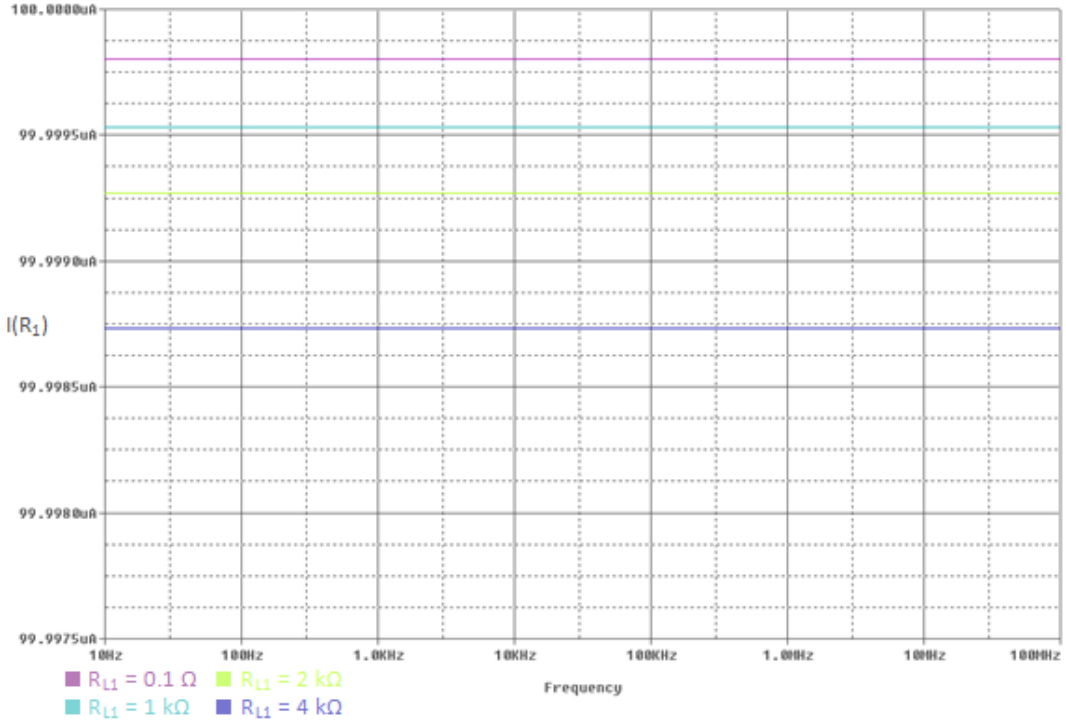


*Figure 3.17: Improved Howland frequency response with ideal op-amps*

*Table 3.6: Improved Howland response with ideal op-amps $R_3$ = 2 KΩ*

| $R_L$ | -1dB Bandwidth | -3dB Bandwidth | $Z_{out}$ at 1 KΩ loading |
|---|---|---|---|
| 0.1Ω | >100 MHz | >100 MHz | 370 MΩ |
| 1KΩ | >100 MHz | >100 MHz | |
| 2KΩ | >100 MHz | >100 MHz | |
| 4KΩ | >100 MHz | >100 MHz | |

Figure 3.17 clearly shows that the bandwidths are effectively infinite. The output impedance is also steady; thus proving that the circuit performance is entirely reliant

on the op-amps used and if better op-amps were acquired the response of the circuitry should improve accordingly.

### *3.4.2.3 20pF Loading*

The Howland model was also tested with 20pF loading for 16 electrode system simulation.

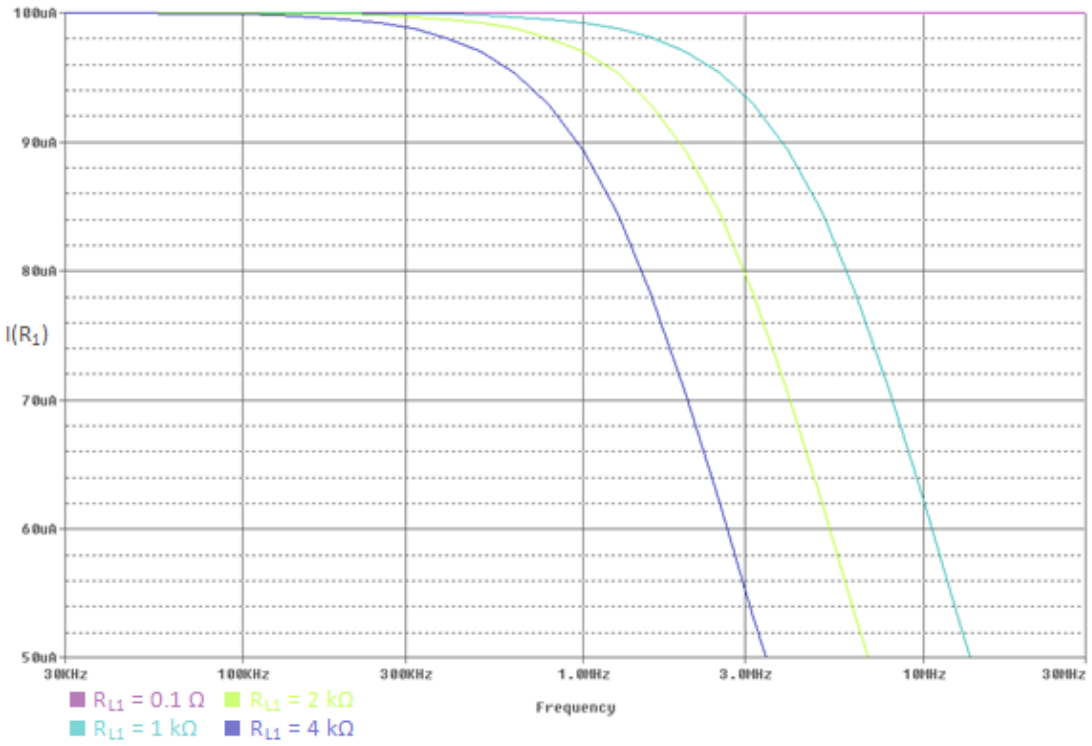


*Figure 3.18: Improved Howland dB points with 20pF loading*

*Table 3.7: Improved Howland response with 20pF loading $R_3$ = 2 KΩ*

| $Rs_L$ | -1dB Bandwidth | -3dB Bandwidth | $Z_{out}$ at 1 KΩ loading |
|---|---|---|---|
| 0.1Ω | >100 MHz | >100 MHz | 370 MΩ |
| 1KΩ | 3.8 MHz | 8.1 MHz | |
| 2KΩ | 1.9 MHz | 4.1 MHz | |
| 4KΩ | 958.1 KHz | 2.1 MHz | |

The Output impedance in this case is once again steady until the bandwidth begins to fall, following a similar shape to that shown in Figure 3.16.

### 3.4.2.4 100pF Loading

The simulation was altered so that the loading capacitance was 100pF and then repeated to show the effects of such loading.

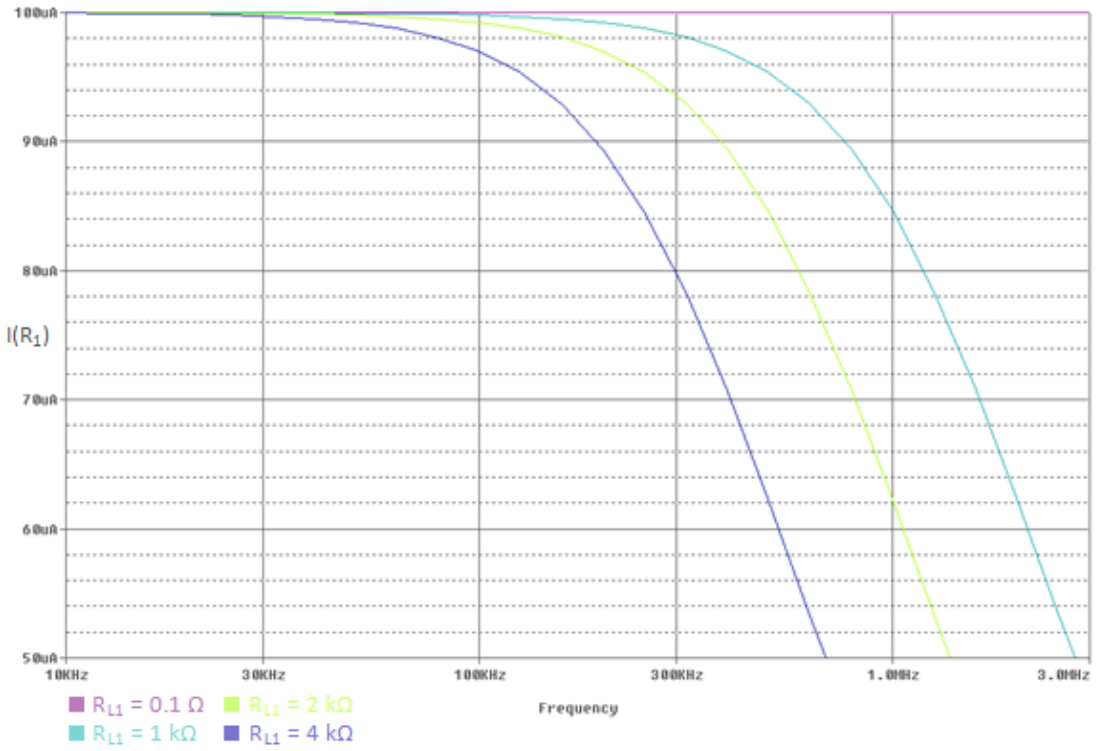


*Figure 3.19: Improved Howland dB points with 100pF loading*

*Table 3.8: Improved Howland response with 100pF loading $R_3$ = 2 KΩ*

| $R_L$ | -1dB Bandwidth | -3dB Bandwidth | $Z_{out}$ at 1 KΩ loading |
|---|---|---|---|
| 0.1Ω | >100 MHz | >100 MHz | 370 MΩ |
| 1KΩ | 758.1 KHz | 1.6 MHz | |
| 2KΩ | 381.5 KHz | 798.0 KHz | |
| 4KΩ | 192.0 KHz | 404.0 KHz | |

As can be seen throughout the two simulations the peak output impedance does not change, however the impedance does drop off earlier thereby reducing the effective bandwidth.

## 3.5 Justification of Circuit

The GIC circuitry does create the higher output impedance values claimed by the American group, it is also affected less by the loading capacitance as predicted. However these output impedance peaks do not cover a large frequency range, this along with the dramatic effect of the bandwidth restrictions within the circuitry during ideal op-amp simulation suggest that the simpler Improved Howland circuit would be of better use within a wide-bandwidth EIT system.

### 3.5.1 Capacitance Loading

Figure 3.20 and Figure 3.21 show the output of the Howland-GIC and the Improved Howland (respectively), the curves in these graphs represent the effect of increased

capacitance loading on the two circuits. It can be seen how this increased loading reduces the bandwidth considerably

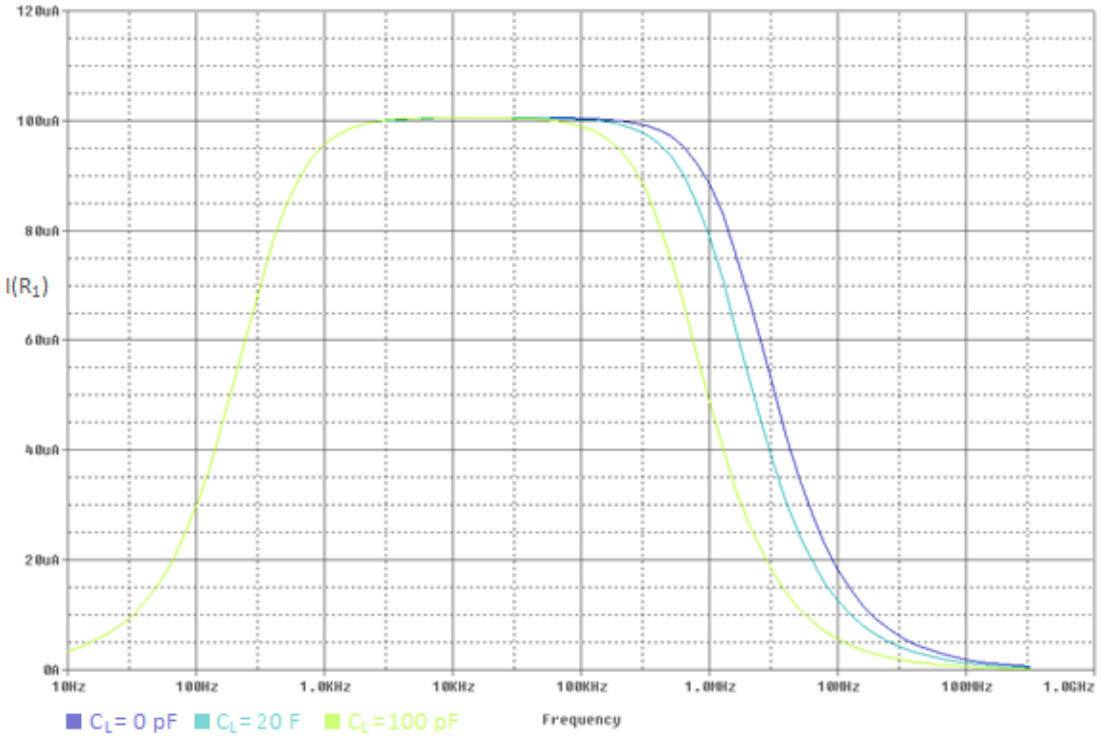


*Figure 3.20: Howland-GIC affect of capacitance loading with ideal op-amps*

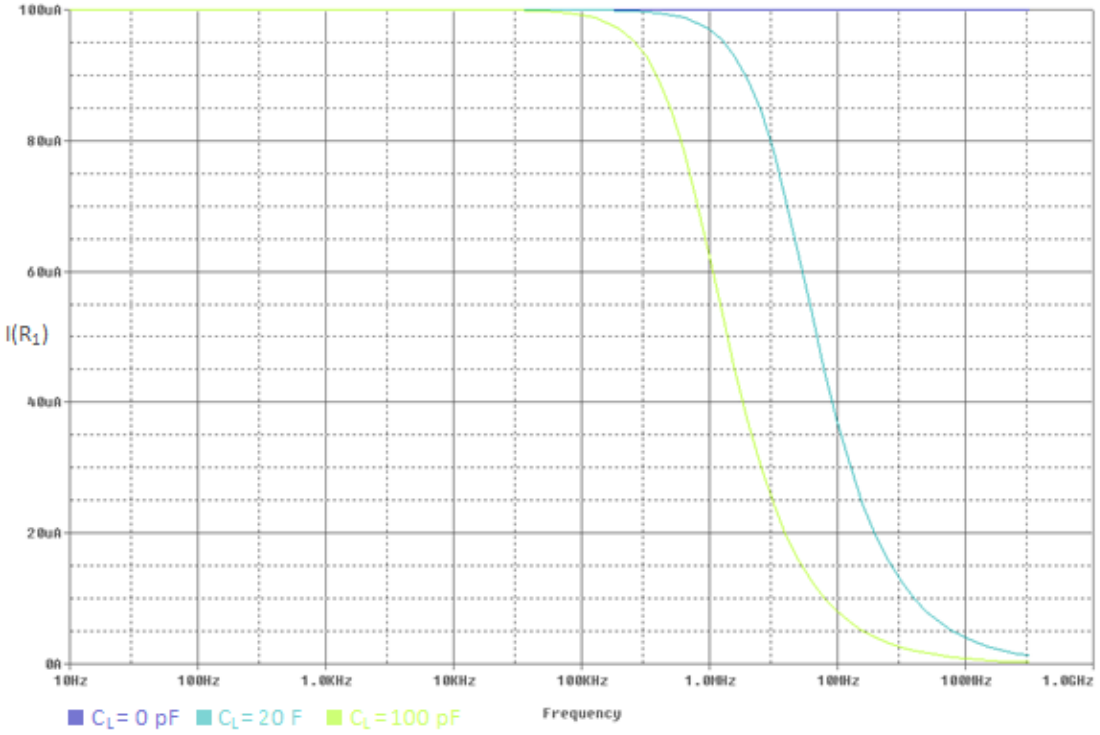


*Figure 3.21: Improved Howland affect of capacitance loading with ideal op-amps*

Comparing Figure 3.20 and Figure 3.21 directly it can be seen that the Howland-GIC circuit is relatively less affected by the capacitance loading, the Howland-GIC bandwidth was already limited by the GIC circuit while the improved Howland model with no loading provided infinite bandwidth; however it is also clear that even with the large reduction in bandwidth the Improved Howland model still provides a better output.

### 3.5.2 Other Op-Amps

Since the ideal op-amp simulation showed that the Improved-Howland circuit performance relied entirely on the chosen op-amp, the output achieved will improve

if a better performance op-amp is found. A search of currently available options was done with the following results with respect to their gain bandwidth product (GBP):

*Table 3.9: Available op-amps and their bandwidths*

| Chip Name | Bandwidth given |
|---|---|
| OPA620 | GBP = 200 MHz |
| MAX4223 | -3dB = 1GHz, -1dB = 300 MHz |
| OPA847 | GBP = 3.9 GHz |
| THS4509 | GBP = 3 GHz |
| THS4508 | GBP = 3 GHz |
| THS4513 | GBP = 2.8 GHz |
| THS3062 | GBP = 2.2 GHz |
| THS3061 | GBP = 2.2 GHz |
| OPA691 | GBP = 2 GHz |
| OPA698 | GBP = 250 MHz |
| OPA2822 | GBP = 240 MHz |
| OPA656 | GBP = 230 MHz |

The MAX4223 op-amp was selected for investigation as it was relatively low cost compared to the larger bandwidth op-amps and provided a more impressive bandwidth when compared to the suggested OPA620 direct replacements.

Furthermore it was easily available to the Leicester group through their existing suppliers.

### 3.5.3 Simulation of MAX4223

The PSpice model for the MAX4223 was available from the MAXIM website and the experiments using the improved Howland model were repeated. [MAXIM N.D.]

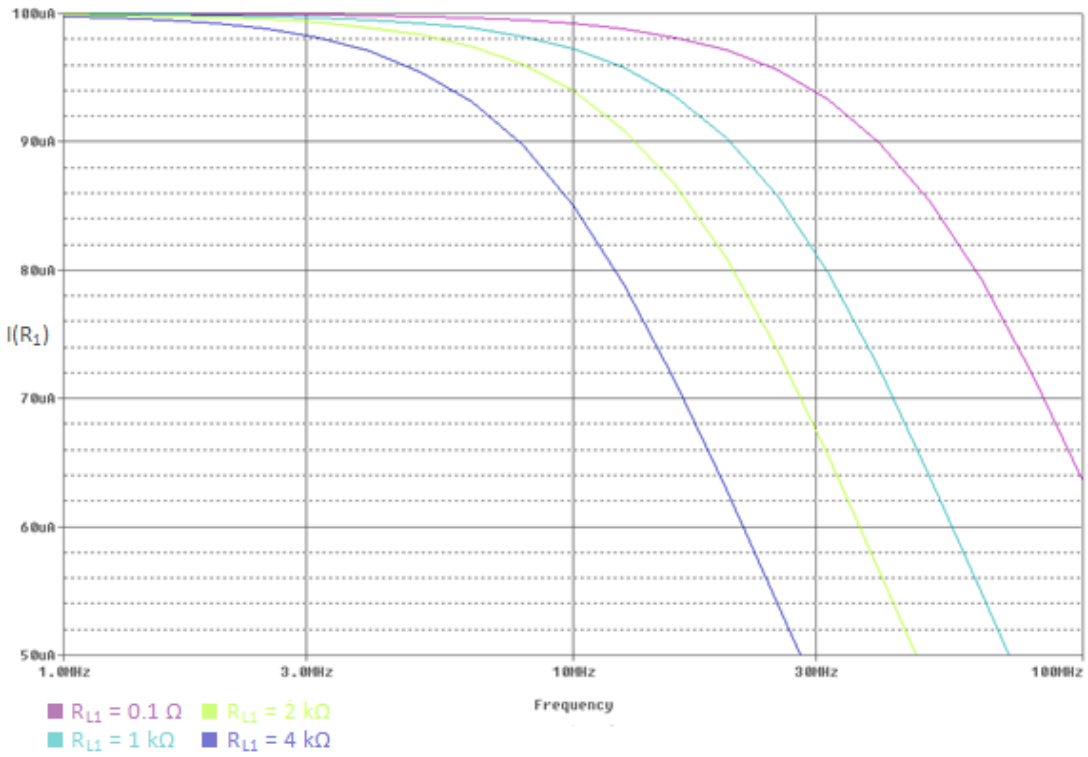


*Figure 3.22: Improved Howland dB points with MAX4223*

*Table 3.10: Improved Howland response with MAX4223 $R_3$ = 2012.8 Ω*

| $R_L$ | -1dB Bandwidth | -3dB Bandwidth | $Z_{out}$ at 1 KΩ loading |
|---|---|---|---|
| 0.1Ω | 39.3 MHz | 83.3 MHz | 37.4 MΩ |
| 1KΩ | 20.2 MHz | 42.3 MHz | |
| 2KΩ | 13.2 MHz | 30.0 MHz | |
| 4KΩ | 7.7 MHz | 16.3 MHz | |

This output is almost identical to the OPA620 for bandwidth; however it is worth noting that the output impedance is higher, showing the MAX amplifier is closer to the ideal response than the OPA620. This impedance is still as high as 4.2 MΩ when the frequency reaches 1 MHz.

It should also be noted that the $R_3$ value was modelled to a lesser degree of accuracy than in the OPA620 simulation so this output impedance could possibly be increased even more.

## 3.6 Conclusions

The output given by the GIC circuit did respond as hoped to some extent, however overall it did not give the sort of output which could be used successfully within our wide-bandwidth EIM system. EIT relies on stability over various frequencies and although the GIC can produce very good results for a few frequencies it does not provide a satisfactorily wide bandwidth.

The Improved-Howland circuit, although it still does not have the values for -1dB bandwidth we would like to achieve, has the advantage of stability over a larger frequency range. It is also a simpler, smaller circuit, which has been shown to improve with better op-amps.

Tables 3.11 and 3.12 show a summary of the results obtained throughout this chapter, it is clear to see that the Improved Howland model provides better bandwidths (both -1dB and -3dB) throughout the simulations. It is worth taking particular notice of the Ideal op-amp simulation as here it can be seen that the circuitry of the Improved Howland does not restrict the output whilst the equivalent results from the Howland-GIC testing show that however good the components used are the output of the circuit is limited to 3.8 MHz -3dB bandwidth as shown in Table 3.2.

*Table 3.11 Outputs gained from the Howland-GIC circuit throughout testing*

| Device | Capacitance loading | -1dB Bandwidth ($R_{L1}$) 0.1Ω | 1kΩ | 2kΩ | 4kΩ | $Z_{out}$ (max) MΩ |
|---|---|---|---|---|---|---|
| OPA620 | Zero | >100 MHz | 1.7 MHz | 847.5 kHz | 424.9 kHz | 120 |
| Ideal | Zero | >100 MHz | 11.8 MHz | 904.9 kHz | 453.2 kHz | 91.8 |
| | 20pF | >100 MHz | 1.3 MHz | 632.1 kHz | 318.3 kHz | 92.1 |
| | 100pF | >100 MHz | 547.8 kHz | 275.0 kHz | 140.0 kHz | 76 |

*Table 3.12: Outputs gained from the Improved Howland circuit throughout testing*

| Device | Capacitance loading | -1dB Bandwidth ($R_{L1}$) 0.1Ω | 1kΩ | 2kΩ | 4kΩ | $Z_{out}$ (max) MΩ |
|---|---|---|---|---|---|---|
| OPA620 | Zero | 59.8 MHz | 21.8 MHz | 13.5 MHz | 7.6 MHz | 5.3 |
| Ideal | Zero | >100 MHz | >100 MHz | >100 MHz | >100 MHz | 370 |
| | 20pF | >100 MHz | 3.8 MHz | 1.9 kHz | 958.1 kHz | 370 |
| | 100pF | >100 MHz | 758.1 kHz | 381.5 kHz | 192.0 kHz | 370 |

Comparing the output impedance values using Table 3.11 and Table 3.12 in a similar way is a little misleading as although the Howland-GIC circuit gave a much higher peak value for output impedance in the non-ideal case this was for one specific frequency which dropped off rapidly as shown in Figure 3.9: Howland-GIC Output Impedance Curve with OPA620. It is worth noting though that whilst using ideal op-amps the Improved Howland model did give a better peak value, as well as having stability over a larger frequency range, this confirms that the choice of op-amp will prove vital within the system. Selected parts of this investigation were presented at the 13th International Conference on Electrical Bioimpedance and the 8th Conference on Electrical Impedance Tomography in 2007. [WANG W 2007b]

Chapter 4 addresses another major issue found in EIT systems; the problems apparent when measuring high frequencies are exposed. A technique involving recording data in the time domain is described as a solution and an investigation is undertaken which attempts to provide a viable alternative to current approaches.

# Chapter 4 Cell Modelling

This chapter introduces the concept of finding values for Cole-Cole model parameters $R_R$, $R_S$ and C from impedance measurement data. It goes on to describe the difficulties involved in collecting enough data using a frequency sweep analysis to accurately describe these values, in particular the issue of measuring data at high frequencies.

Two conventional techniques which have been used to achieve more accurate results within the Leicester group are investigated. Both attempt to deal with the problems found when working with high frequencies by predicting part of the output rather than measuring it, however both methods contain flaws and these issues are highlighted and discussed.

The idea of taking the measurements in a transient sweep rather than across a frequency range is presented as an alternative and experiments are described which show attempts to reach the values of $R_R$, $R_S$ and C from this method.

Following attempts to provide practical results which reflected the encouraging theoretical work further tests within the field are suggested which should, with the correct equipment, present an output which could replace, or be used alongside the

more traditional, frequency approach to improve diagnostic measurements within EIT.

The author was responsible for the majority of the work presented in Chapter 4. Two previously published systems were discussed; the investigation for this was completed by the author. The time and frequency domain tests were completed by the author although the frequency domain tests were completed using equipment and software developed by G. Qiao and G. Sze from the Leicester group.

## 4.1 Frequency Response

As explained in Chapter 2, in order to provide all the information required to produce RSC values for a Cole-Cole model it is important to have impedance outputs over a large frequency range. Clearly the lower and upper frequency results are required in order to read the maximum and minimum outputs, while the curve arc in the central frequencies provides essential details for calculating the capacitance and therefore needs to be recorded accurately.

Due to the wide range of frequency measurements required, specialist equipment is required which can be expensive. Until recently the main apparatus used has been a Network analyser which can handle relatively high frequencies, up to 500 MHz, however it can only provide reading from 2 electrode pairs at a time, therefore the whole test takes a long time to complete. More recently software like NI LabVIEW

has been used which can multiplex various electrodes quickly; however the higher frequency response can be very noisy.

### 4.1.1 High Frequency Issues

Figure 4.1 shows how to identify the Dispersion frequency (also known as the 'relaxation' or 'notch' frequency), it is labelled as Fr within this work. The curves shown relate to the real and imaginary parts of the impedance measured across a frequency range. The dispersion frequency (Fr) occurs when the imaginary plot is at its lowest; this is marked as point 'b'. The point corresponding with this frequency is marked as 'a' on the real axis.

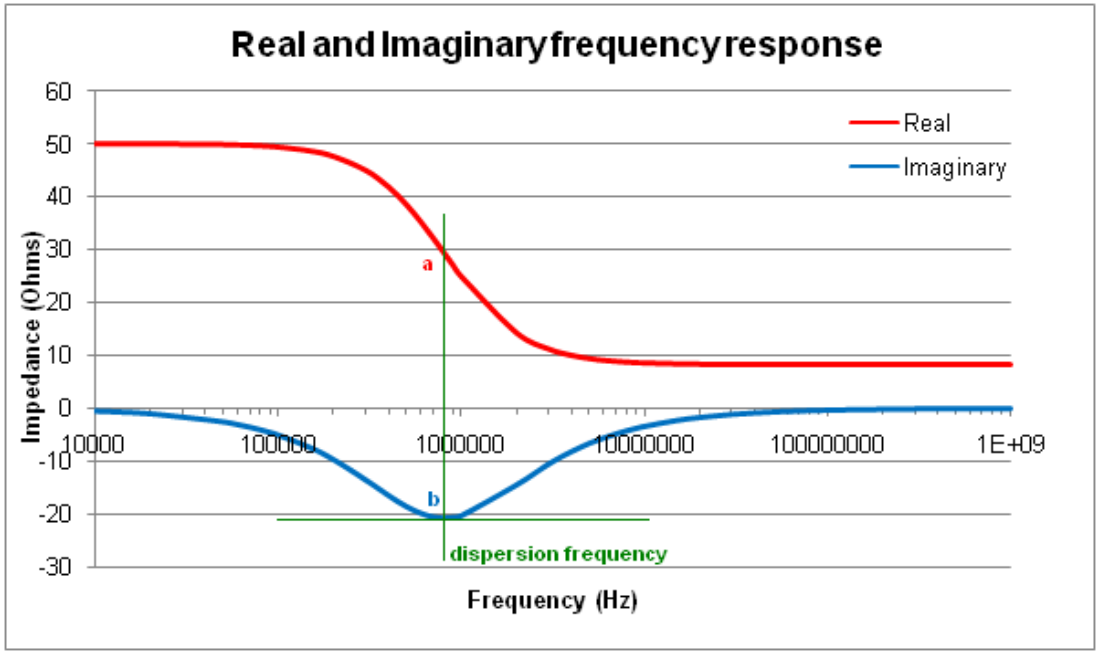


*Figure 4.1: Real and imaginary outputs identifying the dispersion frequency*

Research from the Leicester research group suggested that in order to provide accurate results which could be used to calculate correct values for $R_R$, $R_S$ and C, the frequency bandwidth must be at least 1.3 times Fr [HE 2007].

Due to this required large bandwidth, it had been suggested that the part of the Real impedance output curve which is difficult to measure (the higher frequencies) could be predicted from the existing collected results. This would present a wider "virtual" bandwidth curve without the issues involved in measuring the data directly.

If a technique for this method could be found which proved successful the time taken for measurements could be reduced and the noise incurred in high frequency measurements would be less of a factor.

### 4.1.2 Curve Symmetry Method

One method to predict the higher frequencies was proposed by Miss Yi He (of the Leicester group) in a paper released at the EIT conference in Graz in 2007. The paper presented the argument that the real impedance curve could be described as having rotational symmetry around Fr. [HE 2007]

The lower frequency results were used to provide a curve with the same angular properties as the higher frequency data. The dispersion frequency occurs when the gradient of the real impedance output curve is largest, and can be identified as a valley on the imaginary impedance graph. The paper presented several examples

where this method had been used to accurately predict the second half of the frequency range output.

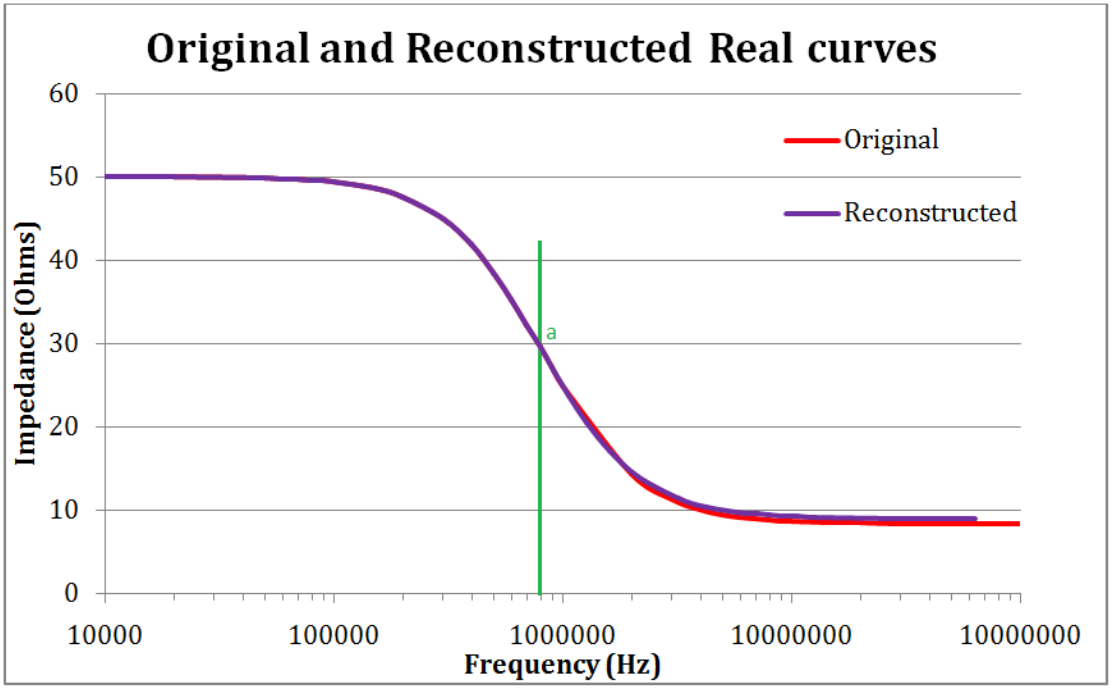


*Figure 4.2: The original and the reconstructed real components*

In Figure 4.2 the red line represents the original real component while the purple line shows the reconstructed real component. The dispersion frequency can be seen marked as a vertical green line, intersecting the curve at point 'a'.

The reconstructed output curve is very similar to the 'real' data; a calculated value for $R_S$ is only 0.5Ω greater than the measured 'real' value, an error of around 7 %.

Although this level of accuracy is acceptable, as the impedance values involved decrease this error will increase and could misrepresent the output.

Data collected from further EIT experiments showed that many of the curves produced were not symmetrical in nature. Any $R_R$, $R_S$ or C values calculated from data which was not accurate would be incorrect. An example of a less symmetrical graph is shown in Figure 4.3, the red line represents the actual output, while blue represents the reconstructed curve.

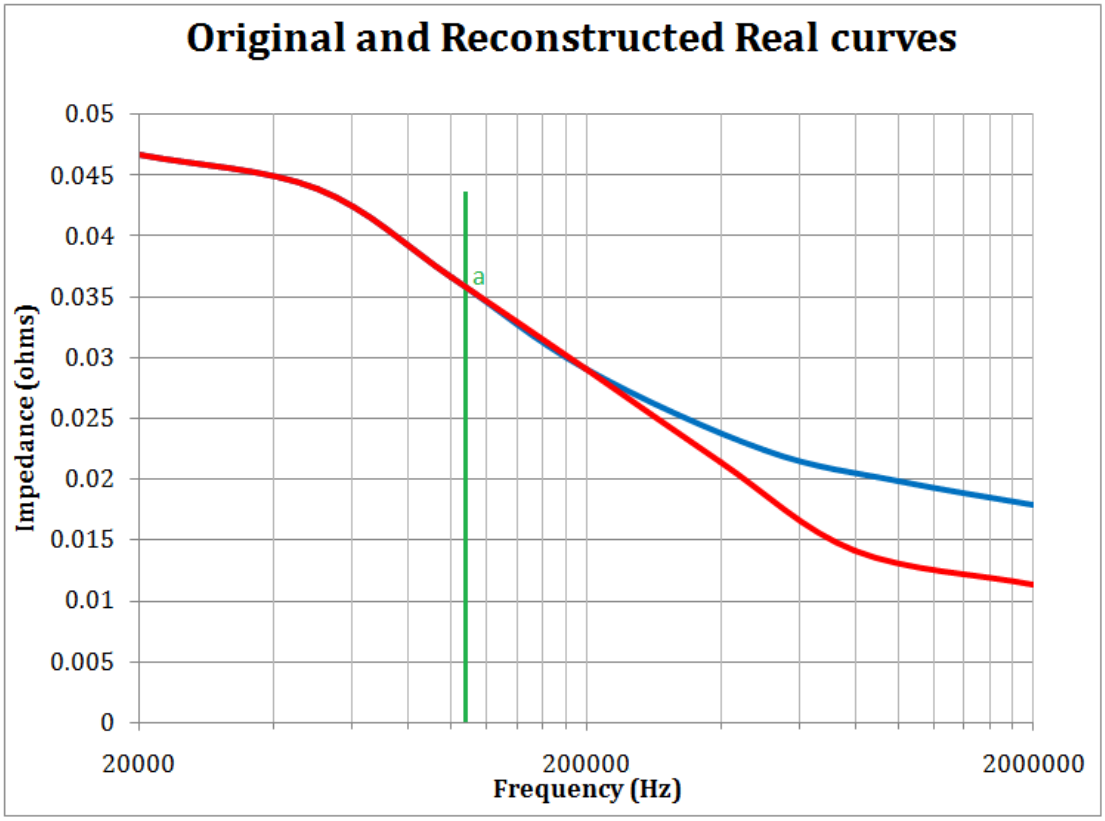


*Figure 4.3: Original and reconstructed curves provided from an EIT measurement, the error in the final value results in an $R_S$ error of 30%.*

A small change in the high frequency settle value can indicate a larger shift in the $R_S$ value; this is due to the parallel nature of the resistance. As $R_S$ increases in comparison to $R_R$ smaller differences in this final value have more of an effect on the reconstructed $R_S$ value and larger errors may be produced. Another issue with the results above is that the amplitude of the signal is below 0.05 ohms which would result in a low signal to noise ratio.

The paper concluded that the new 'symmetrical reconstruction' method provides a good alternative to the original method which can avoid the difficulties found from attempting to measure high frequency EIT data. However this short investigation suggests there are several flaws in its design and as such is not currently a suitable replacement for the original method.

### 4.1.3 3-Point Technique

Another approach investigated by the Leicester group was based on the graph produced by Salter in 1981. It was suggested that the locus for the complex impedance of biological tissue could be plotted along a circular arc. If the Real and Imaginary components of an impedance frequency sweep are plotted against each other, the result is a circular arc with its centre on or below the horizontal axis. [SALTER 1981, MCADAMS 1995]

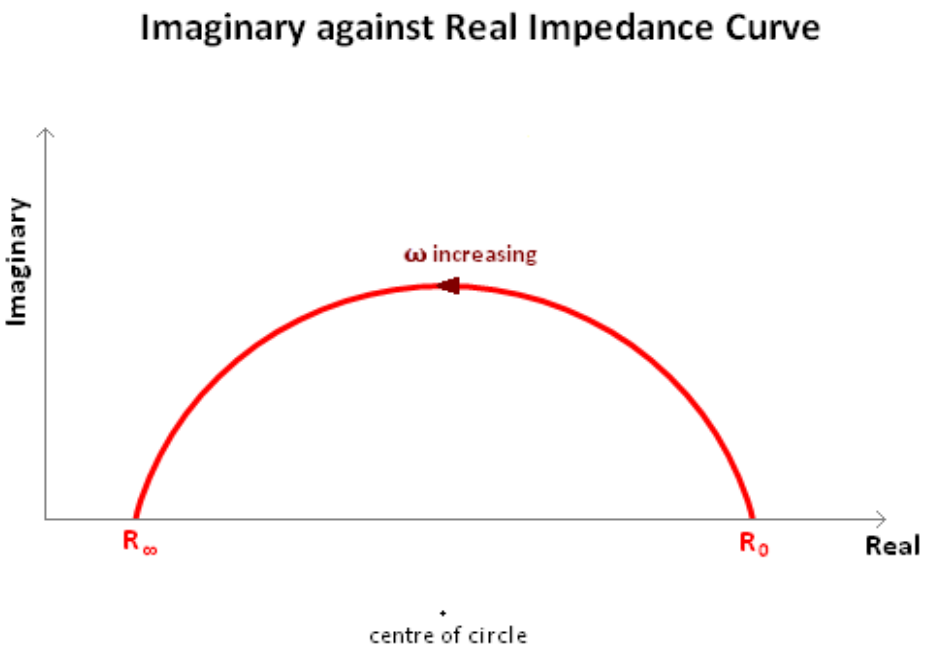


*Figure 4.4: A complex impedance plot showing the curve provided as angular frequency (ω) increases.*

The two intercepts on the curve describe the points where the impedance is purely resistive, these are $R_0$ and $R_\infty$. As the frequency increases the curve is drawn in an anti-clockwise direction. The circular arc is commonly described by the following equation, first published in by Cole in 1940.

$$Z = R_\infty + \frac{(R_0 - R_\infty)}{1 + (j\omega/\omega_0)^\alpha} \quad (4.1)$$

This equation describes the impedance (Z) in terms of the two purely resistive solutions, the angular frequency (ω) and the relaxation factor (α); the range of α is 0-1 (when α = 1 the centre of the circle is positioned on the real axis). [COLE 1940]

It was suggested that if this case were true then not all values needed to be measured, the whole curve could be plotted from measurements taken at only 3 frequencies; since a whole circle can be described from 3 points along its circumference using trigonometry.

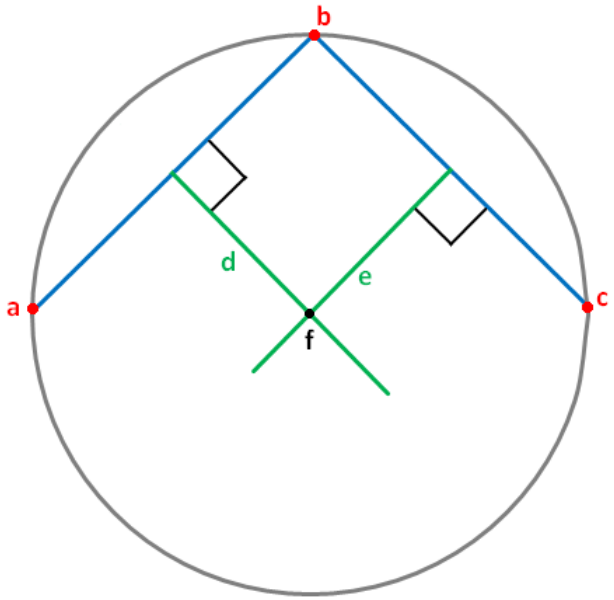


*Figure 4.5: Depiction of circle drawn from 3 points a, b and c*

Figure 4.5 shows how from 3 circumference points (a, b and c) the centre point and therefore the radius of a circle can be calculated. The loci 'ab' and 'bc' are plotted (in blue) which provide the angle and position of the perpendicular lines ('d' and 'e',

emerging halfway along the original loci) which cross to provide the centre position of the circle ‘f’. A radius can simply be calculated from the relative position of any of the original points.

This approach was discussed in detail by Tunstall, where it was argued that it would provide a fast technique for collecting an output for EIT while reducing the noise produced from the high frequency data collection. This would be a huge asset in EIT as it would allow much more accurate calculation of RSC values and overall more definition when comparing various cells. [SALTER 1981, TUNSTALL 2002]

The graph below shows the example used above drawn as real against imaginary. Also plotted is an approximation of the curve taken from 3 complex impedance measurements along the curve.

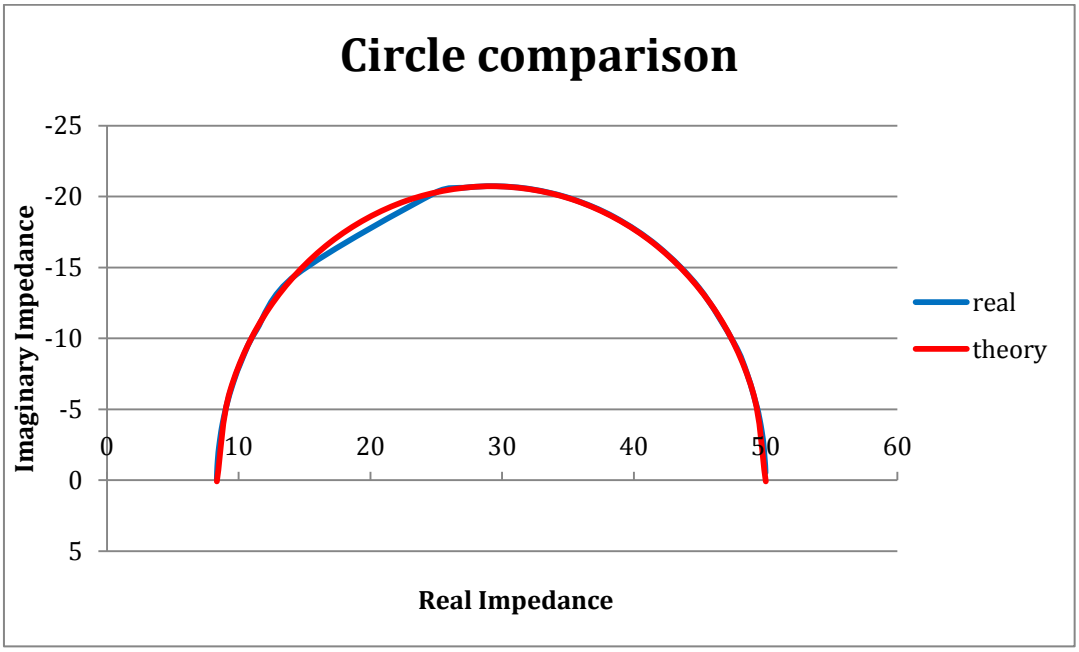


*Figure 4.6: comparing the two circles etc*

The graph clearly shows how the output from the 3-point technique can be very similar to the actual measured outputs. The graph above was created using three specially chosen frequency values (highest, lowest and median from the measured outputs), therefore the graph was expected to follow the actual curve closely, however since the technique was designed to provide the curve from a much smaller frequency range the above curve is not representative of the expected output from this technique. The curve below was reconstructed from 3 low frequency results, in an attempt to predict the higher frequency values:

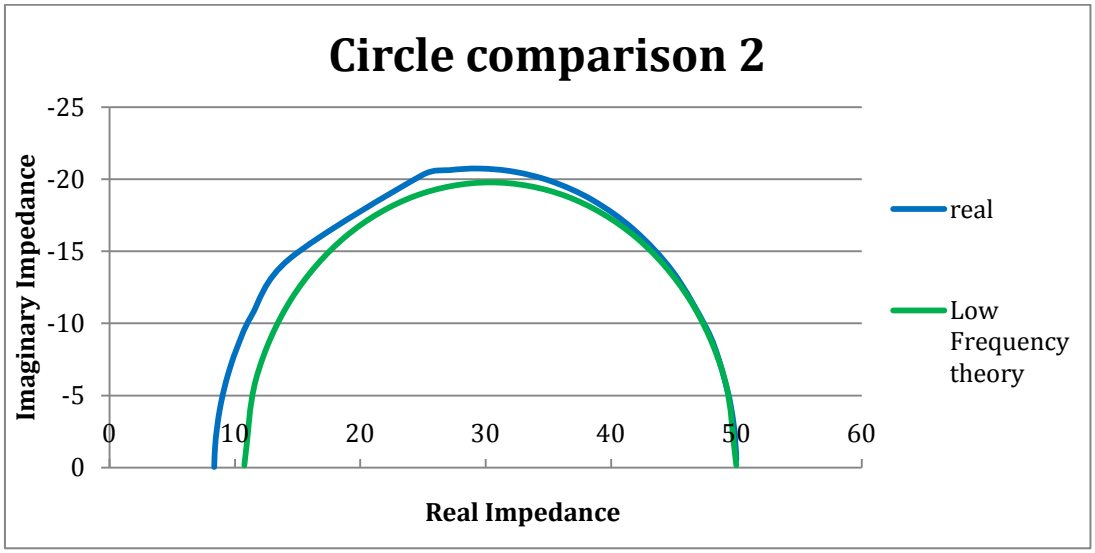


*Figure 4.7: comparison of 2nd circle from low frequency points*

It can be seen from Figure 4.7 that the selection of points used to create the output curve is very important when using this method, however in practise it would be impossible to know whether you were choosing the correct frequency measurements unless you had a 'correct' output curve to compare it to.

It is also clear to see that the real curves above are not perfectly circular, further EIT tests were ran using real data which clarified that the majority of output curves are not perfectly circular. This may be because the Salter curve assumes the nature of the measured sample to be that of the 3 element Cole-Cole model, since living cells do not apply to this model exactly the outputs are not exactly circular in nature, although it is possible to use a circle as a close approximation at times.

Another issue which may present a problem with this method is that spurious voltage spikes can be found at some frequencies. These are generally easy to compensate for by looking at the rest of the results and identifying and eliminating the spike, however if you have only collected limited results it would be difficult to know whether or not one of these measured results is a spike. If spiked data is measured, the reconstructed circle may be wildly inaccurate.

### 4.1.4 Frequency Prediction Issues

In theory, both of the frequency prediction techniques mentioned above are valid ideas for improving the efficiency and speed of frequency testing. These techniques could, in turn, improve the output image quality of some tests, particularly in-vitro experiments greatly. However, due to the large assumptions which are made in the proof of each approach any EIT system which used these techniques may suffer from large inaccuracies produced in the output. These methods could not be used within medical testing where the margin for errors is small.

Since no usable improved method has been discovered with either of these techniques, frequencies up to 1.3 times Fr need to be individually tested in order to create an accurate EIT image and the problems outlined previously all still apply. Therefore it may be a good idea to look into alternative methods of treating the signal.

## 4.2 Modelling in the Time Domain

It was suggested that a transient response may offer an alternative approach to acquiring the impedance data as it allows measurements to be taken in the time domain. The electrical properties of linear and time-invariant objects are exactly the same when measured in time and frequency domain [PLIQUETT 2000]. Time domain measurements therefore should be able to provide useful results over a wide bandwidth in the form of Cole-Cole parameters, although this bandwidth would still be restricted by the equipment used [PLIQUET 2011]. It was further suggested that the frequency response, while often providing good results for RSC values, only takes into account the response of the circuit following the point when the signal has settled on a value, therefore such testing is limited and does not take into account the full response of the sample.

Due to the nature of electronic elements it is clear that a signal cannot simply appear at a certain level. A signal fluctuates or simply increases until it reaches a settling point where the various impedances and inputs are satisfied.

It was thought that there may be some useful diagnostic data to be extracted from the characteristics of the signal fluctuation before the final settled value is reached. Therefore rather than testing the data over a frequency range it could be tested over time, from the point of initial current input until the settled signal is realised.

Clearly this happens almost instantly and the measurements would be difficult to complete. It does mean the tests will be relatively quicker to run than the frequency equivalent as it is recording immediately as opposed to waiting for the settled output before taking a reading. This wait is only a matter of microseconds, however no repetitions at varying frequencies are required, reducing the time for testing further.

Signal to noise ratio is better when considering the frequency domain as often in the time domain the step slopes required can be heavily affected by noise [PLIQUETT 2011]. However there are circumstances when frequency domain measurements are not suited to the application. Time-domain impedance measurements are often completed in situations where fast impedance changes occur as the measurements are quicker to complete [YAMAMOTO 1996, MIN 2008, MIN 2009]. Furthermore it has been suggested that time domain measurements can be advantageous if long cables are required within a wide frequency range system [PLIQUETT 2007].

Several direct comparisons between time and frequency domain measurements have been published [PLIQUETT 2000, PLIQUETT 2011, JARON 1968]. Several of these examples state that the time domain method is preferred in practise, largely due to the speed of the measurements [ALTMANN 2004, BRUCE 2008]. An investigation was completed which tried various methods for screening for heart disease which included both time and frequency domain results, time

domain output was shown to be better and they found a way of combining the various methods to give an improved detection rate [HEITMANN 2009].

There are various techniques for completing time domain testing, one of the highly investigated parts of the system is the choice of input signal, often simply a step or pulse function is used [JARON 1968, ALTMANN 2004, YAMAMOTO 1996, PLIQUETT 2007], however one research group has compared several options and discovered that a chirp signal was preferable for their system [MIN 2008, MIN 2009, MIN 2011].

The various investigations described show that the transient approach can yield impressive results and in some cases can be an improvement on the frequency domain approach. The Leicester group had not investigated this area before and therefore the aim was to produce a time-domain test unit which could be directly compared to the existing frequency-domain EIT system already being used by the group.

### 4.2.1 Derivation of Component Values

In order to investigate a transient approach which could be comparable to frequency EIT several tests were set up to measure the response of this suggested idea. The first of these was a Matlab simulation to show an explanation for the theory.

The transfer function of the Cole-Cole model is described below

$$\frac{1}{Z} = \frac{(R_R + R_S)Cs + 1}{R_R R_S Cs + R_R} \quad (4.2)$$

This transfer function was to be entered into Simulink with an input step function to provide a transient output, however the simulated equations need to match the experimental data and due to the nature of the circuit a load resistor was required to allow the output voltage from the Cole-Cole circuit to be measured:

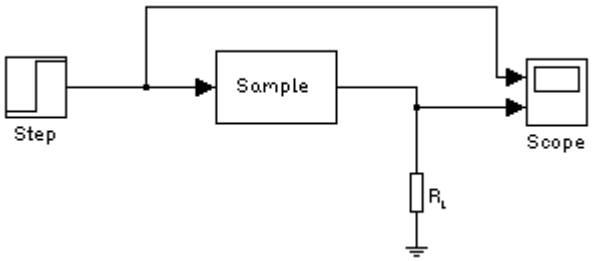


*Figure 4.8: Simulink system diagram*

A step function input is a form of direct current therefore, as discussed in chapter 3, the current must be restricted for safety reasons if the equipment is to be used on living tissue. [BSI 1989]

In order to compare the results collected to a Matlab simulation the Load Resistor $R_L$ needs to be taken into account. Practically there would be contact impedances between the input and the tissue, described below as a Cole-Cole model, however this provides further unknowns into the mathematical model and therefore in this

investigation these impedances are assumed to be negligible, this is discussed further in chapter 4.3.4.

Therefore a new Transfer function must be calculated which incorporates this load resistance.

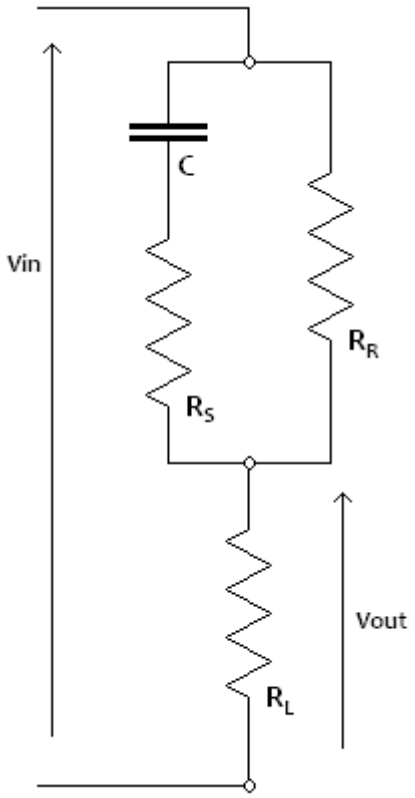


*Figure 4.9: The potential divider provided by the Cole-Cole model and load resistance $R_L$*

The transfer function can be calculated as a potential divider.

$$F(s) = \frac{(R_R.R_L + R_S.R_L)Cs + R_L}{(R_R.R_L + R_R.R_S + R_S.R_L)Cs + R_R + R_L} \quad (4.3)$$

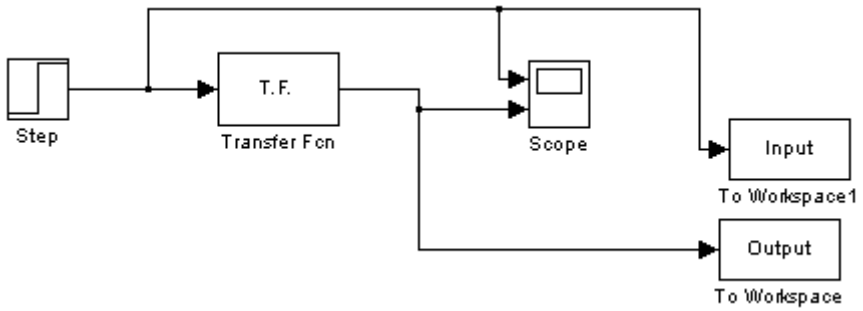


*Figure 4.10: Simulink system diagram*

The output was collected and plotted, an example of which can be seen below.

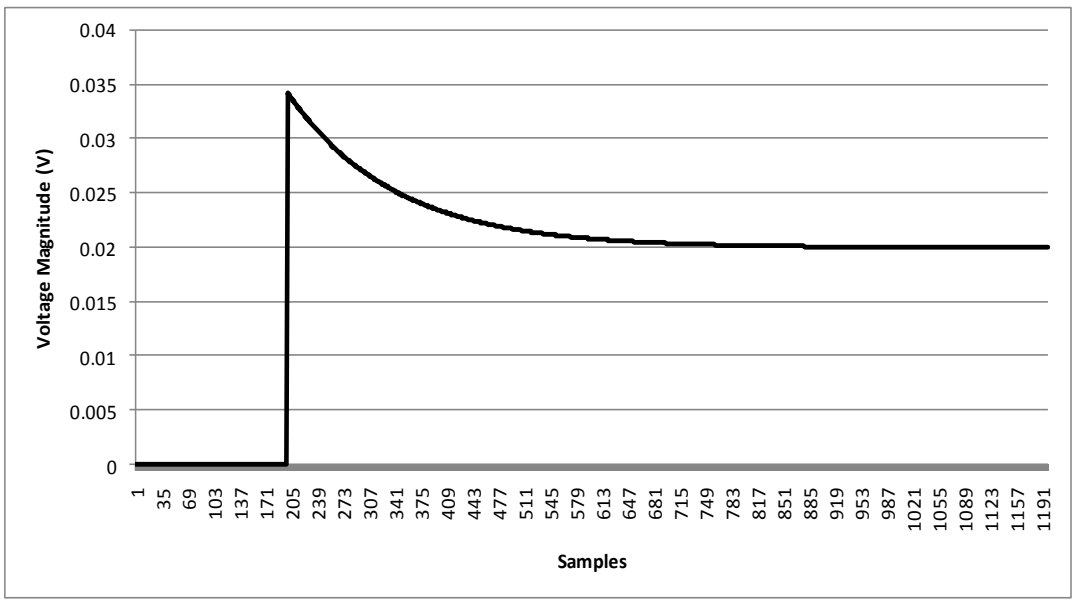


*Figure 4.11: Output from simulink*

The input step was activated at sample 201, the graph shows a similar output to the expected curve; an initial peak which dropped exponentially to a lower settled value.

From this Transfer Function it was possible to work backwards and provide some mathematical working to show values of $R_R$, $R_S$ and C within this particular model.

The following equations describe the theory behind the programming within Matlab which was used to describe the above output curve. It includes methods of working backwards from the Transfer Function to achieve values for the $R_R$, $R_S$ and C values found in the original Cole-Cole circuit, assuming $R_L$ is a known value.

Rearranging the Transfer function gives

$$F(s) = \frac{(R_R + R_S)Cs + 1}{\left(R_R + R_S + \frac{R_R.R_S}{R_L}\right)Cs + \frac{R_R}{R_L} + 1} \qquad (4.4)$$

The Transfer function shown above can be written in a simplified form as

$$\frac{1}{Z} = \frac{Xs + 1}{Ys + Z} \qquad (4.5)$$

Where the following equations apply

$$X = (R_R + R_S) \times C \tag{4.6}$$

$$Y = \left(R_R + R_S + \frac{R_R.R_S}{R_L}\right) \times C \tag{4.7}$$

$$Z = \frac{R_R}{R_L} + 1 \tag{4.8}$$

A step input is then applied

$$\frac{Xs + 1}{Ys + Z} . \frac{1}{s} \tag{4.9}$$

This equation can be re-arranged into the following form which can be used to produce an inverse Laplace transform

$$F(s) = \frac{1}{Z} . \frac{1}{s} + \frac{XZ - Y}{YZ} . \frac{1}{s + {}^{Z}/_{Y}} \tag{4.10}$$

An inverse Laplace transform can be used to convert the frequency domain into the time domain

$$f(t) = \mathcal{L}^{-1}\{F(s)\} \tag{4.11}$$

$$f(t) = \mathcal{L}^{-1}\left\{\frac{1}{Z}.\frac{1}{s} + \frac{XZ-Y}{YZ}.\frac{1}{s+{}^{Z}/_{Y}}\right\} \tag{4.12}$$

The two separate functions within F(s) can be solved individually

$$f(t) = \mathcal{L}^{-1}\left\{\frac{1}{Z}.\frac{1}{s}\right\} + \mathcal{L}^{-1}\left\{\frac{XZ-Y}{YZ}.\frac{1}{s+{}^{Z}/_{Y}}\right\} \tag{4.13}$$

Any constants involved can be taken out of the Laplace function

$$f(t) = \frac{1}{Z}.\mathcal{L}^{-1}\left\{\frac{1}{s}\right\} + \frac{XZ-Y}{YZ}.\mathcal{L}^{-1}\left\{\frac{1}{s+{}^{Z}/_{Y}}\right\} \tag{4.14}$$

The inverse Laplace solutions are as follows

$$\mathcal{L}^{-1}\left\{\frac{1}{s}\right\} = 1 \tag{4.15}$$

$$\mathcal{L}^{-1}\left\{\frac{1}{s+{}^{Z}/_{Y}}\right\} = e^{-(Z/Y)t} \tag{4.16}$$

The complete inverse Laplace transform creates the exponential function below

$$f(t) = \frac{1}{Z} + \frac{XZ - Y}{YZ}.e^{-(Z/Y)t} \tag{4.17}$$

The steady state value

When t = ∞, the exponential will have settled to its final value, $e^{\infty} = 0$

$$f(t = \infty) = \frac{1}{Z} \tag{4.18}$$

Which represents

$$f(\infty) = \frac{1}{Z} = \frac{R_L}{R_R + R_L} \tag{4.19}$$

The peak

When t = 0, the input step begins and therefore this is the point where the initial peak can be seen from the output since $e^0 = 1$

$$f(t=0) = \frac{1}{Z} + \frac{XZ - Y}{YZ} = \frac{X}{Y} \tag{4.20}$$

Which represents in terms of $R_R$ and $R_S$

$$f(0) = \frac{X}{Y} = \frac{R_R R_L + R_S R_L}{R_R R_L + R_R R_S + R_S R_L} \tag{4.21}$$

The Capacitance value

The peak and settled values can be used to find values for the $R_R$ and $R_S$, the capacitance value, however, is determined by the curve of the output.

The curve can be rewritten as:

$$f(t) = f(0)e^{-\frac{t}{\tau}} \tag{4.22}$$

Where

$$\tau = \frac{Y}{Z} \tag{4.23}$$

And $V_0$ represents the height of the exponential curve (a-b in the below diagram)

When t = τ:

$$f(t) = f(\tau) = V_0 e^{-1} = 0.3679 V_0 \tag{4.24}$$

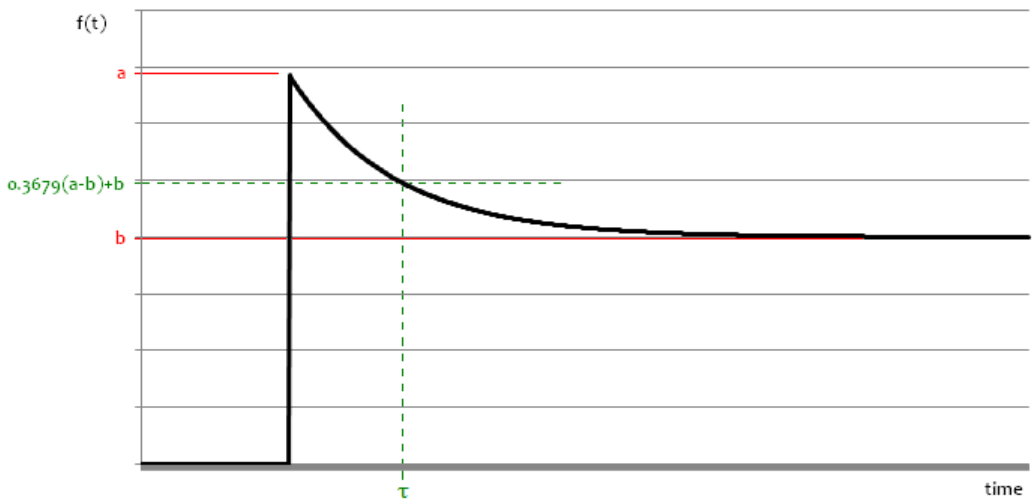


*Figure 4.12: Calculations on exponential curve output*

Tau (τ) is the time constant where the output voltage is approximately 1/3 from the bottom of the curve.

$$f(\tau) = 0.3679(a - b) + b \tag{4.25}$$

It can be seen from the above equations that

$$a = f(0) \tag{4.26}$$

$$b = f(\infty) \tag{4.27}$$

Therefore

$$f(\tau) = 0.3679\big(f(0) - f(\infty)\big) + f(\infty) \tag{4.28}$$

Using this calculation a value for τ can be read off the output graph. As shown previously.

$$\tau = \frac{Y}{Z} = \frac{\left(R_R + R_S + \frac{R_R.R_S}{R_L}\right) \times C}{\frac{R_R}{R_L} + 1} \tag{4.29}$$

The capacitance can then be found from:

$$C = \tau \frac{(R_R + R_L)}{(R_R.R_S + R_R.R_L + R_S.R_L)} \quad (4.30)$$

With these theoretical curve properties the $R_R$, $R_S$ and C values could be derived directly from results taken in a transient experiment.

A program to simulate the data acquisition model was written in Simulink as shown in Figure 4.8. This was tested using a number of Cole-Cole parameters to provide the transfer function. All simulations of the above mathematics provided accurate outputs which tallied with the theoretical work done previously. Further investigations were planned to test the model using real life components, these are described in the following chapters.

## 4.3 Experimental Tests

Tests were set up which would allow the existing Leicester group frequency EIT system to be compared directly with a new transient approach using the theory proven above. The transient set-up was designed to use similar hardware to the existing system in order to make the overall comparison clearer.

### 4.3.1 Frequency Domain Test Set Up

The Frequency tests were run using the existing equipment within the Leicester group.

An HP4194 Impedance Analyser was used to collect the impedance data over a chosen frequency range. The analyser was programmed in Agilent Vee to provide the real and imaginary values from 1 kHz to 12 MHz. [WANG L 2006]

The Analyser provides a differential current output and measures a differential voltage input which it uses to calculate the impedances. For the electronic phantoms the input to the RSC circuit were connected via the HP 16047D test fixture which allows the differential signals to be applied through two terminals.

For the vegetable matter tests a test unit designed by the DMU group was used which allows the pairing of two needle electrodes with two non-invasive electrodes to penetrate the sample injecting the different current and receive the voltage for analysis. [WANG W 2006a, WANG W 2006b]

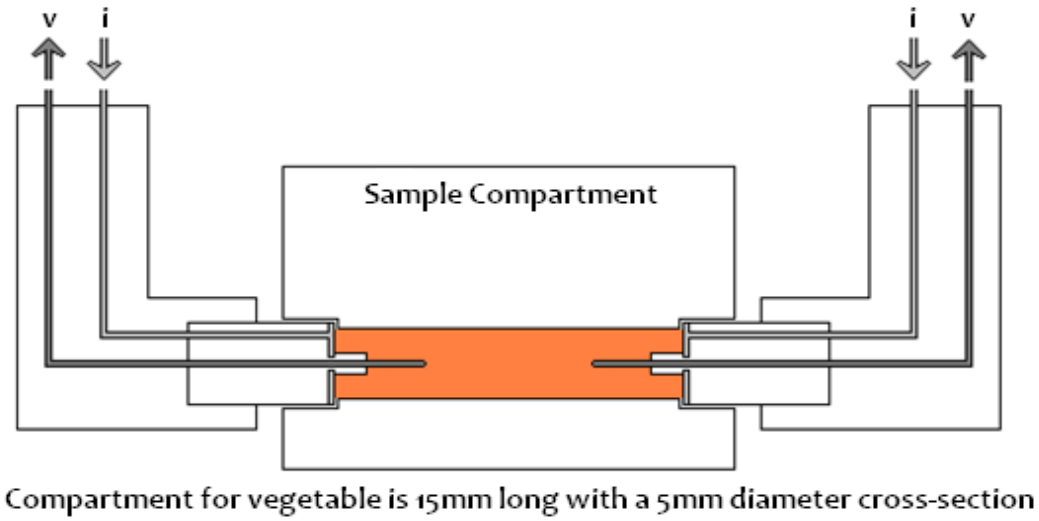


*Figure 4.13: In-vitro testing compartment*
*(differential current input and differential voltage output can be seen)*

Figure 4.13 shows the test unit, the channel for the sample is shaded orange; the two electrode pairs can be seen at either end of this channel connected to the inputs and outputs.

The results were recorded by the analyser and saved, via an Agilent Vee program written for a previous investigation within the Leicester group, onto a computer for analysis.

The Cole-Cole model parameters are calculated using a program provided by Leicester group member G. Sze. This program takes the measured real and imaginary values at various frequencies and outputs values for $R_R$, $R_S$, C, Fr and α (described in chapter 4.1.3). The program completes this task by utilising a Matlab function called

'fminsearch' which requires initial estimates for parameters which can be refined to fit a desired equation.

The equation used within this program is Cole's equation published in 1940, shown previously in this thesis as equation 4. The equation is a function of $R_R$, $R_S$, Fr and alpha, therefore initial estimates for these parameters are required [COLE 1940].

The $R_R$ estimate is taken from an average of the 3 real values recorded at the lowest frequencies, essentially this is the f(0) point on the real curve which, as described in Chapter 2.5.3, is represented by $R_R$. The program was designed for use within a breast screening system; therefore the initial $R_S$ estimate is based on the value of the impedance of 'stroma' tissue within a human breast. The measurements described by Wang in 2001 show that this initial estimate can be set at 0.1. It was suggested that this may provide room for error in applications outside of mammography measurements, however initial tests suggested this would not be the case [WANG 2001]. The Fr estimate is taken as the centre peak of the imaginary curve while since alpha should be between 0 and 1 an initial estimate of 0.1 is used.

These estimations are used as inputs for the 'fminsearch' function which provides optimised values for these parameters which are refined to provide a best fit for Cole's equation (shown previously as equation 4.1).

The capacitance described in the Cole-Cole model is directly related to the other parameters and the program calculates its value using the following equation which was provided by the Leicester group:

$$C = \frac{1}{2\pi(R+S)Fr} \tag{4.31}$$

The work in this chapter compares $R_R$, $R_S$ and C parameters, while further investigations described in Chapter 5 record both Fr and alpha also.

Currently this has proved to be the most reliable process for calculating the Cole-Cole parameters within the Leicester group, however errors can occur if the initial estimations are particularly inaccurate or if the frequency range of the measured data is low.

### 4.3.2 Time Domain Test Set Up

The transient tests were run using NI LabVIEW and an NI PXI board chassis, LabVIEW was programmed to provide a step input via the PXI arbitrary function generator (board number: PXI-4406). The output was recorded by the PXI Multichannel Analogue Input board (PXI-6259) within the chassis and saved directly onto LabVIEW for analysis.

A series resistor was used to bridge the sample output to ground with a constant impedance value which would allow the changing voltage across the sample to be collected. The set-up diagram below shows the placement of this resistor.

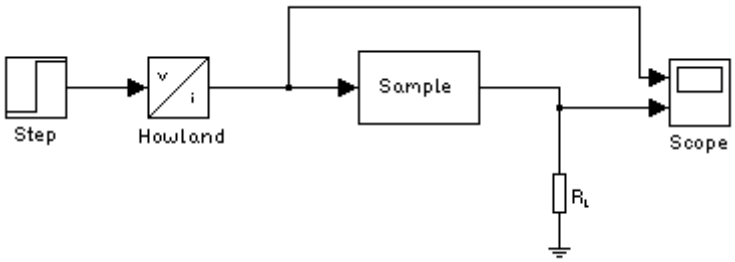


*Figure 4.14: Simulink system diagram*

The voltage step was driven into an optimised version of the Improved Howland model (as described in Chapter 3) to provide a current step input. The step signal generator and the scope were both built into the NI PXI chassis. The first scope input provides the output from the Signal Generator while 2$^{nd}$ one measures the drop output of the test sample.

The generated step function signal was used to test the same electronic phantoms and samples as used in the frequency tests in order to provide a direct comparison between the two.

The test unit block used in the frequency tests was modified for use in the transient experiments; the newer version had only 1 input and output as there were no differential voltages.

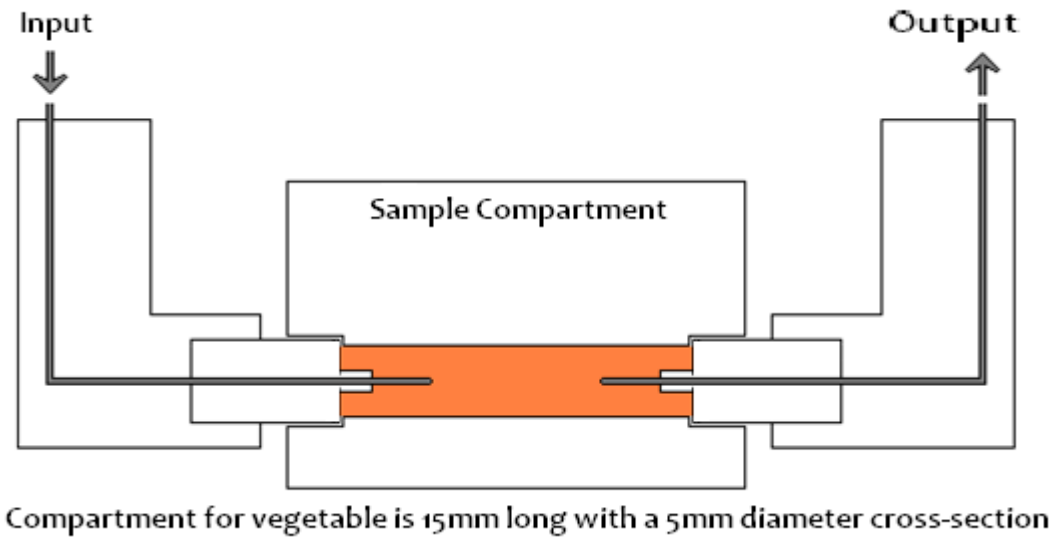


*Figure 4.15: Modified in-vitro testing compartment*

### 4.3.3 Electronic Phantom

Two electronic Cole-Cole phantoms were made to test the respective outputs from frequency and transient testing. The phantoms were simple 3 component circuits containing the $R_R$, $R_S$ and C found in the Cole-Cole model, the values for each are found in Table 4.1. $R_L$ in each model was 51Ω.

*Table 4.1: Real values of the two electronic phantoms*

| | Phantom 1 | Phantom 2 |
|---|---|---|
| $R_R$ | 51Ω | 130Ω |
| $R_S$ | 9Ω | 12Ω |
| C | 3.3nF | 33nF |

The experiments were setup as described earlier and output curve for the time-domain method was realised. It can be seen in figure 4.17.

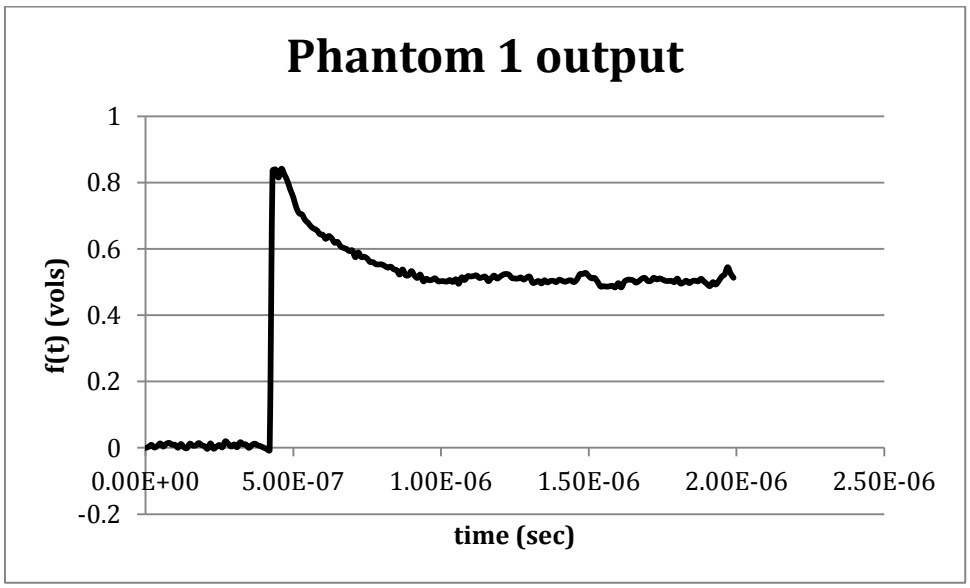


*Figure 4.16 Output from time-domain test of 1st electronic phantom*

Values for f(0) and f(∞) can be read from the curve in Figure 4.16 as 0.84 V and 0.51 V respectively. From equation (4.28) a value for f(τ) can then be calculated as 0.63 which corresponds to a τ value of 2.1E-7.

$R_R$, $R_S$ and C values can be calculated from re-arranged the equations previously described:

$$R_R = \frac{\left(1 - f(\infty)\right) \times R_L}{f(\infty)} = \frac{(1 - 0.84) \times 51}{0.84} = 9.7\ \Omega \qquad (4.32)$$

$$R_S = \frac{R_R R_L - f(0) R_R R_L}{f(0) R_L + f(0) R_R - R_L} = \frac{(9.7 \times 51) - (0.84 \times 9.7 \times 51)}{(0.84 \times 51) + (0.84 \times 9.7) - 51} = 11.8\ \Omega \qquad (4.33)$$

$$C = \frac{\tau \times (R_R + R_L)}{R_R R_L + R_R R_S + R_S R_L} = \frac{2.1^{-7} \times (9.7 + 51)}{(9.7 \times 51) + (9.7 \times 11.8) + (11.8 \times 51)} = 5.79\ \text{nF} \qquad (4.34)$$

The same method was used to calculate the impedance values for the second electronic phantom. Table 4.2 shows the calculated impedance values from both of these tests.

*Table 4.2: Calculated values of the two electronic phantoms, using transient approach*

| | Phantom 1 | Phantom 2 |
|---|---|---|
| $R_R$ | 49.7Ω | 21.8Ω |
| $R_S$ | 11.8Ω | 13.6Ω |
| C | 4.9nF | 18.4nF |

It is clear that these results are not very accurate, for Phantom 1 $R_R$ and $R_S$ are relatively good values, while C is quite far removed from the correct value. The output for Phantom 2 provides less impressive results, the $R_S$ value is fairly similar to the correct value, however this value relies on the value of $R_R$, and this is wildly incorrect, suggesting the accuracy of $R_S$ is more coincidental, the capacitance calculated for this phantom is almost half the expected value.

More traditional EIT measurements using frequency analysis were also recorded using The Leicester Group's Impedance Analyser system and existing RSC extraction software. Table 4.3 shows the final results from this method for comparison.

*Table 4.3: Calculated values of the two electronic phantoms, using a traditional EIT approach*

| | Phantom 1 | Phantom 2 |
|---|---|---|
| $R_R$ | 51Ω | 131.4Ω |
| $R_S$ | 8.9Ω | 14.2Ω |
| C | 2.7nF | 34nF |

The values extracted from the frequency method are much nearer to the actual values.

From these two sets of results it appears that the frequency test results are much closer to the expected values, with an average error of only 6.96% percent, compared to 37.16% percent for the transient results.

### 4.3.4 Discussions

The results above describe inaccuracies in the output of the transient tests on the known electronic phantom values. There are several reasons for these issues, the main problem being that the input square wave was of poor quality. All calculations were based on the assumption of a square wave input, however the best input curve achieved from the NI LabVIEW equipment was not strictly square. The graph below describes the input wave achieved for these tests.

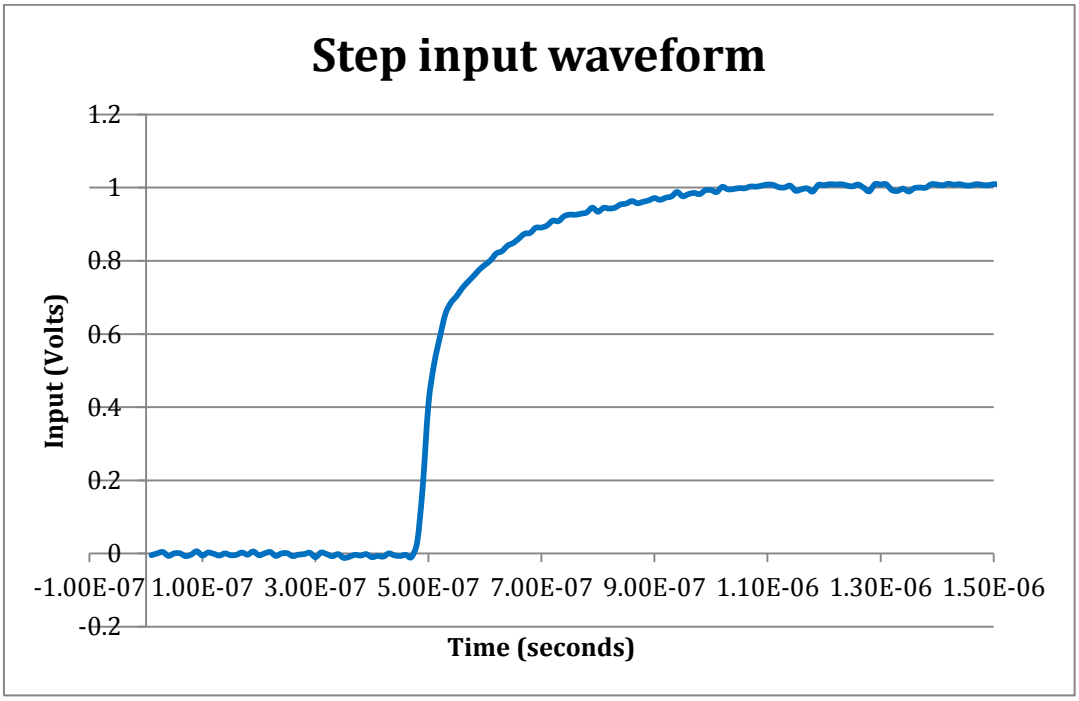


*Figure 4.17: Input square wave achieved from LabVIEW generator with a smoothing filter, produced at a sample rate of 1E-8 $s^{-1}$.*

As can be seen the initial step from 0 to 1V is not a simple step, rather a curve which needs further time to settle at the expected 1V final value. Due to this, the output value peak at the initial f(0) point is compromised and does not work within the set equations proven with the theoretical step in Matlab.

If this square wave were closer matched to the theoretical equivalent the following mathematics should have provided much more accurate output values. Unfortunately due to the large difference of this it is difficult to suggest where other errors occur as it cannot be certain how inaccurate the results would be had this input been of better quality. Several different function generators were used during

initial experiments including a Blackstar Function Generator Jupiter 500, however the NI PXI Arbitrary Waveform Generator (AWG) was chosen as it can be controlled through LabVIEW and therefore allowed the whole system to be integrated within one program.

It was expected, however that the final value for f(∞) would be correct, and therefore provide a good value for $R_R$ as this value relies only on the value of $R_L$ and f(∞), this appeared to be the case in the first phantom test, however the following tests did not continue this trend. This detail infers that there were other errors inherent in the system which could not be fully observed due to the input. One suggestion for this error is that the electrode-skin contact impedance would affect the results. This variable was not included in the mathematical model as it would have increased the number of unknowns and made the equations impossible to solve, however in a practical situation it may have a considerable effect.

In comparison the frequency results for the phantom tests were more accurate and suggest that the standard EIT method is of high quality and very reliable

## 4.4 Comparing the time domain approach

Following the completion of the above tests several discussion topics are apparent which can be used to compare the techniques and essentially decide the fate of transient testing.

### 4.4.1 Advantages

The equipment, when compared to Frequency testing, is a lot cheaper, NI Labview can run on a standard PC, and is much more portable.

The mathematical model is simple and the calculations to provide values for $R_R$, $R_S$ and C are simple in comparison with the frequency testing. The tests completed in this chapter did not involve any imaging of the results and therefore Cole-Cole parameter values can be acquired very quickly.

The time domain tests are very simple to run, operator training would be straightforward as the LabVIEW program handles nearly all of the functions. A simple front end could be designed so that the operator would not need to worry about any of the background calculations.

The frequency domain tests used a network analyser for data acquisition. The program required to communicate with the analyser is not capable of the complex mathematics used to calculate the final parameter values therefore the data needs to be transferred to a separate program for analysis. This may allow further opportunities for human error, in comparison the time domain tests were completed entirely within LabVIEW.

### 4.4.2 Shortcomings

Currently it is difficult to provide an accurate step input, however perhaps a larger budget may allow this to be achieved using state-of-the-art wave generators. The system described provided a spike at f(0) which was smoothed with a filter at the output, this filter overcompensated and the curve shown above was the best output achieved.

Figure 4.18 shows the input step function before and after the filter compensation.

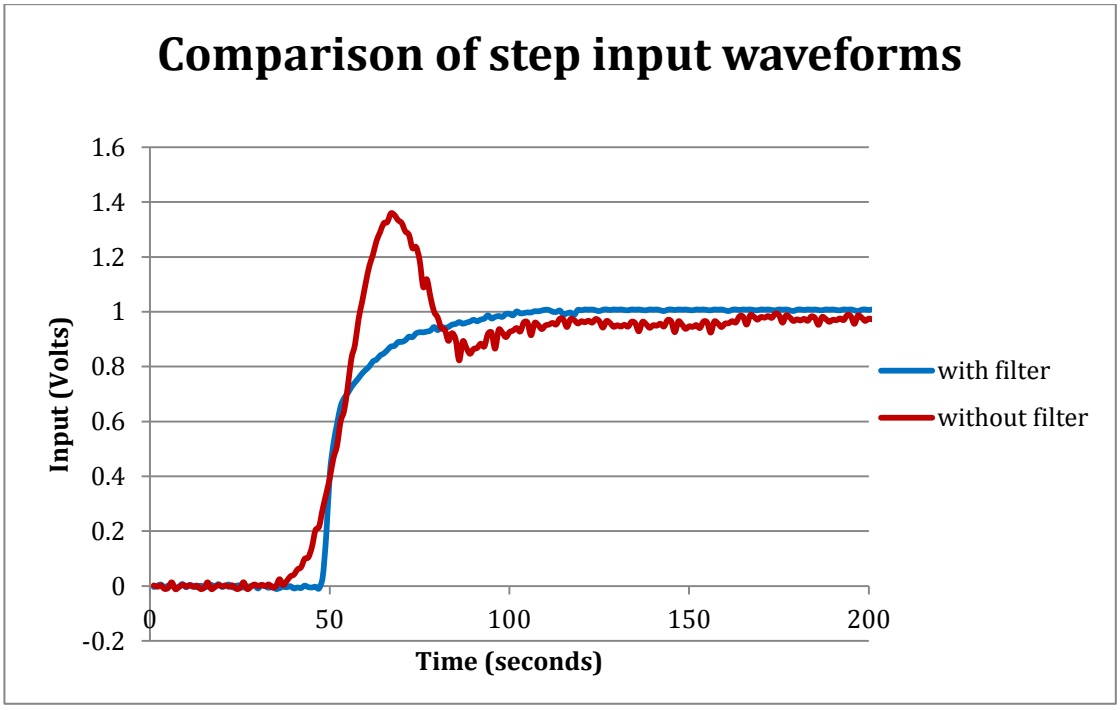


*Figure 4.18: Input waveforms produced by the NI LabVIEW arbitrary waveform generator with and without a smoothing filter*

It was shown empirically that the results from the smooth filtered input were far superior to those from the un-filtered spike input. However this is still a concern as the results are affected by the inaccuracies of the input signal.

If the error at the input cannot be reduced; the mathematical model described will not give the correct output.

### 4.4.3 Conclusions

Currently the transient results do not provide the correct output, although there are advantages over the standard frequency method, without further improvements the technique cannot be used.

The major drawback with the transient process is the input signal. With more time spent on the system it may be possible to reduce the inaccuracies in the waveform by improving the filter at the input. Alternatively further work could be used to develop an approach in which the curve input is highly repeatable and could be compensated for within the mathematics. Through this approach the transient sweep may still prove a useful diagnostic approach as mathematically all Cole-Cole parameters can be obtained from a step function.

There is a real possibility that with improved equipment this approach could achieve accurate Cole-Cole parameters, although from the tests described here the frequency domain method provides superior results. It is suggested that possibly

using both frequency and transient techniques together may provide enough information to solve any issues found with the individual approaches.

Chapter 5 describes an investigation using a traditional frequency approach to EIT, the aim in this work is to distinguish between normal and cancerous cells within mouse pancreata. In-vitro tests were completed using three different techniques. Promising initial results suggest that the EIT can provide a successful diagnostic solution for this research.

# Chapter 5 Micro Impedance Measurements

The Leicester group collaborated with a group from Warwick University to investigate cancer within mouse pancreatic cells. This work was intended to distinguish cancerous cells from normal cells within the pancreas. Two separate ideas were eventually tested, one testing the whole pancreas with an electrode array, while the other tested individual pancreatic islets (collection of hormone producing cells).

The islet testing used 2 different techniques; one was based on patch clamping and used a micro-electrode; the other incorporated a manufactured Micro Electrode Array (MEA).

The author was project manager for the islet testing completed within the EPRSC project. All tests in this piece of work were planned, organised, completed and analysed by the author. Other members of the team were involved in completing the tests, in particular Guofeng Qiao and Linda Cheung.

The whole pancreas testing was managed by G. Qiao. L. Cheung and the author were heavily involved in planning and completing the tests. G. Qiao was responsible for the design of the test apparatus for these tests. Analysis of these results were completed by G. Qiao and Gerald Sze.

Preliminary results from this study were published in 2008. [WANG 2008]

## 5.1 EPSRC Project

A group at Warwick University has been investigating cancer within mouse pancreata as it is known that this disease acts in a similar way to tumours developed in humans.

In the mouse pancreas are groups of cells referred to as 'Islets of Langerhans', these islets contain different types of cells, one of which, beta cells, manufacture an important protein known as c-Myc. This protein becomes active under cancerous conditions; the Warwick group has developed a method of turning this activity on and off. [PELENGARIS 2002, PELENGARIS 2004]

Tumours regress almost entirely when this activity is turned off. The aim of their research was to force all the cancerous cells to regress to a normal state by turning off this protein's activity, which would in effect cure the cancer. A small number of the cells (called "escapers") resist the treatment and continue to grow. The group wished to investigate the properties of these cells in order to learn more about why they can resist the treatment and how they can be treated in order to cure the cancer completely. [PELENGARIS 2006]

Unfortunately since there are hundreds of islets within each mouse pancreas and thousands of beta cells within each islet, the search for these escapers is long and

difficult. The current technique is to dissect the islet into slices which can then be dyed and viewed under a microscope. This process is expensive. It also kills and damages the pancreas cells; so making any further tests on them practically impossible. This dissection process confirmed that the majority of the islets are found at the head of the pancreas, with none being found in the tail.

EIT was pursued as a method for locating 'escaper' cells as it had been suggested that the technique may be able to distinguish between cell types without making direct contact with the cells themselves. The objective was to use EIT to identify and locate the cells within the pancreas so that they could then be extracted for investigation. EIT's non-invasive nature would leave the cells undamaged following the scan so further testing after identification would not be compromised.

Fully grown mice pancreata can differ in length from around 20mm to 50mm and also vary in shape. The majority of those tested within this research however were around 25-30mm, as can be seen in figure 5.1. The Islets of Langerhans, which contain the escaper cells measure on average 150µm in diameter. Clearly due to the size of the islets the differences in the output readings will be minimal making the whole task very difficult as a high level of accuracy will be vital. [PELENGARIS 2006]


*Figure 5.1: Image showing size of an extracted pancreas, it is clear to see the pancreas is around 25mm, samples tested ranged from 23mm to 31mm in length.*

Ideally the whole mouse would be scanned and the cells located in-vivo. The cells would still be alive when the researchers look into why they did not regress.

Unfortunately, the pancreas is very small compared to the mouse and is often found in a slightly different position within the mouse's body. It is also surrounded by larger organs, making measurements challenging. For this research the pancreata were extracted with the EIT search done *in-vitro*. *In-vivo* studies were planned for later, when (and if) the measurement approach had been demonstrated.

## 5.2 Whole Pancreas Testing

The initial pancreas testing was designed to scan the whole extracted mouse pancreas using a specially designed test unit. The results were captured by computer for analysis.

The test unit applied the drive and receive electrodes in a linear formation along the pancreas. The electrodes were designed to both drive and receive the signal which was programmed using the computer based software, LabVIEW. The results from cancerous and normal pancreata could then be compared to show if a difference could be identified by EIT testing.

The tests were run using fully healthy and fully cancerous pancreata in order to show an initial distinction. It was intended that further tests could be done towards identifying, the more difficult to locate, escaper cells once the initial results had provided a promising outcome.

Over the course of experimentation the system went through several iterations, the final test system ran entirely using NI Labview. Two programs were designed and built, one which controlled the temperature of a heating system which elevated the test unit to replicate mouse body temperature, while the second was used to inject a differential current and receive a differential voltage via the electrodes. All results were saved through this program as real and imaginary impedance data.

### 5.2.1 Whole Pancreas Test Unit

A unit was designed by the Leicester Group to hold the pancreas and apply the electrodes in the same position to each sample of tissue. This unit had two separate parts; an upper, detachable, compartment containing the electrodes and a groove for positioning and easy access to the pancreata, the lower, base, part allowed a

connection from an NI Chassis to the electrodes, via sprung, gold plated connectors. The two parts could be secured together to create a good electric connection between the output cable and the tip of the electrodes. An earlier version on this system is described by Qiao in 2008. [QIAO 2008]

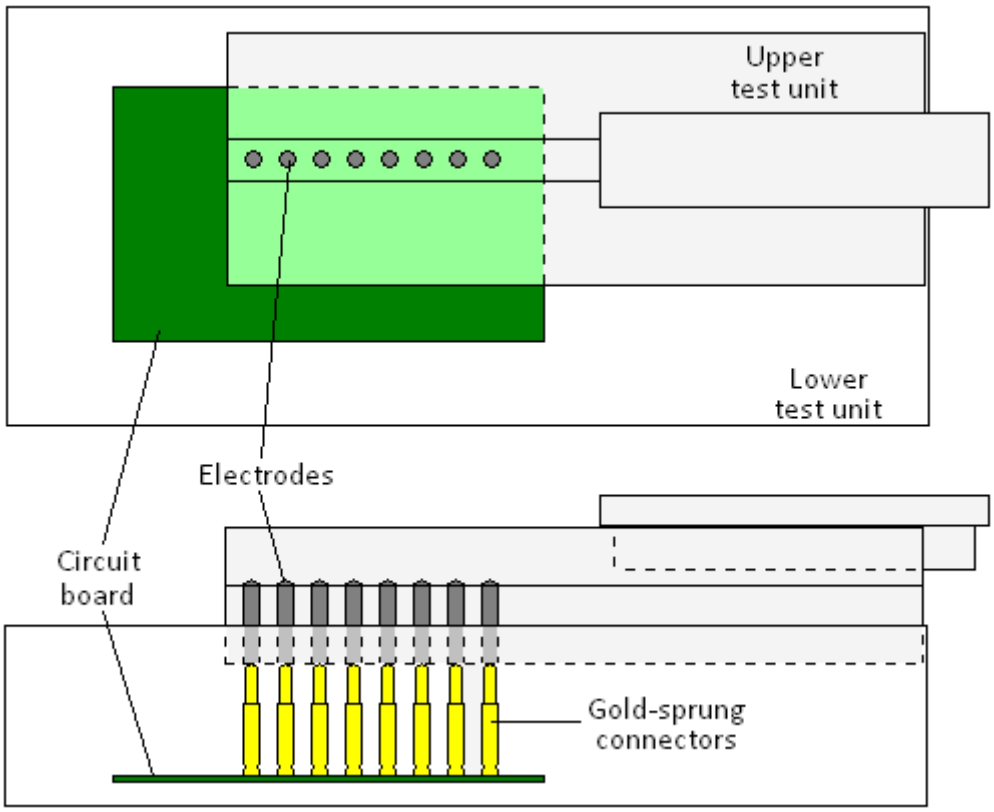


*Figure 5.2: Plan and Side view of whole pancreas test unit, showing both upper and lower parts of the unit, the upper compartment is shaded.*

The test unit was connected to a National Instruments PXI chassis which was controlled from a PC running LabVIEW.

#### 5.2.1.1 Heating System

The upper part of the test unit included a channel which allowed a heating system to pump water around the chamber via flexible hoses; this allowed the temperature of the pancreas to be controlled throughout the test.

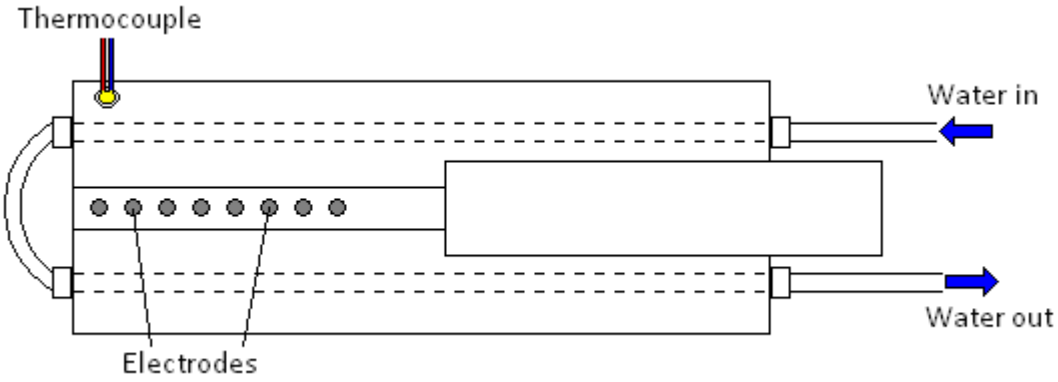


*Figure 5.3: The heating channel shown within the upper part of the whole pancreas test unit, the arrows indicate the flow of water through the system.*

As the long term plan for this project was to test for cancer in vivo it was important to keep the cell properties similar to those of in vivo tissue. The heating system was employed to keep the pancreas as close to mouse body temperature as possible and so avoid the dramatic changes in the reaction of cells with a change in temperature.

A thermocouple placed inside the test unit can be seen in the top left corner of Figure 5.3, and was used as a guide for an NI LabVIEW program to regulate the temperature throughout the system. The NI chassis provided the outputs which were used to control the heating system.

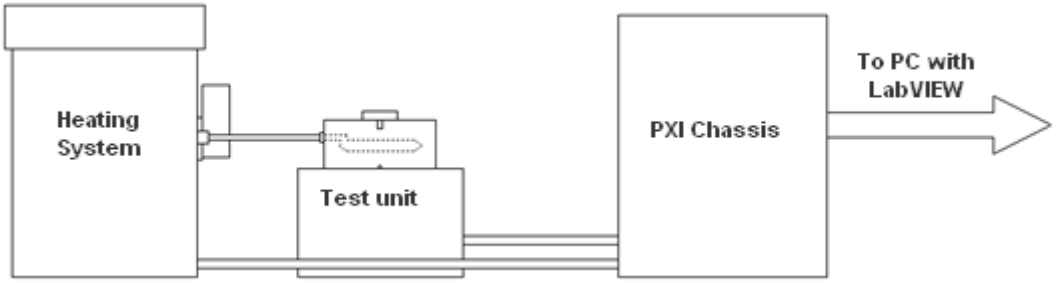


*Figure 5.4: The test set up of the whole pancreas testing*

Figure 5.4: The test set up of the whole pancreas testing shows the relative positions of the main equipment used in the whole pancreas tests. The heating system on the left was a water tank with a pump which was controlled by the PXI chassis. Heating elements within the tank were controlled automatically with reference to the thermocouple.

A block diagram of the whole system is shown in Figure 5.5 showing how the heating system and both parts of the test unit were interconnected.

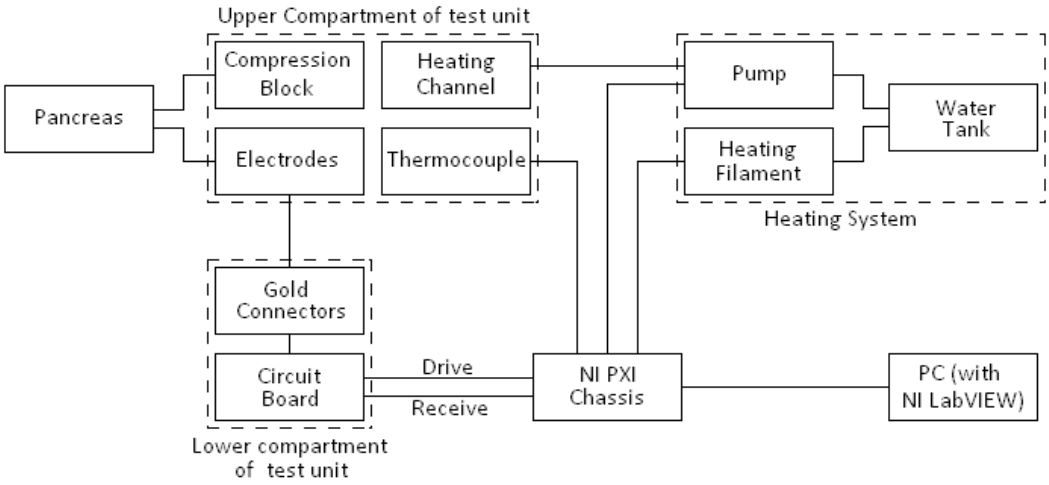


*Figure 5.5: A block diagram of the whole pancreas test unit*

### 5.2.2 Electrode Configuration

The electrode array was programmed to collect two separate sets of data for each test.

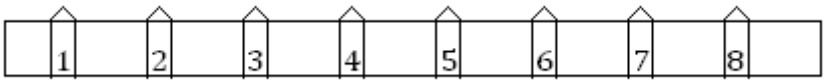


*Figure 5.6: Whole pancreas testing electrode array diagram*

Figure 5.6 shows the planar array of electrodes. There were 8 electrodes in total and 2 separate configurations were recorded within the experimental procedure.

*Table 5.1: Whole pancreas testing electrode configuration 1*

| Drive 1 | Drive 2 | Receive 1 | Receive 2 |
|---|---|---|---|
| 1 | 8 | 1 | 2 |
| 1 | 8 | 2 | 3 |
| 1 | 8 | 3 | 4 |
| 1 | 8 | 4 | 5 |
| 1 | 8 | 5 | 6 |
| 1 | 8 | 6 | 7 |
| 1 | 8 | 7 | 8 |

The table above shows the first configuration of electrodes, it is clear to see how the differential current was input at either end of the array, while the output was received at various points along the array, always from adjacent electrodes.

*Table 5.2: Whole pancreas testing electrode configuration 2*

| Drive 1 | Drive 2 | Receive 1 | Receive 2 |
|---|---|---|---|
| 1 | 4 | 2 | 3 |
| 2 | 5 | 3 | 4 |
| 3 | 6 | 4 | 5 |
| 4 | 7 | 5 | 6 |
| 5 | 8 | 6 | 7 |

The second configuration provided outputs where the drive and receive pairings were always the same distance apart which would hopefully provide results with more similar values of magnitude.

### 5.2.3 Timing of Tests

Initial tests were carried out using an HP 4145 Network Analyser and the Agilent Vee program. This provided the intended drive/receive voltages.

This system was found to be too limited for our purposes, as only 4 electrodes could be connected to the analyser at a time. We could reconfigure the electrodes using a built in bank of switches, and so obtain results.

Unfortunately, the relatively slow measurements performed by the analyser, combined with the manual switching required between each measurement caused the overall procedure to be quite slow and we found the pancreata deteriorated over the course of one test.

Later, with the NI equipment we were able to test different pancreata at known intervals following extraction. Measurements were taken at 3 different temperatures the graph in Figure 5.7 shows how the Resistivity value increases over time. It was suggested this was likely to be due to cells dying within the pancreas.

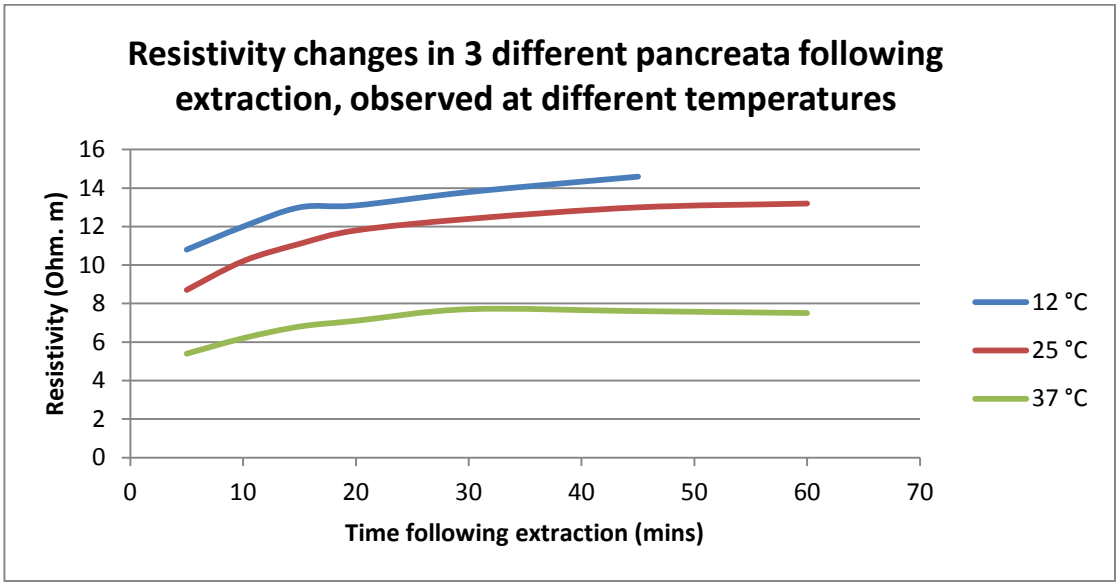


*Figure 5.7: The deterioration of the pancreata post mortem*

It was found that at 37 degrees centigrade the impedance measurements settled around 30 minutes after extraction. With the HP analyser it took about this long to continue a run of tests with various electrode configurations and since the pancreata were degrading during the test the comparisons may have been flawed. However if the tests were completed once this degradation had slowed to a stable value it is possible that the comparisons would be more useful, but as Figure 5.7 suggests the resistivity values of the sample would have changed since the extraction and therefore were no longer representative of an *in vivo* test.

The NI kit solved this issue as the LabVIEW program could be made to change the electrode configuration automatically, so was a lot faster and avoided manual switching. Results were therefore completed within 3 minutes after extraction as this

provided enough time for the correct positioning of the sample in the test unit and the observations of the extracted organ.

### 5.2.4 Summary of Tests

The final set of results from this technique produced data from 8 separate pancreata. Four of which were normal and four cancerous.

It has been shown previously that the majority of the Islets of Langerhans within a pancreas are at the head end of the pancreas, therefore the most useful results would be from the electrode configuration which measured over this area. It was also decided that the 2$^{nd}$ electrode configuration provided the best output as the drive electrodes were closer to the receive electrodes and therefore the current at this point would be stronger, so any alterations from the change in Islet properties would be more easily detected. Also, in the 1$^{st}$ configuration the inputs were driven at either end of the pancreas, and any biasing at these extremes could alter the output unfavourably.

Due to the degradation mentioned previously the results were taken from those tests completed 3 minutes after the pancreas extraction, due to the nature of the test this was the fastest time possible from culling the mouse to the pancreas being extracted and positioned appropriately in the test unit.

The pump and heating element were controlled automatically by a monitoring program which kept the temperature within the compartment at around 37 degrees centigrade, this being the internal temperature of the mice and shown previously to have the lowest resistivity change following extraction (see Figure 5.7).

### 5.2.5 Test Procedure

The procedure at the animal house involved several stages which required a minimum of 3 technicians to complete them correctly.

Firstly a mouse was culled and the pancreas extracted. Temperature readings were taken of the pancreas in-vivo and following extraction to monitor the change during this process.

While this was taking place the upper compartment was heated by the water pumping system to body temperature so that the pancreas did not dip in temperature following extraction.

The upper compartment was then disconnected from the heating system so that the pancreas could be placed onto the electrodes making sure the head and tail of the pancreas where at the correct ends of the array, the pancreas was also compressed to make sure all the electrodes made a good connection with the tissue.

The upper compartment containing the pancreas was secured onto the lower compartment and the heating tubes were reconnected. Once these connections were made the LabVIEW programs were activated to begin the water pumping and take the first readings.

### 5.2.6 Results

The NI equipment took measurements from various frequency inputs, these were taken and entered into a Matlab program designed by the Leicester group to extract values for $R_R$, $R_S$, C, Fr and α as described in Chapter 4.3.1.

Table 5.3 shows these calculated values split into two parts, the top half shows the results gained from the four normal pancreata, while the lower half shows those of the cancerous tissue. The table also includes averaging and standard deviation values for aiding the comparison of cancerous and non cancerous samples.

*Table 5.3: Calculated values from 8 mouse pancreata*

| Normal | | | | | |
|---|---|---|---|---|---|
| | $R_R$ | $R_S$ | C | Fr | Alpha |
| p1 | 6.006 | 0.5 | 155.81 | 157 | 0.217 |
| P3 | 6.052 | 0.547 | 168.546 | 143.106 | 0.193 |
| P5 | 6.186 | 0.618 | 157.769 | 148.255 | 0.255 |
| P7 | 6.455 | 0.558 | 160.426 | 141.469 | 0.187 |
| Average | 6.17475 | 0.55575 | 160.6378 | 147.4575 | 0.213 |
| STD | 0.201834 | 0.048527 | 5.601254 | 6.987918 | 0.030854 |

| Cancerous | | | | | |
|---|---|---|---|---|---|
| | $R_R$ | $R_S$ | C | Fr | Alpha |
| P2 | 5.258 | 0.7 | 135.254 | 197.474 | 0.201 |
| P4 | 5.883 | 0.661 | 131.984 | 181.142 | 0.211 |
| P6 | 5.956 | 0.634 | 139.501 | 172.869 | 0.208 |
| P8 | 6.201 | 0.71 | 120.043 | 191.843 | 0.258 |
| Average | 5.8245 | 0.67625 | 131.6955 | 185.832 | 0.2195 |
| STD | 0.40141 | 0.035217 | 8.355691 | 10.98034 | 0.026006 |

The average values from this table can be seen represented in Figure 5.8, the standard deviation is shown as error bars.

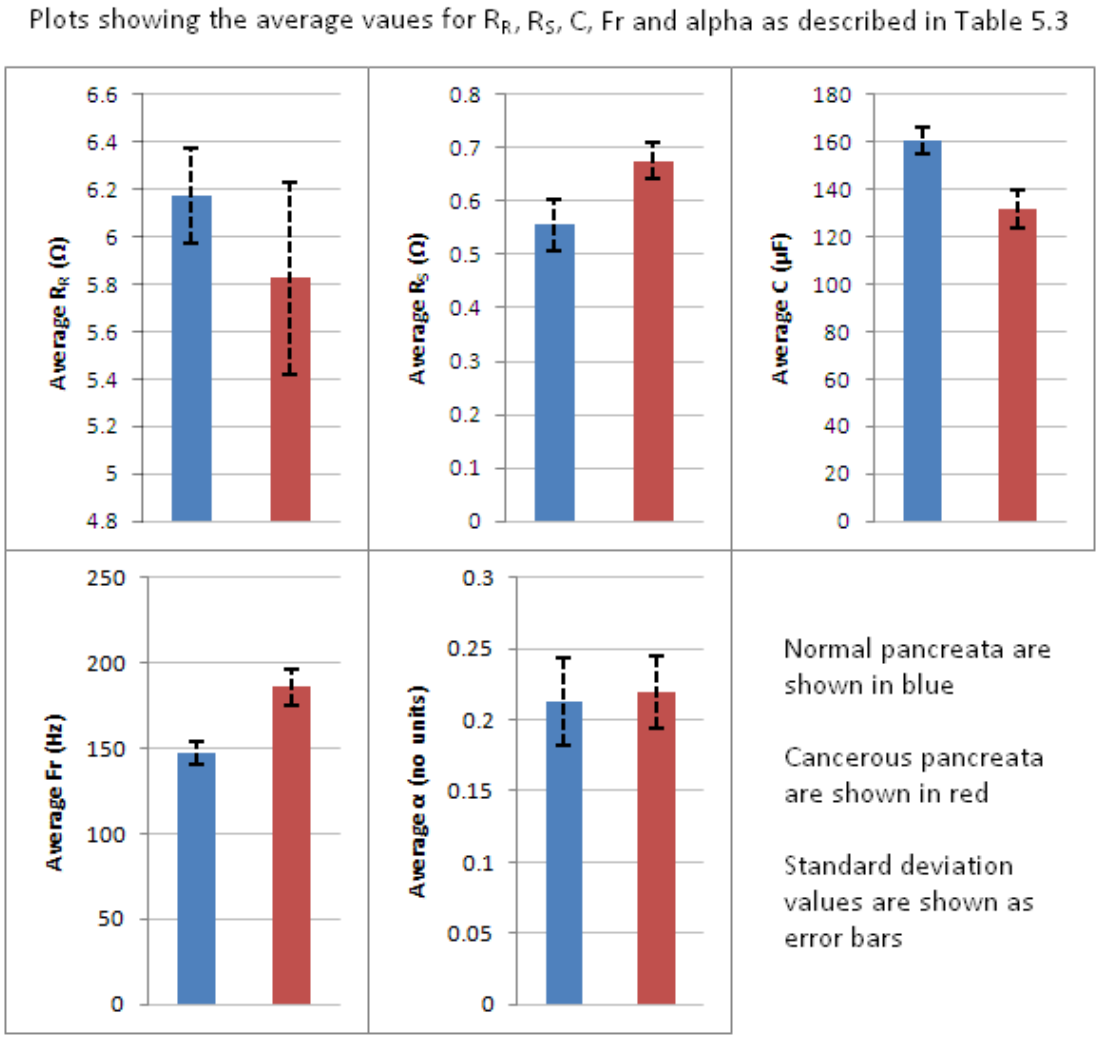


*Figure 5.8 Bar charts showing comparison between cancerous and normal pancreata parameters. Plots represent averages and standard deviation.*

The results shown in Table 5.3: Calculated values from 8 mouse pancreata and Figure 5.8 show several noticeable differences from the cancerous and normal pancreata. The $R_R$ values, which represent the extra-cellular resistance, appear higher for normal tissue although the standard deviation shows that these results should not be

relied upon to distinguish between cancerous and normal samples. The values for the intra-cellular resistance, $R_S$, are lower for normal tissue.

The cancerous values of relaxation frequency (Fr) and membrane capacitance (C) are also different, higher and lower respectively.

The Alpha values calculated for the tests are slightly lower in Normal tissue, however the difference is not as clear as the other results so this derived parameter does not look as if it provides a useful distinguishing criterion and therefore little can be concluded from this particular element.

### 5.2.7 Interpretation means Islet Testing

The results provided suggest a difference in the cell measurements from healthy to cancerous tissue. All 3 of the Cole-Cole model parameters provide differing values which could be used to identify the health of the pancreas. It is more clear within the results for $R_S$ and C, however since these values represent properties within the cell itself that is to be expected. It appears that the cancer growth weakens the cell membrane and increases the internal resistance of the islets.

Since the test results provided promising outcomes the next phase of the testing was begun.

The cancerous pancreata in this test included several hundred cancerous islets and therefore the differences measured may be more identifiable than the effect caused by one escaper islet, therefore further tests were designed to provide a difference between cancerous and normal tissue at the islet level. If a measurable difference could be identified at the islet level it may be a useful reference in attempting to identify the escaper cells as the research continued.

## 5.3 Patch Clamping Approach

Patch Clamping is a technique used to measure, among other things, ion channels surrounding individual cells. In order to achieve measurements of such small objects an approach was devised which allows microscopic electrodes to be attached directly to an individual cell. The cell voltage can be controlled and clamped at a specific value while the change in ion current is measured.

This approach has similar themes to EIT, controlling the voltage (or more often in EIT, the current) input and measuring the resulting current (or voltage). From this approach it should be possible, as it is in EIT, to present the impedance of the measured object.

It was suggested that if patch clamping technology was used an EIT measurement for a single islet could be achieved. This could provide a clear indication as to the effect of the cancerous beta cells on the overall impedance of an islet.

Patch clamping uses extremely fine pipettes which contain a small electrode. These pipettes can be attached directly onto individual cells using suction. This allows for a very tight seal between the pipette and the cell, so that when a voltage is applied through the electrode all the current must flow through the cell before it can reach an earth connection – typically this is underneath the cell(s) being tested. [MOLLEMAN 2003]

### 5.3.1 Experimental Set Up and Procedure

Figure 5.9 shows a block diagram of the patch clamping style experiments completed at Warwick University. Much of the equipment was kept inside a faraday cage in order to minimise impact of stray electrical noise on the results.

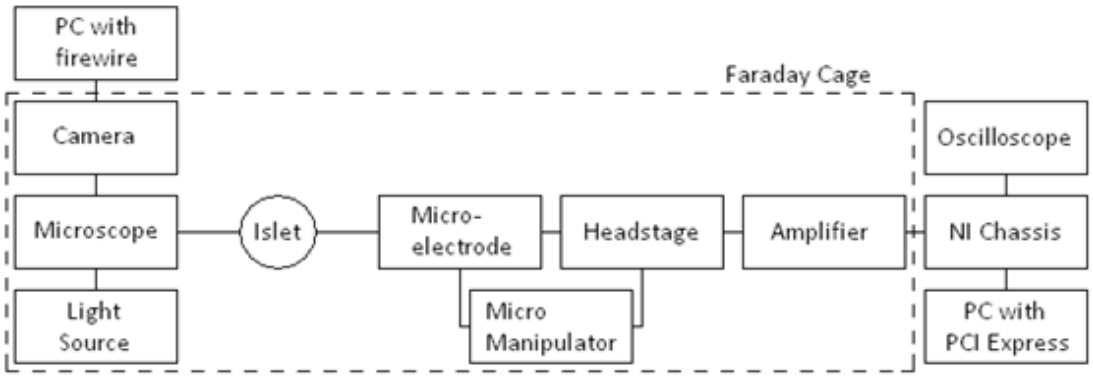


*Figure 5.9: The set up connections used within the cell patching experiments.*

The Islet was placed in a petri-dish which was held under the microscope within the faraday cage. The microscope had an external light which allowed the test to be viewed, since the microscope needed to be in the faraday cage the whole

experiment was viewed on an external PC screen via a video camera attached to the top of the microscope. Images from the microscope could also then be recorded for later analysis and explanation.

The glass pipette containing the micro-electrode was positioned using a micromanipulator, this allowed microscopic movements to be applied so that the electrode could be lined up exactly with the islet. The manipulator also held the headstage, which provided the voltage output to the electrode.

The headstage was connected to the patch-clamping amplifier which was used to apply the input voltage and monitor its level. This was routed through the NI Chassis and could be viewed on the oscilloscope and the Laptop.

The islet was kept in a pool of sustaining medium in order to prevent it from dying. The medium used for all the experiments was RPMI with 10mmol glucose added. The culturing medium had previously been used by the Warwick research group. [PASCAL 2008] Tests completed by the Leicester group showed the medium conductivity was around 12.3 mS/cm at room temperature which would allow the current to reach the tissue. The micro-manipulator was adjusted until the glass pipette was touching the islet directly at its tip. Suction was then applied to the pipette which allowed the islet to be partially drawn into the capillary. The islet was positioned using the manipulator so that a contact with the earth ring was made. The relative positions of these components can be seen in Figure 5.10.

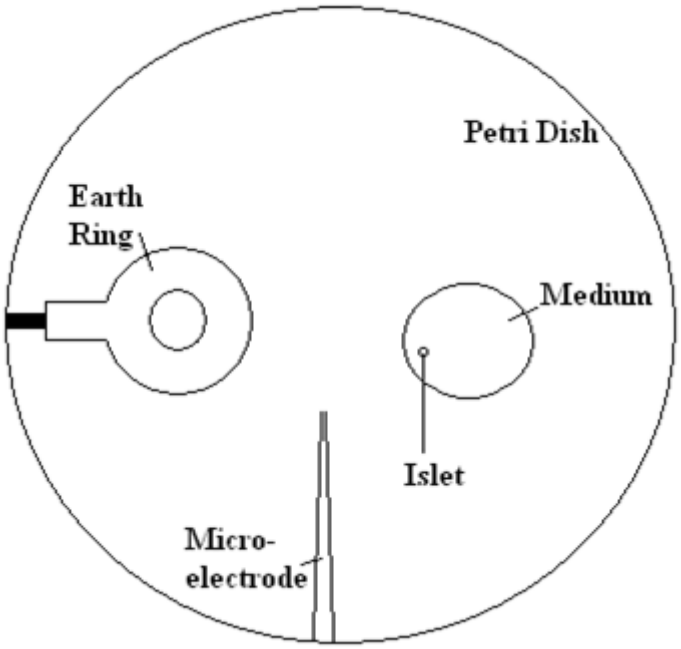


*Figure 5.10: A plan of the petri-dish and the components used in islet patching*

The view from the microscope camera did not show the whole petri dish, 3 still images from the camera are shown in Figure 5.11. These show an islet, a glass capillary and an islet being sucked into a glass capillary respectively.

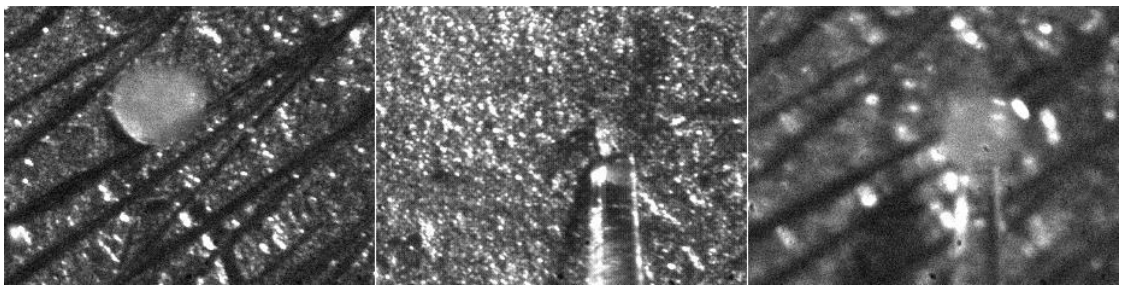

*Figure 5.11: Photos from the islet patching tests*

## 5.4 Experimental Output

The outputs from this test method were inconsistent; some of the tests seemed to show a difference between cancerous and non-cancerous islets, while most were marred by large amounts of noise and other interference, so those results which looked promising could not be reported with any conviction.

Throughout the testing there was a constant need to alter the experiments in an attempt to address the noise and related issues, which took longer to rectify than initially assumed, further information on the details of the complications can be read in appendix A.

Unfortunately, due to time and budget restrictions, and the limited capability of the equipment the full extent of patching-style experiments planned were not realised. The tests did not reach a point where a typical EIT curve could be plotted.

It became apparent that in order to provide results to a high standard which could be presented in a report at the end of the initial funding period a new approach would be needed. The approach which was investigated was a more traditional electrode array method as it was thought that some results could be quickly achieved and further investigation into islet impedance could be completed if the funding were continued.

## 5.5 MEA Approach

Since the previous tests failed largely due to the untested nature of the experimental procedure it was hoped that an approach could be found which used existing technology to provide impedance readings for the islets, therefore a Micro Electrode Array (MEA) was bought for the testing.

An MEA is a manufactured set of micro-electrodes which can be wired into a control system which will allow current injection and measurement from any selected electrode within the array. The electrodes have uniform positioning as part of a grid.

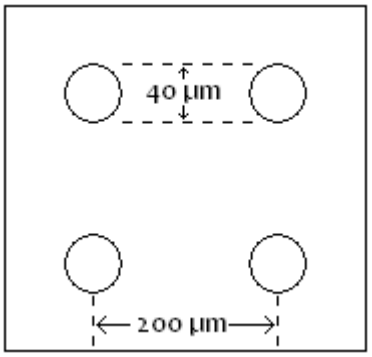


*Figure 5.12: The spacing measurements of the MEA*

As can be seen in Figure 5.12 the electrodes in the MEA were 40 µm in diameter and were set 200 µm apart. Each electrode was the shape of a conical point which reached 50-70 µm high from its base. The array used contained 60 electrodes (8x8, but with corner electrodes omitted); however only 4 were used in the islet tests run by the Leicester group.

### 5.5.1 Experimental Set Up and Procedure

An islet was positioned on the array in the centre of 4 electrodes, the drive and receive signals were once again programmed into these electrodes using NI LabVIEW.

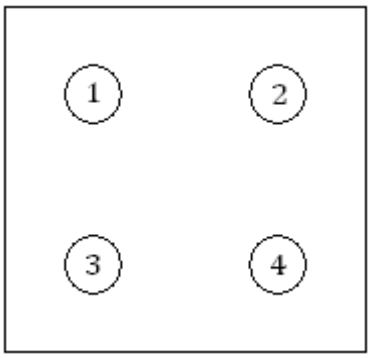


*Figure 5.13: Islet testing electrode array diagram*

In this testing a 2 electrode system was employed; the drive and the receive pairs were the same 2 electrodes. The input voltage, Vin, was provided by a voltage to current convertor while the output, Vout, is produced in parallel to the 2 electrodes in the system.

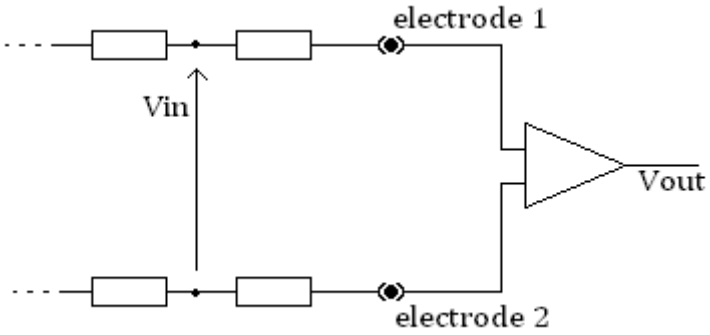


*Figure 5.14: The circuit using 2 electrodes*

The NI LabVIEW was programmed to provide the inputs and read the outputs from the MEA system, therefore the system ran through the readings automatically once the islet was in place. Four different positions of this pairing were used to collect a signal. The table below shows the positions measured from.

*Table 5.4: Electrode configurations used in islet testing*

| Electrode 1 | Electrode 2 |
|---|---|
| 1 | 2 |
| 1 | 3 |
| 1 | 4 |
| 2 | 3 |

These configurations cover the horizontal, vertical and both diagonal approaches to testing the islet using 2 of the 4 shown electrodes.

The MEA was built into a dish which enabled a thin layer of the sustaining medium (RPMI with added glucose was again used) to be used to cover the electrodes; this improved the connection from the electrodes to the islet to be tested.

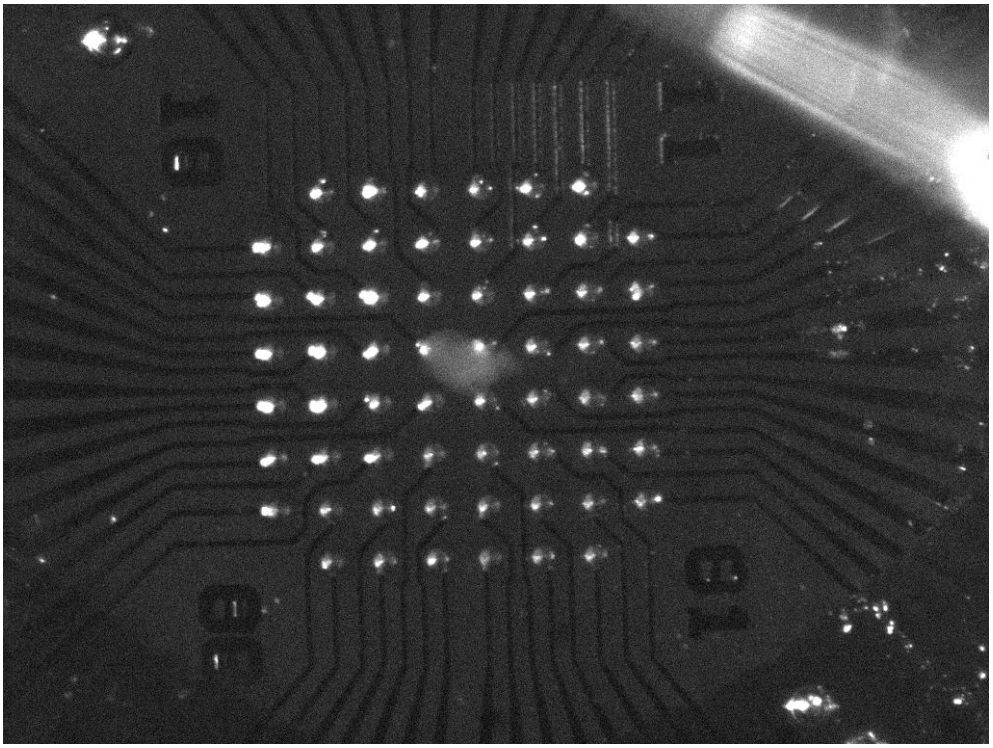

*Figure 5.15: Photo showing an islet positioned on the MEA*

Figure 5.15 shows an islet positioned between the central 4 electrodes of the MEA for testing. Positioning the electrode proved tedious as in order to move the cells a patch clamping suction method was used to clamp onto the sample before repositioning it and releasing the suction. Unfortunately the nature of the islets

when immersed in medium made this repositioning unpredictable, and often involved repeated positioning attempts.

Once the islet was correctly in place, between the 4 central electrodes, the test procedure could begin.

### 5.5.2 Results

Table 5.5 compiles the results calculated from the outputs of electrodes 1 and 2.

*Table 5.5: Cole-Cole parameters extracted from impedance measured across pancreatic islets using electrodes 1 and 2*

| Normal | | | | | |
|---|---|---|---|---|---|
| | $R_R$ | $R_S$ | C | Fr | Alpha |
| Islet_1 | 10.736 | 128.792 | 22.813 | 50 | -0.999 |
| Islet_2 | 12.002 | 70.919 | 90.935 | 21.107 | -0.143 |
| Islet_5 | 10.429 | 136.822 | 69.183 | 15.623 | -0.168 |
| Average | 11.05567 | 112.1777 | 60.977 | 28.91 | -0.43667 |
| STD | 0.8338 | 35.95592 | 34.79448 | 18.46915 | 0.487155 |

| Cancerous | | | | | |
|---|---|---|---|---|---|
| | $R_R$ | $R_S$ | C | Fr | Alpha |
| Islet_3 | 11.384 | 58.596 | 71.315 | 31.891 | 0.055 |
| Islet_4 | 10.087 | 91.378 | 50.511 | 31.054 | 0.438 |
| Islet_6 | 10.197 | 180.062 | 46.081 | 18.153 | -0.153 |
| Average | 10.556 | 110.012 | 55.969 | 27.03267 | 0.113333 |
| STD | 0.719175 | 62.84041 | 13.47334 | 7.701396 | 0.299787 |

The table shows that in this case the $R_R$ and $R_S$ values are very different, the $R_S$ value being much higher than the calculated $R_R$ values. This was not expected. Figure 5.6 shows the normal and cancerous average values as bar charts.

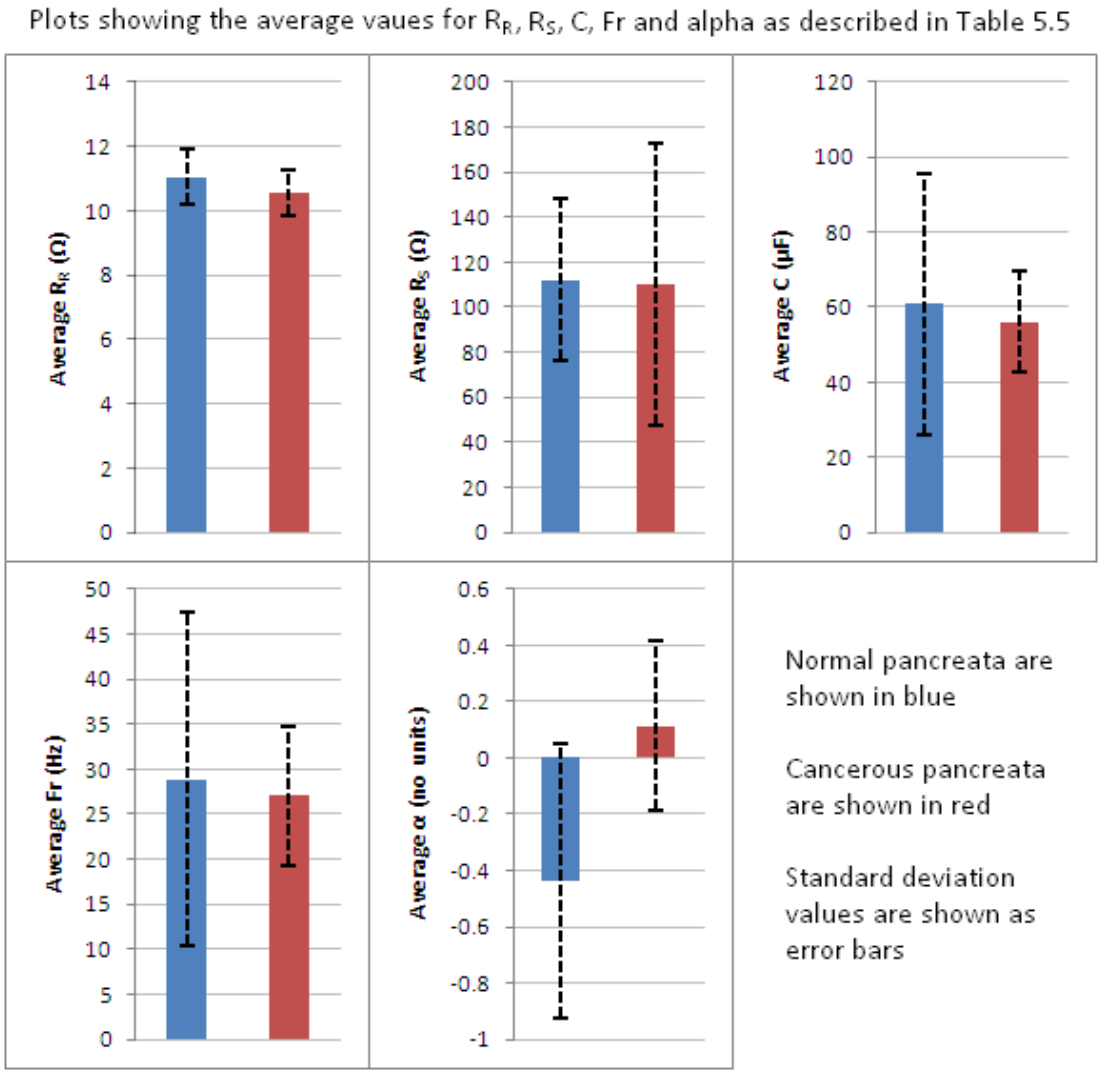


*Figure 5.16 Bar charts showing comparison between cancerous and normal islet parameters. Plots represent averages and standard deviation.*

The standard deviation of the $R_S$, C and Fr values are very high, indicating that the results are not reliable for identifying cancerous or non-cancerous data. To reiterate this issue, none of the average values when comparing between cancerous and non-cancerous are different enough to be easily definable. The standard deviation of the R values is impressive; however the average values are so similar that it would still be impossible to distinguish between them. The alpha results provided a standard deviation which was greater than the average value, which means they are even less reliable.

Similar results were apparent at all electrode configurations.

## 5.6 Conclusions

The conclusions for both the whole pancreas and the islet tests are discussed below. The whole pancreas experiments provide positive results which suggest further investigation would be worthwhile.

### 5.6.1 Whole Pancreas Conclusions

The results collected using the whole pancreas testing unit were promising and showed that there are indeed differences to be found between normal and cancerous pancreata, the differences can be observed across the various Cole-Cole parameters but are most noticeable for C and Fr.

It was originally expected that a larger difference may be observed over values obtained for extra-cellular resistance, represented by $R_R$, as cancerous growth provides cell alignment restructuring and often a change in the density of cells can be observed. However, although a slight difference was shown, it was not the clearest indication of cancer; the change was not precise enough to avoid mis-identification.

The membrane properties C and Fr were expected to provide some differences as membrane proteins such as the glucose transporter (Glut-2) are down-regulated in the cancerous cells. Unfortunately these results did not provide any recognisable differences between the normal and cancerous tissue.

### 5.6.2 Islet Conclusions

The islet results are less encouraging. The results do not indicate an identifiable characteristic in cancerous pancreata. Following the promising results from the whole pancreas testing, this is disappointing.

The main reason suggested for the poor results from these tests was the experimental practise, which involved surrounding the islets with a conducting medium to allow a good connection between the electrodes and the islet. It has been suggested that the current flowed through the medium with very little passing through the islet as intended, the medium conductivity was measured as around 12.3 mS/cm at room temperature, therefore this may be the case. This would explain the lack of distinction between the normal and cancerous results shown in Figure

5.16. It can be seen from the whole pancreas results, shown in Figure 5.8, that the normal and cancerous tissues can provide differing results and if the medium biased the experiment for the islet tests these differences would be heavily diminished.

Another primary concern with regards to these tests was the lack of refinement with the experimental design and procedure, some suggested refinements are described in Section 5.7. The time spent on improving the whole pancreas testing unit was considerable, many different models were used and various experiments were carried out to identify areas which could be improved before final testing. This eroded the time which was left for improving the islet testing, especially once the new MEA system was employed. A total of 4 tests were carried out using the MEA compared to more than 15 tests done using different variations of the block testing unit. Several other islets tests were done; however these were completed using variations on the patch clamping based system; which unfortunately didn't provide results soon enough for the project and was not comparable to the final MEA tests.

With more time spent improving the test procedure and the analysis programs the use of islets to provide data may be useful, but the current results are inadequate to identify the distinguishing characteristics.

## 5.7 Future Testing

There is scope for further investigation in this area; all testing methods require further refinement to improve the frequency response bandwidth and the electrode connection method.

Also, there would almost certainly be great improvements made if the operation of the tests could be standardised further, especially when applying the electrodes, to improve the connection to the tissue/islets.

The whole islet testing did provide some useful outputs and therefore suggests that an improved future output should be achievable. It is suggested however that, since some of the issues with the islet testing have been identified, it would be of use to the investigation for further islet tests be completed with these improvements implemented first. This may give a clearer indication as to the affect of cancerous beta cells on the $R_R$, $R_S$ & C values within the pancreas. This would suggest what results could be expected from whole pancreas tests and may allow improved analysis of the results.

There are areas for improvement regarding controlling the environment within the MEA testing (in a similar manner to the use of the heating system within the whole pancreas testing) which could lead to improved outputs. The Leicester group have already begun plans to investigate further in this respect.

The islet patching method provides a solution to the issue found in MEA testing as the current is forced to pass through the islet in order to complete a circuit. If it was possible to combine the system used for the MEA tests and the hardware of the patching method the output may provide results comparable to those obtained from the whole pancreas. Therefore there is definitely scope to continue work along these lines in future research. There were many issues which became apparent while completing these tests initially, some of which are described in Appendix A, all of these would need to be addressed before new tests could be completed. A description of potential experiments is below; suggestions for improvements are included along with a timescale suggested for optimising the progress of the tests.

In order to fully conclude the potential of these tests it is recommended that a programme of tests be planned with time for incremental improvements in procedure between each session. Sufficient time must be set aside which would allow for the improvements to be fully investigated. The study must begin with all the correct equipment with a view that the equipment will be available throughout the testing period otherwise delays may be incurred and the improvements may falter.

If this project were to be undertaken again it is recommended that a series of up to 20 tests be planned, no more than two a week, allowing time in between each for adjustments and improvements to the equipment and procedure. If a test is known

to be inadequate there is little point in completing further tests if no improvements to the system have been made. This means a minimum of 10 weeks would be needed to complete the testing once all the equipment and biological samples were prepared. It is advisable to allow an additional 2 weeks in case of any unforeseen circumstances.

Initially a large amount of funding would be required to set up the experiments with all the correct equipment and biological samples. The tests would need a supply of islets from an animal research department, this would mean either the tests should be carried out near to the animal house or the islets would need to be transported safely to a separate site, the tests should all be planned in advance so that the animal house know how many pancreata to provide for the testing and what condition they need to be in. One mouse can provide more than enough islets for each test and these islets can be stored for up to 3 days, therefore if the tests are planned correctly it may be possible to complete both tests within one week using islets from a single mouse. A minimum of 20 mice will be needed if this is possible in order to provide the cancerous and non-cancerous islets for each of the 20 tests, a maximum of 40 mice would be needed if the tests are planned further than 3 days apart. However it may be decided while planning that both cancerous and non-cancerous islets may not be needed for early testing as these runs will be used to investigate the method and progressively improve the initial system, so fewer mice would be required overall.

The lab where the tests were to be set up should be free from electrical and acoustic noise as testing on such a small scale makes it very susceptible to interference. It should be assessed as to what other tests are being completed simultaneously within the room and any specific times when these tests are to be undertaken, this should ensure that no tests are compromised by interference from other machines – such as vibration tests etc. Furthermore equipment such as an anti-vibration table and a faraday cage are essential in order to ensure the test results are unaffected by these external issues. The anti-vibration table needs to be large enough to hold the microscope with a micro-manipulator mounted onto it.

Once it is certain the tests will not be compromised by external factors it is important to select the correct equipment for the tests themselves, in particular a good microscope, at least 60x zoom (if available an inverted microscope should be trialed for the application as these are used in traditional patch clamping and allow easier access above the islet to manoeuvre the pipette). It should have a mount for a manipulator which would provide clear access for the patching electrode to be applied and a fully functioning amplifier, along with the appropriate headstage and all the required software, to apply the current to the islet via the electrode. PCs will be needed to control the inputs and also to monitor the microscope view, these should be strategically placed to not interfere with the test and yet be close enough that it is not awkward for the operator to complete his/her task.

As previously discussed the promising results provided by the whole pancreas testing show that there is a measurable difference between cancerous and non-cancerous mouse pancreata. It is known that the cells which are affected by this cancer are the beta cells within the islets of langerhans, therefore the future islet tests should provide correlating but superior results. Furthermore the concentration of beta cells within an islet will be much higher than within the whole pancreas, this should allow the islet testing to be more sensitive to the changes brought about by cancer.

It is still unproven whether EIT could be used to determine the position of escapers with an otherwise healthy pancreas; however the investigative tests described above could bring the project nearer to a conclusion.

# Chapter 6 Review, Conclusion and Future Work

This thesis has covered several areas of research within the field of EIT and in each section new approaches to the subjects have been investigated. This conclusion describes these novel contributions as well as explaining where there are opportunities for continued investigation within the different areas.

## 6.1 Howland Model

The investigation and analysis work established that the improved Howland model was the most appropriate circuit to provide a current source for EIT purposes and was a secure foundation for future work of the Leicester group.

The analysis and circuit comparison using the PSpice simulation program showed that the improved Howland response could be enhanced further as improved op-amps became available.

It has been shown that capacitance loading effects were significant contributors to the limits of the EIT measurements, and the development and adoption of improved op-amps would make a significant improvement to EIT performance. The quality of the results presented in this thesis was limited by the quality of the op-amps used, and so improvements are possible with components with better specifications.

### 6.1.1 Future Work

Howland based current sources are still a major part of many of the leading EIT systems, including the Leicester group. Improved output and stability is therefore always desirable and it is useful to have an approach which can be improved over time. The improved Howland model can be updated continuously as further op-amps are made available and work will need to be ongoing to ensure that the outputs provided are of the best available quality.

## 6.2 Time Domain Experiments

EIT systems can struggle with high frequency limitations. The Leicester group designed and implemented two approaches to address these limitations. The investigation reported in this thesis showed that both approaches have promise, but neither are yet able to fulfil this promise.

A transient sweep was explored as an alternative to standard EIT measurements. The method explored was comparable to the Leicester Group's current frequency approach, but the results indicated that this approach is sensitive to noise that can arise, and this noise can lead to spectacular errors.

The investigation explored use of a square wave input, as such a step function incorporates an infinity of frequencies, and so can, in principle, deliver the required Cole-Cole parameters.

The theoretical results were promising, but in the experiments the results were not as successful. This was found to be due, at least partly, to the limitations of the input square wave source used, the filter compensation of the original spike meant that the signal produced was more curved than the ideal step input which was used to provide the mathematic formula for the Cole-Cole parameters. The errors in the system meant that it was shown that the frequency tests provided more accurate parameter values than the time domain results.

### 6.2.1 Future Tests

The theory suggests that experimentation with more appropriate square wave sources will provide a set of results which are comparable with the more standard frequency domain tests but bring associated benefits in measurement speed. Further theoretical work may find a form of input signal that is closer to practical technological devices and suggest signal analysis that produces useful results. Therefore future tests in this area are highly recommended as this may prove to be a very useful technique within EIT. If it is not a full replacement for frequency scan EIT, it could be used alongside it in order to provide an output which combines the two methods as has been suggested by Heitmann and therefore provide more accurate assessments of the Cole-Cole parameters [HEITMANN 2009].

## 6.3 Mouse Pancreas Tests

The results gained from the whole pancreas tests were promising, and, as expected, the work showed clear differences between cancerous and non-cancerous pancreata. The work and analysis reported in this thesis confirm that EIT is capable of cancer diagnosis in whole pancreata.

The patch clamping experiments were not successful, as it became clear that significant improvements in the measurement protocol and in some of the experimental equipment would be necessary to achieve usable results. Various enhancements were identified and one in progress, but the project was terminated before these refinements were attempted.

The differences shown between the cancerous and normal pancreata suggest that EIT is a technique which could provide some insight into this area of research, however the scope of the experimental precision required was shown to be great and therefore much more work is needed to make the approach valid.

### 6.3.1 Future Tests

As described in chapter 5 there is certainly potential for further tests to be completed using the patch clamping method, but careful planning and the appropriate equipment are needed to ensure similar difficulties are not encountered.

The value of this work is to provide further insight into the differences between cancerous and non-cancerous cells at an islet level, this information could then be used to enhance the analysis completed on the whole pancreas.

Once this analysis can be improved further whole pancreas tests should be completed, first of all to see if the differences can be identified with greater ease, but also to investigate the theory of whether EIT can detect a single 'escaper' within an otherwise healthy pancreas, as this in essence was the original aim of the project.

## 6.4 MEA Tests

Since the MEA experiments were rushed the results, although disappointing in terms of measurable differences, were not unexpected. The block testing had shown that a similar test approach worked well for the larger scale tissue investigation and therefore it was hoped that the MEA tests would provide a similar level of differentiation. Unfortunately due to the limited period which was available towards the end of the project there was no time for refinement of the technique in the same way which had benefitted the whole pancreas tests. There was only time for 2 test runs once the equipment arrived and, as shown in chapter 5, the output collected from these did not provide any useful results. There were many inherent issues which were not solved in the timescale provided. The main issue which was encountered was that the medium the islets were suspended in was conductive to the point that the current favoured this route and therefore the impedance

measured was affected little by the islet. This led to the parameter results for cancerous and normal islets being very similar.

### 6.4.1 Future Tests

The work of this thesis gives a foundation of the optimism of the group about the future of MEA testing of islets since the basis of the experiments is the same as those found in the successful whole pancreas approach. The group plans to continue this approach and further testing work following their move to Sussex University. With the purchase of more appropriate equipment, including a new microscope, many of the difficulties reported in this thesis report will be overcome and hopefully some improved results will follow. Tests should begin before the end of 2011 with a hope to publishing some results in the New Year. The new project plan offers a timescale to allow the group to look into the issues which became apparent and deal with them effectively before undertaking the final tests.

# Appendix A

Appendix A is an edited extract from an informal report submitted while the patch clamping tests were in progress. It discusses various issues with the patch clamping technique and tools. It was prepared for the other members of the group who were not present at the actual testing in order to report progress and to suggest improvements which address the issues. The report has been significantly shortened to avoid duplication with the 'method' sections of Chapter 5 of this thesis.

Although the information included in this appendix is not appropriate for the main body of the thesis, it may be of value to someone attempting further experiments within a similar field. This version is aimed at such an audience.

## Report on Islet Testing - Improvements to be considered

### Problems

There have been several major problems during the testing; I have tried to outline them here.

***The amplifier*** The amplifier we borrowed from Prof. Ian Forsythe is a very good patch clamping amplifier, however since we are not doing standard patch clamping the bandwidth is too limited to cover the 5 MHz we usually hope to achieve – a built

in low pass filter restricts the bandwidth further. Since we are no longer doing standard patch clamping, our recent experiments cannot make use of the functions the amplifier is designed to provide. Our simple use is to transmit the input signal (generated by the NI kit) to the head stage and back again.

There have been repeated discussions concerning designing and making a new amplifier, or buying a new one. I have asked for quotes from 2 companies (so far without results). My recommendation is to use a simple amplifier which will transmit our signal. After the islet testing is complete, we may indeed need the sophistication of a patch clamping amp for the beta cell testing, we can pursue this then.

***The NI kit software*** The software itself still seems quite amateurish, I have suggested a few updates to Nevis, some of which are now in place, but I think it would be better (and quite feasible) for the whole thing to be done automatically, rather than the current situation where the operator chooses the sampling rate etc. All the results would be comparable and the operator would be able to concentrate on more useful aspects. There should be one button 'collect data' and the system should set its own input magnitude according to where it saturates etc. The operation of the islet sucking is complicated enough without having to worry about whether the system has managed to record data or just an offset value.

***Microscope*** The microscope we are using is an Olympus SZX9 which requires manual turning of the zoom and focus functions. As these are attached to the side of the

microscope neck any adjustment causes the microscope to move its focus point. Such movement makes it very difficult to get a good image of the islet for manipulation using the micro-electrode. As there is no stage guide on the microscope all movement of the Petri-dish being viewed must be done by hand, which is imprecise, and, within the space constraints of the faraday cage, clumsy. Quite often this leads to other movement or disconnections.

The maximum zoom of the microscope is just enough for current experiments so long as we restrict our experiments to large islets. If we intend to move onto beta cell testing we will need a lens with zoom capabilities of at least 10x what we have now. Finally, although the micro-manipulator was supplied with a mount for attaching to Olympus microscopes our microscope is too old to fit this mount. This means that the manipulator has to be placed in front of the scope. This blocks precious desk space needed for moving the Petri-dish.

***The faraday cage*** The faraday cage previous improvised by Dr Wang did serve to show that a faraday cage is essential to the experiments. However, it is its not large enough to include the camera and the design prevents access to the eye pieces. While it is possible to view using the camera screen, this creates problems for those more used to conventional microscopy.

Also, I have concerns over the safety of our current faraday cage. It is made from cut chicken wire, and the ends, where it was cut to shape, are very sharp, creating the

risk of users (and other staff passing) cutting themselves. Personal (and bloody) experience has demonstrated this risk!

***Anti-vibration needs*** Following the tests done in the lab in Warwick I think an anti-vibration table really vital to get good results, especially for when the project moves to beta cells. Currently even minor movement, such as someone leaning on the desk, can disrupt an experiment by moving the microscope out of position; cause noise to appear in the readings from disturbing contact between the electrode and the earth; or break the electrode by snapping it on the earthed ring.

We are very careful to avoid these problems whilst testing, but other researchers in the busy lab can easily transmit disturbances (e.g. from vibrating/spinning testing devices) through the connected benches. Any such disturbance like this damages our outputs and means repeating experiments.

The main problem with an anti-vibration system is the space it will take up, there certainly isn't any room for one in the areas we have been working at Warwick Uni. If we intend to use one, we will need to secure a different working area.

***The 'sucking' technique*** My main concern with this technique is the lack of accuracy and the difficulty of repeatability. There are 4 outcomes which occur regularly when trying to use the technique:

1) The islet is partially sucked into the pipette and the rest falls off when lifting the electrode up

2) The islet is partially sucked into the pipette and the rest needs to be cut off using a cutting needle

3) The islet is fully sucked into the pipette and therefore is useless as we cannot guarantee the current will pass through it

4) The islet falls apart and is useless.

Obviously options 3 and 4 are bad, but do happen quite often, especially on the more fragile cancerous islets.

Option 2 isn't good as the needle isn't appropriate for precision cutting above or below the glass electrode when there is no depth perception. This, in conjunction with the vibration problem has caused the breakage of a many pipettes at this stage of the experiment.

Option 1 is the least bad option, but the amount sucked and measured is different for every experiment. The islet membrane is inevitably broken, so we are not measuring the islet in its entirety. This is a source of uncontrolled variation and so

inaccuracy. While the membrane is not as affected by cancer as beta cells we are unable to assess the impact on overall results.

***The earth ring connection*** The earth ring connection causes several problems:

1) The ring is flat and the electrode approaches at an angle. We tried to adjust the ring position for a perpendicular approach, and so improve the contact between them. However, this also made it harder to tell through the microscope when contact was established, and we were not able to improve results in this way.

2) The ring gets dirty regularly – medium dries on it and pipettes break on it – so keeping it clean can be difficult, or even knowing whether it is clean or not. We have had to resort to scratching the surface away.

3) The overall connection to the ring doesn't appear to be adequate, and the problem seems to lie with the medium used. I recommend trials with other media.

***The medium*** As the medium used in out experiments is conductive (13mS/cm), we assumed that this would be conductive enough to for the experiments. This does not seem to be the case, and I have experimented with a pipette without an islet. Only a weak current flows, suggesting that the base case conductivity (without an islet) is unduly low.

Originally, the medium was chosen to maximise the life of the islet within it. In other patch clamping experiments two media are used, one for the pipette and one surrounding the cells. There may be complications in the biology, (beyond my current understanding and scope) but a relevant literature search should suggest effective, or proven, alternatives that it would be helpful to explore.

## Equipment Required

A laptop with both PCI express and firewire card; This would save on equipment needing to be carried from university to university each time an experiment is underway, also the camera is not used once the connection is made so there would be no cross-over of operation, 1 PC/laptop should be able to handle the work.

A new microscope; as described above there are several issues with the current available microscope, in particular the movement caused when adjusting the zoom/focus. Following this, obviously the greater the zoom, the more accurate our tests can be. Also I recommend that the chosen scope enables direct mounting of the manipulator was mounted onto the microscope.

A new amplifier; a broader band amplifier is essential for higher frequency data. A bandwidth of 50kHz is the best we can currently achieve assuming we overcome noise and saturation issues, and this is unlikely to be enough to secure good R, S and C values.

Anti-vibration table; this would be very useful now, as we are held back by vibration and movement interference. For beta cell testing is will be essential, and will need adequate space to mount it.

## Summary

In summary the tests so far have achieved results, with some usable data. However, the essential refinement of the testing technique has prevented us replicating tests over separate week. To get good results we need further equipment and experiment time to deal with the significant issues we have identified. Without this we risk unsatisfactory results that will need repeating on a complete system.

# References

Adler, A. and Lionheart, W. R. B. (2006). Uses and abuses of EIDORS: An extensible software base for EIT, *Physiol. Meas.* **27**: S25-S42

Adler, A. et al. (2009). GREIT: a unified approach to 2D linear EIT reconstruction of lung images, *Physiol. Meas*. **30**: S35-S55

Altmann, M. Et al. (2004). Prediction of lamb carcass composition by impedance spectroscopy, *Journal of Animal Science*. **82** (3):816-825

Assenheimer, M. et al. (2001). The T-Scan technology: electrical impedance as a diagnostic tool for breast cancer detecton. *Physiol. Meas.* **22**: 1-8

Attardo, E. A. et al. (2011). Jacobian optimization for 3D electrical impedance tomography via GPU acceleration, *11th Electrical Impedance Tomography Conference Proceedings, Bath, UK* pg 263 – 266

Barber B. C. (2005). EIT: The view from Sheffield **In** Holder, D. S. *Electrical Impedance Tomography: Methods, History and Applications*, 423-449. Bristol, UK: IOP Publishing Limited.

Barber, D. C. and Brown, B. H. (1984). Applied Potential Tomography (Review Article). *J. Phys. E:Sci. Instrum.* **17**: 723 - 733

*Black's Medical Dictionary.* (2005). 41st Edition. London, UK: A & C Black 2005

Boas, D. A. et al (2001). Imaging the body with diffuse optical tomography. *IEEE Signal Proc. Mag.* **18** (6): 57-75

Borsic, A. et al. (2010). Electrical Impedance Tomography Reconstruction for Three Dimensional Imaging of the Prostate, *Physiol. Meas.* **31** (8): S1

Brewer, N. et al. (2007). Systematic Review: The Long-Term Effects of False-Positive Mammograms, *Annals of Internal Medicine*. **146** (7): 502-510

British Standards Institution (BSI). (1989). BS EN 60601-1:1990. *Medical electrical equipment. General requirements for safety.* Milton Keynes: BSI

Bruce, P.G. (2008). The power of electrochemical impedance techniques, http://ca.cariescan.com/assets/ClinicalReferences/file21.pdf, date accessed 07/05/2011

Cancer Research UK. (2008a). *CancerStats report – Breast Cancer UK*, Cancer Research UK

Cancer Research UK, Information Resource Centre. (2008b). *Breast Cancer*, http://info.cancerresearchuk.org/cancerstats/types/breast/mortality/, Date accessed 28/11/2008

Cancer Research UK, Information Resource Centre. (2008c). *Breast Cancer*, http://info.cancerresearchuk.org/cancerstats/types/breast/survival/#stage, Date accessed 28/11/2008

Cole, K. S. (1940). Permeability and impermeability of cell membranes for ions, *Cold Spring Harbor Symp, Quant. Biol*. **8**: 110–22

Cole, K. S. and Cole, R. H. (1941). Dispersion and absorption in dielectrics. *J. Chem. Phys.* **9**: 341-351

De Vries, P. M. J. M. (2007). What separates us from turning EIC and EIT into successful clinical bed-side instruments? *IFMBE Proc. of XIII ICEBI &VII EIT, Graz, Austria*. **17**: pp 3

Diagnostic Sonar. (2009). *3 Generations of Ultrasonic Experience,* http://www.diagnosticsonar.com, Date accessed 20/10/2009

EIDORS. (2011). EIDORS - News, http://eidors3d.sourceforge.net/news.shtml, Date accessed 14/07/2011

Fabrizi, L. et al. (2009). A comparison of two EIT systems suitable for imaging impedance changes in epilepsy. *Physiol. Meas.* **30**(6): S103-S120

Fentiman, I. S. (1998). *Detection and Treatment of Breast Cancer, 2nd Edition*. London: Martin Dunitz

Food and Drug Administration (FDA), U.S. Department of Health and Human Services. (1999a). *FDA approves new breast imaging device*, http://www.fda.gov/bbs/topics/ANSWERS/ANS00950.html, Date accessed 01/12/2008

Food and Drug Administration (FDA), U.S. Department of Health and Human Services. (1999b). *TransScan T-Scan 2000 - P970033, Summary of safety and effectiveness data*, Food and Drug Administration

Forsythe, J. et al. (2011). Optical breast shape capture and finite-element mesh generation for electrical impedance tomography, *Physiol. Meas.* **32**: 797-809

Foster, K. R. And Schwan, H. P. (1989) the electric capacity of tumors of the breast, *Journal of Cancer Research* **10**: 340

Fricke, H. and Morse, S. (1925). The electric resistance and capacity of blood for frequencies between 800 and 412 million cycles, *J. Gen. Physiol.* **9:** 153–67

Fricke, H. and Morse, S. (1926). The electric capacity of tumors of the breast *Journal of Cancer Research* **10:** 340-376

Grieve, B. D. et al. (2010). An accessible electrical impedance tomograph for 3D imaging, *Trans. Inst. Meas. Control.* **32** (1): 31-50

Grychtol, B. I. (2011). The importance of shape: thorax models for GREIT, *11th Electrical Impedance Tomography Conference Proceedings, Bath, UK* pg 230 – 233

Haltiwanger, S. (2003). The Electrical Properties of Cancer Cells, http://www.royalrife.com/haltiwanger1.pdf, date accessed 06/04/2011

Hartov, A. et al (2005). Breast cancer screening with electrical impedance tomography **In** Holder, D. S. *Electrical Impedance Tomography: Methods, History and Applications,* 167-185. Bristol, UK: IOP Publishing Limited.

Hartov, A. et al. (2011). Systems and methods for combined ultrasound and electrical impedance imaging, *United States Patent Application Publication* US 2011/0034806 A1

He, Y. et al. (2007). Preliminary study of a Cole-Cole model curve fitting method for Electrical Impedance Tomography. *ICEBI 2007, IFMBE Proceedings* **17**: 436–439

Heitmann, A. et al. (2009). Screening of heart diseases with multivariate short-term heart rate variability analysis, *World Congress on Medical Physics and Biomedical Engineering.* **25** (7): 285-288

Henderson, R. P. and Webster, J. G. (1978). An impedance camera for spatially specific measurements of the thorax *IEEE Trans. Biomed. Eng.* **25:** 250-254

Holder, D. S. (2005). Introduction to biomedical electrical impedance tomography **In** Holder, D. S. *Electrical Impedance Tomography: Methods, History and Applications*, 423-449. Bristol, UK: IOP Publishing Limited

Holder, D. (2010). *Electrical Impedance Tomography of brain function,* UCL Department of Medical Physics and Bioengineering Research publications - Further Reading. http://www.ucl.ac.uk/medphys/research/eit/pubs/brain_EIT_overview.pdf, Date accessed 20/07/2011

Horowitz, P. and Hill, W. (1989). *The Art of Electronics*. Cambridge, UK: Cambridge University Press

Huang, J-J. et al. (2011) development of Electrical Impedance Spectroscopy and Tomography System, *International proceedings of Chemical, biological & Environmental Engineering* **16:** 135-140

IARC Handbooks of Cancer Prevention (2002). *Breast Cancer Screening.* Volume 7. Lyon: IARC Press

Imaginis. (2009). *Frequently Asked Questions about Mammography and Breast Cancer,* http://www.imaginis.com/breasthealth/faq-mammo2.asp, Date accessed 16/08/2009

IMT. (2008). Impedance Medical Technologies – Multifrequency electrical impedance mammograph, http://www.medimpedance.com, date accessed 24/02/2011.

Jaron, D. et al. (1968). A mathematical model for the polarization impedance of cardiac pacemaker electrodes, *Medical and Biological engineering and computing.* **6**(6):579-594

Jossinet, J. et al. (1985). A quantitative technique for bio-electrical spectroscopy, *J. Biomed. Eng*, **7** (4): 289–294

Jossinet, J. et al. (1988). A hardware design for imaging the electrical impedance of the breast, *Physiol. Meas.* **9** (Supplement A): 25-28

Jossinet, J. (1998) The impedivity of freshly excised human breast tissue *Physiol. Meas.* **19** (1): 61-76

Kao, T-J. et al. (2008). Regional Admittivity Spectra With Tomosynthesis Images for Breast Cancer Detection: Preliminary Patient Study, *IEEE transactions on medical imaging.* **27** (12): 1762-1768

Kopans, D. B. (1998). *Breast Imaging, 2nd Edition.* Philadelphia: Lippincott-Raven

Lee, E. J. et al. (2011). Breast EIT using a new projected image reconstruction method with multi-frequency measurements, *11th Electrical Impedance Tomography Conference Proceedings,* Bath, UK pg 278 – 281

Macdonald, J. R. (1991). Impedance Spectroscopy, *Annals of Biomed. Eng.* **20** (3): 289-305

Maxim Integrated Products (N.D.). *MAX4223 Family Macromodels*, www.maxim-ic.com/tools/spice/operational_amplifiers/macro/MAX4223.FAM, Date Accessed 06/04/2006

McAdams, E. T. and Jossinet, J. (1995). Tissue impedance: a historical overview *Physiol. Meas.* **16** (suppl): A1–A13

McEwan, A. et al. (2006). A comparison of two EIT systems suitable for imaging impedance changes in epilepsy. *Physiol. Meas.* **27** (5): S199

Min, M. et al. (2008). Broadband excitation for short-time impedance spectroscopy, *Physiol. Meas.* **29** (6): S185

Min, M. et al. (2009). Comparison of rectangular wave excitations in broad band impedance spectroscopy for microfluidic applications, *World Congress on Medical Physics and Biomedical Engineering* **25** (7): 85-88

Min, M. et al. (2011). Broadband spectroscopy of dynamic impedances with short chirp pulses*, Physiol. Meas.* **32**: 945-958

Mieog, J. S. D. et al. (2011). *Toward Optimization of Imaging System and Lymphatic Tracer for Near-Infrared Fluorescent Sentinel Lymph Node Mapping in Breast Cancer,* Annals of Surgical Oncology, http://dx.doi.org/10.1245/s10434-011-1566-x, date accessed 24/08/2011

Molleman, A. (2003). Patch Clamping: An Introductory Guide to Patch Clamp Electrophysiology. Chichester, England: John Wiley & Sons

National Cancer Institute (NCI), U.S. National Institute of Health. (2002). *Improving methods for Breast Cancer Detection and Diagnosis,* http://www.cancer.gov/cancertopics/factsheet/Detection/breast-cancer, date accessed 01/12/2008

NHS Cancer Screening Programme. (2007). NHS Breast Screening Programme, www.cancerscreening.nhs.uk/breastscreen, date accessed 15/08/2008

Office for National Statistics (ONS). (2007). *Cancer Statistics registrations: Registrations of cancer diagnosed in 2004*, England. Series MB1 (No.35)

Oh, T. I. et al. (2011). Fully parallel multi-frequency EIT system with flexible electrode configuration: KHU Mark2, *Imaging.* 32: 1-15

*Oxford Reference Concise Medical Dictionary.* (1994). 4th edition. Oxford, UK: Oxford University Press

Parker, R. W. (2005), Circuits I have known, http://controlsignalconverter.com/docs/circuits_i_have_known.pdf, Date accessed 24/02/2008

Pascal, S. M. A. et al. (2008). Effects of c-MYC activation on glucose stimulus-secretion coupling events in mouse pancreatic islets, *American Journal of Physiology, Endocrinology and Metabolism*. **295** (1): E92-E102

Pease, R. A. (2008). A Comprehensive Study of the Howland Current Pump, *National Semiconductor Application Note* **1515**: 1-10

Pelengaris, S. et al. (2002). Suppression of Myc-induced apoptosis in beta cells exposes multiple oncogenic properties of Myc and triggers carcinogenic progression. *Cell* **109** (3): 321 – 334

Pelegaris, S. et al. (2004). Brief inactivation of c-Myc is not sufficient for sustained regression of c-Myc-induced tumours of pancreatic islets and skin epidermis. *BMC Biology* **2** (26): 1-14

Pelengaris, S. & Khan, M. (2006). The Molecular Biology of Cancer. Oxford, UK: Blackwell Publishing

Pikkemaat, R. et al. (2011) High speed multi-frequency EIT device, *11th Electrical Impedance Tomography Conference Proceedings,* Bath, UK pg 37 – 40

Pliquett, U. et al. (2000). Evaluation of fast time-domain based impedance measurements on biological tissue, *Biomed Tech (Berl).* **45**(1-2): 6-13

Pliquett, U. et al. (2007). High frequency and low concentration – limitation for impedance measurements, *ICEBI 2007, IFMBE Proceedings* **17**: 12–15

Pliquett, U. et al. (2011). Front end with offset-free symmetrical current source optimized for time domain impedance spectroscopy*, Physiol. Meas.* **32**: 927-944

Pollard, B. J. et al. (2011). Functional electrical impedance tomography by evoked response (FEITER): Sub-second changes in brain function during induction of anaesthesia with propofol: 7AP1-6, *European Journal of Anaesthesiology* **28**: 97–98

Prasad N, S. et al. (2008). Breast imaging using 3D electrical impedance tomography, *Biomed Pap Med Fac Univ Palacky Olomouc Czech Repub*. **152**(1):151–154.

Qiao, G. et al. (2008) Investigation of in-vitro bioimpedance test system for mouse pancreas. *Proc. of IX EIT conf.* Hanover, USA. 44: 159-162

Radiologyinfo.org, developed jointly by The American College of Radiology and The Radiological Society of North America. (2008). Mammography, http://www.radiologyinfo.org/en/info.cfm?pg=mammo, date accessed 15/08/2008

Ross, A. S. et al. (2003). Current source design for electrical impedance tomography, *Physiol. Meas.* **24**: 509–516

Salter, D. C. (1981). *A study of some electrical properties of normal and pathological skin in vivo,* Ph.D. Thesis, University of Oxford

Scharfetter, H. et al. (2007). Spectroscopic 16 channel magnetic induction tomography: The new Graz MIT system. *ICEBI 2007, IFMBE Proceedings* **17**: 452–455

Schweiger, M. and Arridge, S. R. (1999). Optical tomography reconstruction in a complex head model using a priori region boundary information. *Phy. Med and Biol.* **44**(11): 2703-2721

Sequin, E. K. (2009). Imaging of cancer in Tissues using an Electromagnetic Probe, MSc Thesis, Ohio State University

Soulsby, C. T. et al. (2006) Measurements of gastric emptying during continous nasogastric infusion of liquid feed: electrical impedance tomography versus gamma scintigraphy, *Clin. Nutr.* **25**: 671-680

*Taber's Cyclopaedic Medical Dictionary.* (1997). 18th edition. Philadelphia, USA: F.A. Davis Company

Tizzard, A. et al. (2010).Generation and performance of patient-specific forward models for breast imaging with EIT. *J. Phys.: Conf. Ser*. **224** (1): 012034

Trokhanova, O. V. et al. (2008). Dual-frequency electrical impedance mammography for the diagnosis of non malignant breast disease, *Physiol. Meas.* **29** (6): S331

Trokhanova, O. V. et al. (2011). Using of electrical impedance mammography for monitoring of the efficient of dyshormonal breast diseases treatment, *11th Electrical Impedance Tomography Conference Proceedings,* Bath, UK pg 222 – 225

Tsui, P. H. et al. (2008). Classification of breast masses by ultrasonic Nakagami imaging: A feasibility study. *Physiol. Meas.* **53**: 6027-6044

Tunstall, B. (2002). *An investigation into the use and limitations of electrical impedance mammography as a clinical diagnostic tool*, Ph.D. Thesis, Leicester De Montfort University

Wang, L. et al (2006). Preliminary report of optimisation of in-vitro studies with an in-vitro specimen measuring system *Proceedings of VII EIT*, Seoul, Korea

Wang, W. et al. (1998). The design of De Montfort Mk2 electrical impedance mammography system, *EMBS Proc. of 20th Ann. Int. Conf. of IEEE, Hong Kong, China.***2** 1042-1043

Wang, W. et al. (2001). Preliminary results from an EIT breast imaging simulation system, *Physiol. Meas.* **22** 39-48

Wang, W. et al. (2006). Study and comparison of the repeatability errors from different bio-electrodes under various conditions for EIT *Proceedings of VII EIT*, Seoul, Korea

Wang, W. et al (2006). Investigation on biomedical measurement accuracy in electrode-skin tests *Proceedings of XI IFAC MCBMS* **6** (1): 147-150

Wang, W. (2007). *EIM in DMU*, Unpublished presentation presented internally at De Montfort University

Wang, W. et al (2007) A Comprehensive Study on Current Source Circuits In: *Proceedings of XIII ICEBI &VIII EIT, Graz*

Wang, W. et al (2008). Preliminary results from a study of pancreatic tissue for cancer identification using electrical impedance measurement *9th Electrical Impedance Tomography Conference*, Hanover, USA pg 130-133

Warren, S. L. (1930). A roentgenologic study of the breast. *The American Journal of Roentgenology and Radium Therapy.* **24**: 113-124

Wi, H. & Woo, E. J. (2009) Design of KHU Mark2 Multi-frequency EIT System, *10th Electrical Impedance Tomography Conference Proceedings,* Manchester, UK

*Wiley Encyclopaedia of Biomedical Engineering.* (2006). vol. 2. Hoboken, New Jersey, USA: John Wiley & Sons

Yamaguchi, T. F. et al. (2011). Practical human abdominal fat estimation utilising electrical impedance tomography, *11th Electrical Impedance Tomography Conference Proceedings, Bath, UK.* pg 17 – 20

Yamamoto, Y. et al. (1996). Instantaneous measurement of electrical parameters in a palm during electrodermal activity, *IEEE Transactions on instrumentation and measurement.* **45** (2):483-487

Yang, F. et al. (2010). MEFS - MIND electrical impedance tomography forward solver, *Engineering in Medicine and Biology Society (EMBC), 2010 Annual International Conference of the IEEE.* pg 3105-3108

Yoo, P.J. et al. (2011). Parallel multi-frequency EIT system with self-calibration: KHU Mark2.5, *11th Electrical Impedance Tomography Conference Proceedings,* Bath, UK pg 109 - 112

Zhou, L. et al. (2011). Magnetoacoustic tomography with magnetic induction (MAT-MI) for breast tumor imaging: numerical modeling and simulation. *Phy. Med and Biol.* **56** (7): 1967-1984